INFORMATION TO USERS

This manuscript has been reproduced from the microfilm master. UMI films the text directly from the original or copy submitted. Thus, some thesis and dissertation copies are in typewriter face, while others may be from any type of computer printer.

The quality of this reproduction is dependent upon the quality of the copy submitted. Broken or indistinct print, colored or poor quality illustrations and photographs, print bleedthrough, substandard margins, and improper alignment can adversely affect reproduction.

In the unlikely event that the author did not send UMI a complete manuscript and there are missing pages, these will be noted. Also, if unauthorized copyright material had to be removed, a note will indicate the deletion.

Oversize materials (e.g., maps, drawings, charts) are reproduced by sectioning the original, beginning at the upper left-hand corner and continuing from left to right in equal sections with small overlaps.

Photographs included in the original manuscript have been reproduced xerographically in this copy. Higher quality 6" x 9" black and white photographic prints are available for any photographs or illustrations appearing in this copy for an additional charge. Contact UMI directly to order.

ProQuest Information and Learning
300 North Zeeb Road, Ann Arbor, MI 48106-1346 USA
800-521-0600

UNIVERSITY OF OKLAHOMA

GRADUATE COLLEGE

MODELING INTERPOROSITY FLOW FOR IMPROVED SIMULATION OF NATURALLY FRACTURED RESERVOIRS

A Dissertation

SUBMITTED TO THE GRADUATE FACULTY

in partial fulfillment of the requirements for the

degree of

Doctor of Philosophy

By

GHERSON PEÑUELA-PINEDA

Norman, Oklahoma

2002

UMI Number: 3045836

UMI Microform 3045836

ProQuest Information and Learning Company
300 North Zeeb Road
P.O. Box 1346
Ann Arbor, MI 48106-1346

MODELING INTERPOROSITY FLOW FOR IMPROVED SIMULATION OF NATURALLY FRACTURED RESERVOIRS

A Dissertation

APPROVED FOR THE MEWBOURNE SCHOOL OF

PETROLEUM AND GEOLOGICAL ENGINEERING

By

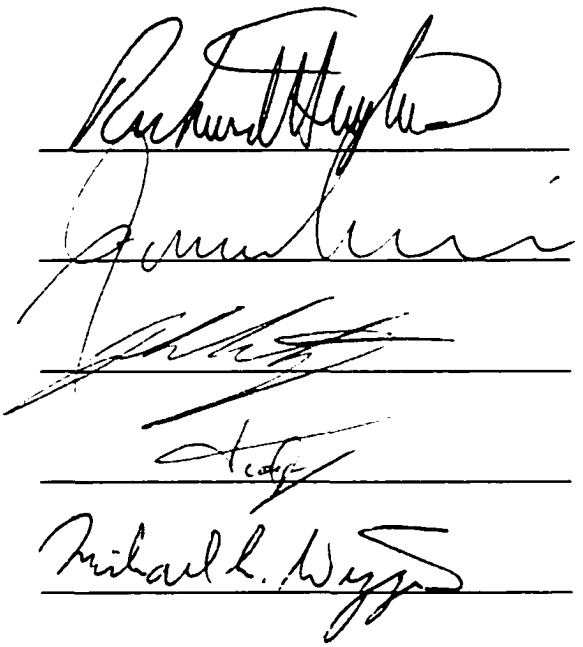

ACKNOWLEDGEMENTS

I wish to express my deepest gratitude to my doctoral committee co-chairs, Dr. Faruk Civan and Dr. Richard G. Hughes, for their continuous guidance and motivation during the entire period of this study. The basic content of this research was the outcome of very productive discussions during our weekly meetings. This work would have not been accomplished without their guidance and encouragement.

Deep appreciation is also extended to Dr. Michael L. Wiggins, Dr. Jean-Claude Roegiers, and Dr. John P. Castagna for their time, assistance and willingness to serve as members of my doctoral advisory committee.

I would also like to express my gratitude to all professors and staff in the Mewbourne School of Petroleum and Geological Engineering who helped me during my studies at The University of Oklahoma.

Special thanks go to the United States Department of Energy for the financial support throughout my doctoral study.

A further note of appreciation goes to my Colombian friends for their encouragement.

I affectionately dedicate my thesis to my parents, Matías Peñuela and Gladys Pineda de Peñuela, and to my brothers, Anderson and Jahisber, for their understanding, encouragement and support that bolstered me up to conclude this work.

The author gratefully acknowledges the permission for inclusion of Figs. 2.1-2.3, 3.1 3.2, 3.4, 4.1-4.14, 5.1, 5.2, 6.1-6.9 and Tables 2.1, 4.1-4.3, 5.1, 5.2, 6.1, 6.2 by the Society of Petroleum Engineers; and Fig. 3.5 by Society of Exploration Geophysicists in this dissertation.

TABLE OF CONTENTS

LIST OF FIGURES

LIST OF TABLES

ABSTRACT

An accurate interporosity flow equation incorporating a time-dependent shape factor is derived and verified for improved dual-porosity modeling of pressure depletion and waterflooding of naturally fractured reservoirs. The interporosity rate equation expresses the exchange rate in terms of the oil-phase pressure gradient in the matrix, effective flow area and fluid permeability at the matrix/fracture interface, fluid viscosity and a variable matrix-block shape factor, computed as a flow correction factor to Darcy's law. This approach can accommodate the flow directed from matrix to fractures while representing the permeability anisotropy of interconnected fractures as a tensor. The model equations are expressed in dimensionless forms for convenient integration into conventional numerical simulators for accurate simulation of pressure depletion and waterflooding of naturally fractured reservoirs. Implementation of flow correction factors is also demonstrated by modifying a dual-porosity, dual-permeability reservoir simulator.

Fine-grid numerical simulation of a matrix block is performed to verify the flow equation using the time-dependent flow correction factor. Numerical experiments with various size matrix blocks indicate that the flow correction factor varies with time and converges to the steady-state value reported in the previous studies for single-phase flow. The flow correction factor for single-phase flow converges to a steady-state value at a speed proportional to the reciprocal of total compressibility, while the flow correction factor for two-phase flow converges at a speed proportional to the slope of the capillary

pressure curve evaluated at the average water saturation present at the matrix/fracture interface. It is shown that the single-phase flow correction factor converges much more rapidly to its steady-state value than the two-phase flow correction factor.

The applicability of the time-dependent flow correction factor is also extended and demonstrated for gas-condensate systems by taking advantage of pseudofunctions that reduce the miscible two-phase problem to a single-phase problem.

This study demonstrates that considering the time-dependency of the shape factor alleviates the errors associated with using constant shape factors in fractured reservoir simulation with minor modifications in the interporosity flow model. Results from the numerical examples presented in this study indicate that the physical phenomena considered in the present model would predict shorter water breakthrough times and less oil recovery from the matrix, compared with predictions of the current numerical simulators using constant shape factors. Specifically, water breakthrough time and oil recovery predicted by the present model are about half of those predicted by current numerical simulators using constant shape factors, based on a 10 years production period from a naturally fractured reservoir.

CHAPTER 1

INTRODUCTION

A naturally fractured reservoir is a porous rock formation in which stresses have created planar discontinuities that either positively or negatively affect fluid flow. From the viewpoint of petroleum reservoir engineering, these naturally occurring fractures represent both challenging modeling problems as well as opportunities for reservoir development. The combination and application of knowledge from different branches of science is required in order to take full advantage of their presence in a hydrocarbon-bearing formation. Classic books by Jaeger and Cook,[1] Aguilera,[2] Reiss,[3] van Golf-Racht,[4] and Nelson[5] provide details on fracture formation, characterization and mathematical simulation through simple models that capture some of the typical characteristics of naturally fractured reservoirs.

Even though a substantial amount of research has been devoted to geomechanics, geology and reservoir engineering since the abovementioned publications, high-priority research needs were recently identified.[6] Some of these studies include further research on the origin and development of fracture systems; fracture detection methods; effects of coupling between stress and flow; effects of coupling between chemical processes, flow, and temperature in rocks; development of improved conceptual models as bases for more

realistic and efficient numerical models of fluid flow and transport; and additional in-situ facilities to test these numerical models.

Much research on naturally fractured reservoir modeling has focused on conceptual models that accurately represent the matrix/fracture fluid transfer because of its importance in reservoir performance. Most naturally fractured reservoirs are characterized by high initial production rates that later drop to much lower stable flow rates. The later period of production is controlled by the matrix/fracture interaction through the interporosity flow rate. During this period, the permeable matrix replenishes fractures with hydrocarbon fluids, which are produced from the high conductivity pathways to the wellbore.[5] Hence, fluid expansion is the primary mechanism for hydrocarbon recovery. On the other hand, successful implementation of a secondary or tertiary recovery project in a naturally fractured reservoir requires an accurate matrix/fracture interaction model. Some of the mechanisms investigated in order to estimate and predict the interporosity flow rate include gravity and capillary effects,[7,8] reinfiltration,[9,10] and capillary continuity throughout the matrix blocks,[11,12] and cocurrent and/or countercurrent imbibition phenomena.[13,14] In waterflooding, capillary imbibition is generally the most important recovery mechanism.[15]

Some field and laboratory observations have been studied through numerical simulation, which typically assumes that there are two continua, matrix and fractures, within each simulation gridblock. Flow equations are written for each system with a matrix/fracture transfer function to relate the loss or gain of matrix fluids to or from the fracture. This fluid transfer rate is commonly calculated as a function of the pressure difference between the matrix and fracture systems, matrix flow capacity and matrix

geometry considered through a constant shape factor. However, in spite of the great level of current model sophistication, the highly anisotropic and heterogeneous nature of a fractured formation makes fractured reservoir modeling a challenging task, frequently with uncertain results in forecasting.

This study presents a new conceptual model to determine the interporosity flow rate in naturally fractured reservoirs. The new model is used to investigate time-dependent effects on the matrix-block shape factors by defining a flow correction factor based on Darcy's law. This approach is shown to be an improved way to model naturally fractured formations because it correctly accounts for nonlinear pressure and saturation gradients within matrix blocks without using fine-grid numerical simulation.

A literature review is presented in Chapter 2. The proposed conceptual model is introduced in Chapter 3, and the types of fractured reservoirs are identified. A time-dependent flow correction factor is then introduced for single-phase systems, and a correlation to estimate the correction factor in terms of dimensionless variables is derived in Chapter 4. The application of the flow correction factor to gas-condensate systems by means of appropriate pseudofunctions that account for the reduction of gas mobility because of liquid condensation at the matrix/fracture interface is presented in Chapter 5. An extension of the flow correction factor to multiphase black-oil systems is presented in Chapter 6. Correlations for the flow correction factor and relative permeabilities at the matrix/fracture interface are presented that are based on numerical experiments with a conventional finite-difference simulator. These correlations are expressed in dimensionless form for convenient integration into current simulators. Finally,

implementation of flow correction factors in a dual-permeability, dual-porosity reservoir simulator is presented in Chapter 7.

CHAPTER 2

LITERATURE REVIEW

In recent years, numerical simulation of naturally fractured reservoirs has received significant attention because of increased exploration and development of more challenging, deeper reservoirs that are characterized by compartmentalization, heterogeneity, and anisotropy. Highly efficient computers have helped engineers to model fractured reservoirs faster and with more detail. In this section, commonly used approaches for naturally fractured reservoir modeling and interporosity flow estimation are reviewed.

2.1 Reservoir Modeling

There are three basic models that are used for numerical simulation of naturally fractured reservoirs: Discrete network models, equivalent continuum models, and hybrid techniques, which combine features of both discrete network and continuum models.[6] In discrete network simulation, a population of individual fractures is modeled while in equivalent continuum models, effective rock and fluid parameters are assigned to large volumes of the rock mass. Although the selection of any particular model depends on the reservoir and the type of fluid flow behavior to be numerically simulated, in general, the equivalent continuum modeling approach may be used to simulate reservoir rocks that

have undergone multiple and extensive deformations (high fracture density) and/or any formations where matrix permeabilities are large enough that fluid flow is not influenced by any individual fracture or series of fractures that form a conducting channel.[6] Because of the relevance to this study, the most important equivalent continuum models – single-porosity, dual-porosity, and dual-permeability models – are briefly reviewed in the following.

2.1.1 Single-Porosity Models

Even though single-porosity models are used to simulate reservoirs where all the storage capacity is assumed to reside in the fractures, they may also be applied in fractured reservoirs where interporosity flow between porous matrix and fractures is an important factor. An example of a single-porosity model application was presented by Agarwal *et al.*,[16] who simulated a giant, fractured chalk reservoir in the North Sea. They pointed out that one of the most challenging tasks was to account for the fluid transfer between porous media and fractures. To circumvent this difficulty using a single-porosity reservoir model, they developed pseudorelative permeability functions. This development consisted of a two-stage upscaling process. Initially, detailed modeling of stacks of individual matrix blocks using a dual-porosity model was performed. Then, the relative permeability curves generated in the previous stage were applied to generate field scale dynamic pseudofunctions by history matching of the fine-grid simulation. Even though the single-porosity approach has an advantage from the viewpoint of computational effort, it has the problem of selecting an appropriate model for fluid exchange while preparing the pseudorelative permeability curves using a dual-porosity reservoir model.

An additional difficulty is encountered during simulation when the operating conditions are changed because a new set of dynamic pseudofunctions needs to be calculated; for instance, when waterflooding after gas flooding.

2.1.2 Dual-Porosity Models

Dual-porosity models simulate reservoir systems composed of two different types of porosity that coexist in a rock volume. It is usually assumed that the matrix blocks consist of a set of porous rock systems that are not connected, have high storage capacity and low transmissibility. On the other hand, the fracture system is assumed to be an interconnected porous medium of low storage capacity and high transmissibility. Flow from the reservoir to the wellbore only occurs through the fracture system.[17] Several idealizations to the matrix/fracture system geometry in a simulation gridblock have been developed such as the sugar cube,[17] parallel horizontal fracture[18] and match-stick column models.[3] A variation of dual-porosity models is the multi-porosity model, which assumes a fracture set that interact with two groups of matrix blocks with distinct permeabilities and porosities.[19]

2.1.3 Dual-Permeability Models

The first dual-permeability model was formulated by Barenblatt *et al.*[20] and numerically solved by Hill and Thomas.[21] This approach models a continuous matrix media allowing matrix-matrix and fracture-fracture flow between simulation gridblocks. The flow equation for phase α in the fracture system is given by:

$$\nabla \cdot \left[\frac{\bar{\bar{k}}_f k_{r\alpha f}}{\mu_{\alpha f} B_{\alpha f}} \left(\nabla p_{\alpha f} - \rho_{\alpha f} g \nabla D \right) \right] = \frac{\partial}{\partial t} \left(\phi_f \frac{S_{\alpha f}}{B_{\alpha f}} \right) - \tilde{q}_\alpha \quad \text{.....2.1}$$

where $\tilde{q}_\alpha$ is the interporosity flow rate per unit volume of rock. The subscript α represents water, oil and gas phases. A similar set of equations may be defined for multiphase fluid flow in the interconnected matrix media. See Chapter 7 for additional details.

An important drawback of dual-permeability models is that they require greater computing time and data storage than dual-porosity models.[22] Modifications to the initial formulation have extended this model to handle compositional fluids.[23] However, the most important modification to dual-porosity and dual-permeability models has been the incorporation of different fluid transfer functions for interporosity flow modeling.

2.2 Interporosity Flow Modeling

In traditional dual-porosity and dual-permeability simulation of fractured reservoirs, the interporosity flow rate is proportional to a shape factor, which is taken as a constant value obtained for an assumed matrix-block size and geometry. Other approaches that do not use shape factors are also available. In general, fluid transfer models can be grouped into two broad categories depending on the fluid system in the reservoir. Single-phase models have been applied in well test analysis while multiphase models have been predominant in modeling secondary and tertiary recovery in naturally fractured formations.[24]

2.2.1 Single-Phase Models for Interporosity Flow

For single-phase fluid systems, two main approaches can be found depending on whether shape factors are required to determine the interporosity rate. Models that do not require

shape factors use the superposition principle to compute the interporosity rate from the amount of fluids flowing from the matrix to the fractures per unit of fracture volume owing to the matrix pressure variation as the fracture pressure changes.[25,26] Other approaches that do not need shape factors will be reviewed under the section that compares models for multiphase fluid systems. On the other hand, two groups of models can be identified when shape factors are used. One group only considers the matrix geometry while the other uses only the fracture geometry in shape factor calculations. A discussion and comparison of models that use shape factors are presented in the following.

2.2.1.1 Matrix-Based Shape Factors

Barenblatt *et al.*[20] proposed a model for naturally fractured reservoirs that is analogous to a model used for heat transfer in a heterogeneous medium. They assumed that the outflow of fluids from matrix blocks into the fractures is steady-state and that the fluid transfer rate is a function of the viscosity of the fluid, the pressure drop between the matrix and fracture systems, and matrix-rock properties related to geometry and porous interconnectivity in the matrix block. According to Barenblatt *et al.*, the fluid transfer rate per unit volume of rock is calculated from the following expression:

$$\tilde{q} = \frac{\sigma k_m}{\mu}\left(\bar{p}_m - p_f\right) \qquad 2.2$$

where σ is a shape factor related to the specific surface of the fractures, $\bar{p}_m$ and p_f are the average pressures in the matrix and fracture domains, respectively, and $\tilde{q}$ is the fluid transfer rate between the matrix and fracture.

Several researchers have adopted Eq. 2.2 for modeling interporosity fluid transfer in both dual-porosity and dual-permeability models in single- and multiphase flow. However, there is little agreement among the reported studies on the value of the shape factor. Bourbiaux *et al.*[22] presented a comparison of shape factors found in the literature. **Table 2.1** is a modified version of the Bourbiaux *et al.* table,[22] reporting the numerical value of the product σL^2 as calculated by different researchers. The L parameter may represent the fracture spacing for one set of parallel fractures, the side length of a square formed between two normal sets of fractures, or the side length of an isotropic cubic matrix block obtained from the intersection of three normal sets of fractures.

TABLE 2.1 – INCONSISTENT VALUES OF THE REPORTED GEOMETRIC FACTORS, σL^2 (AFTER PENUELA *ET AL.*[27])

Mathematical approximations	Matrix Geometry		
	Slab	Square-Column	Cube
Warren and Root[17] (Analytic)	12	32	60
Kazemi *et al.*[28] (Numeric)	4	8	12
Thomas *et al.*[29] (Numeric)	--	--	25
Coats[30] (Analytic)	8	16	24
Kazemi and Gilman[24] (Analytic)	--	--	29.6
Lim and Aziz[31] (Analytic)	9.9	19.7	29.6
Quintard and Whitaker[32] (Numeric)	12	28.4	49.6
Noetinger *et al.*[33,34] (Stochastic)	11.5	27.1	--
Bourbiaux *et al.*[22] (Numeric)	--	20	--

Warren and Root[17] presented an application of Eq. 2.2 in their dual-porosity model for well test analysis by assuming that the interporosity flow occurs under pseudo-steady state conditions. They proposed an analytical approximation to estimate the shape factor

assuming uniformly distributed sets of parallel fractures. A schematic of three normal sets of fractures is shown in **Fig. 2.1**.

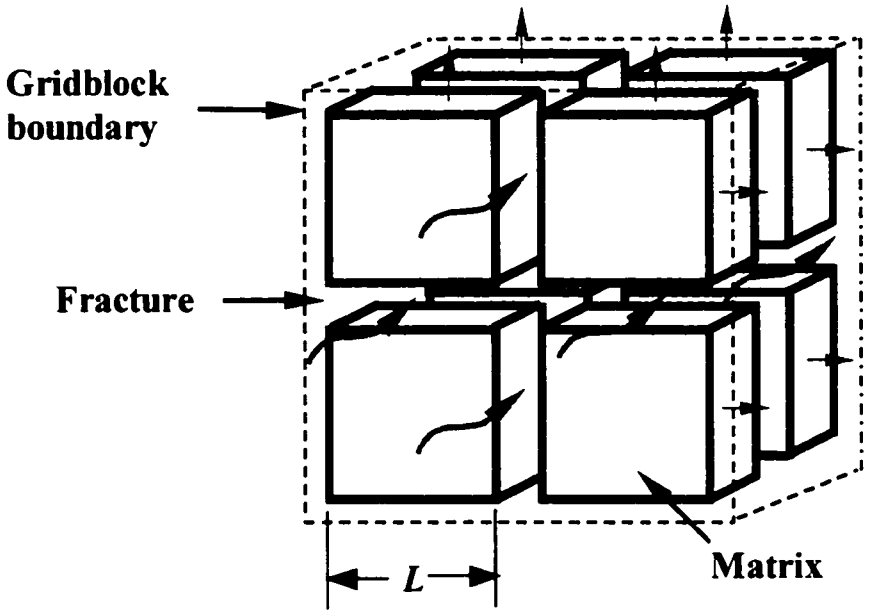

Fig. 2.1 – Gridblock in the dual-porosity model with three normal sets of parallel fractures following Warren and Root[17] (From Penuela *et al.*[27])

For this matrix/fracture system, Warren and Root[17] did not present a derivation of their equation but expressed the shape factor as:

$$\sigma = \frac{4n(n+2)}{L^2} \qquad \text{2.3}$$

where n is the number of normal sets of parallel fractures.

Kazemi *et al.*,[28] Thomas *et al.*[29] and Coats[30] presented various expressions for the shape factor that were verified through numerical solutions of multiphase flow equations similar to those proposed by Warren and Root for a single-phase, dual-porosity model. For instance, using a standard seven-point finite difference formulation of a single-phase,

flow problem, Kazemi *et al.*[28] obtained the following shape factor for a three-dimensional homogeneous matrix block:

$$\sigma = 4\left(\frac{1}{L_x^2}+\frac{1}{L_y^2}+\frac{1}{L_z^2}\right) \quad \text{..... 2.4}$$

where the L_x, L_y, and L_z are the block lengths along x, y, and z-direction, respectively. Equation 2.4 inherently assumes a linear pressure gradient between the fracture and the center of the matrix block.[31] As observed in Table 2.1, shape factors computed from Eq. 2.4 have the lowest values. Hence, this approach is likely to underestimate the efficiency of the energy available to produce single-phase fluids from a matrix block.

Lim and Aziz[31] verified and extended the shape factors for dual-porosity simulation presented by Kazemi and Gilman[24] by combining the analytical solutions of the pressure diffusion equation for various matrix blocks. By using matrix blocks of regular shapes, Lim and Aziz[31] obtained improved shape factors that consider the geometry of the system and the physics of fluid transfer without using the pseudo-steady state assumption. The significance of their approach is that the derived shape factors properly account for nonlinear pressure gradients in the matrix. For the general case of an anisotropic, rectangular matrix block, they reported the following expression for the shape factor:

$$\sigma = \frac{\pi^2}{k_m}\left(\frac{k_x}{L_x^2}+\frac{k_y}{L_y^2}+\frac{k_z}{L_z^2}\right) \quad \text{..... 2.5}$$

where k_m is the geometric average matrix permeability.

2.2.1.2 Fracture-Based Shape Factors

In the solution to the problem of flow of water in fractured media, Duguid and Lee[35] considered a porous medium with several fractures, which were approximated as cylindrical tubules of elliptical cross-sectional area. These cracks have average dimensions, are randomly distributed throughout the matrix, and have porous walls that allow fluid transfer. A representation of their model is shown in **Fig. 2.2**.

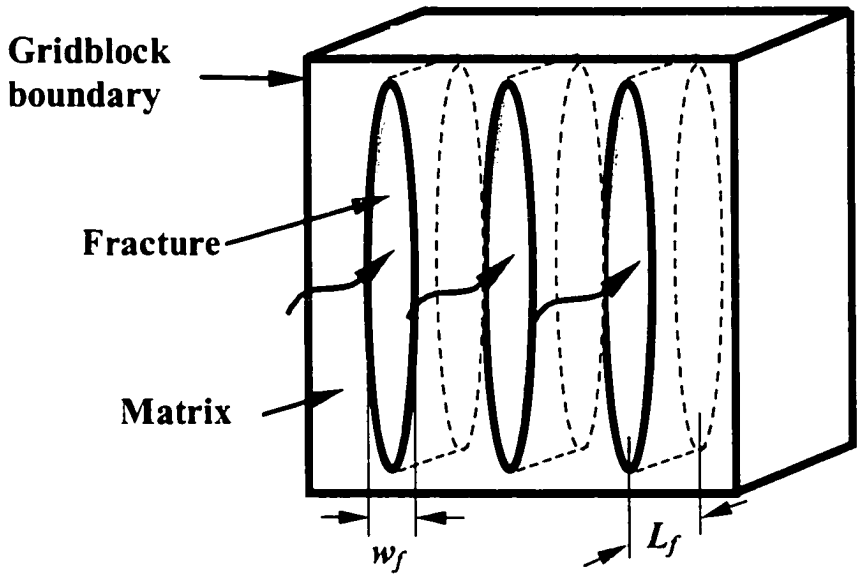

Fig. 2.2 – Gridblock in the dual-permeability model following Duguid and Lee[35] (From Penuela *et al.*[27])

The formulation of the flow transfer term assumes a 1D flow from the matrix to the fracture with fluid flow between the matrix and the fracture. The fracture fluid pressure is assumed constant at the interface. Duguid and Lee[35] provided an approximation for the fluid transfer rate per unit volume of rock that can be written in a more convenient form as:

$$\tilde{q} = \frac{\sigma k_m}{\mu}\left[(p_m - p_f) + 2\sum_{j=1}^{\infty}(-1)^j (p_m - p_i)e^{-j^2 t_D} + 2\sum_{j=1}^{\infty}(p_f - p_i)e^{-j^2 t_D}\right] \quad \text{..... 2.6}$$

where the dimensionless time is:

$$t_D = \frac{2\pi^2 k_m}{\phi_m \mu c_t L_f^2} t \quad \text{..... 2.7,}$$

and the shape factor:

$$\sigma = \frac{16}{\pi}\frac{\phi_f}{w_f L_f} \quad \text{..... 2.8.}$$

Even though the fluid transfer rate as defined by Eq. 2.6 approaches the constant value predicted by steady-state solution, given by Eq. 2.2, a direct comparison cannot be made between Duguid and Lee model and the previous approaches using matrix-based shape factors for the following reasons. The shape factors presented in Eqs. 2.3 through 2.5 are expressed in terms of block geometric properties while Eq. 2.8 is in terms of fracture geometric properties (w_f, L_f). Moreover, the shape factors calculated from Eqs. 2.3 through Eq. 2.5 are independent of fracture porosity. Finally, the shape factor according to Eq. 2.8 is independent of fracture spacing, which is an important characteristic in determining block size in most dual-porosity models.

The importance of models for single-phase fluid systems is that they provide a boundary limit for the flow problem where no effects from multiphase interactions are present. For an ideal fluid transfer function, a single-phase flow model should account for the appropriate effects of both the matrix and the fracture as a system. Currently, most models only consider the effect of either the matrix or the fracture geometry on fluid

transfer. There are no models available accounting for the combined effect of the coupled fracture and matrix media where each system has different geometrical characteristics.

2.2.2 Multiphase Models for Interporosity Flow

Hydrocarbon production by pressure depletion, secondary or tertiary recovery may require flow of a multiphase fluid through the reservoir. The complexity of having more than one fluid flowing through the matrix/fracture interface has been represented with a series of models that consider gravity and capillary effects. Methods to obtain the fluid exchange functions are based on geometric factors, subdomains and empirical parameters, also called empirical transfer functions.

2.2.2.1 Geometric Factor Methods

Geometric factor methods extend single-phase models for fluid transfer to multiphase flow in fractured media by including terms that account for gravity and capillary effects and modifying the shape factor.

Although the pioneering works of Birks,[36] Aronofsky *et al.*[37] and Mattax and Kyte[38] on oil displacement by water laid the foundations for matrix/fracture interaction modeling, the implementation of the shape factor proposed by Barenblatt *et al.*[20] was the most important step toward the mathematical description of the interporosity flow rate. Warren and Root[17] associated the shape factor with the size and geometry of the rock matrix and detailed a procedure to estimate it via well test analysis. Several researchers have proposed modifications to extend the single-phase flow equations of Warren and Root to multiphase flow.

The first modification consisted of the use of effective permeability instead of the absolute permeability. Kazemi *at al.*[28] evaluated fluid effective permeability at the average saturation in the matrix to account for additional resistance to flow owing to the presence of other phases. Thomas *et al.*[29] followed the same approach for flow from the matrix to the fracture, but they computed the fluid relative permeability as a product of the fluid saturation in the fracture and fluid relative permeability evaluated at the matrix fluid saturation when flow is from the fracture to the matrix. This approach was intended to account for the fractional coverage of a gridblock by a fluid.

Kazemi's original multiphase flow model[28] did not account for gravity effects. These effects were later added by Gilman and Kazemi[39] as follows:

$$\tilde{q} = \sigma k_m \left[\omega \left(\frac{k_r}{\mu B} \right)_{am} + (1-\omega) \left(\frac{k_r}{\mu B} \right)_{af} \right] \left[(p_{am} - \rho_{am} g D_m) - (p_{af} - \rho_{af} g D_f) \right] \quad \text{..... 2.9}$$

where ω is a weighting factor that takes a value of one if flow is from matrix to fracture, and is zero when flow goes from fracture to matrix. D_m and D_f are elevations of the matrix and fractures required to account for the gravity head in both media. A more complex version of Eq. 2.9 was introduced by Gilman and Kazemi,[8] who incorporated additional terms to account for gravity effects owing to fracture elevation differences between adjacent gridblocks.

Sonier *et al.*[40] incorporated gravity effects in a dual-porosity formulation following a similar approach. However in their model, the weighting function was applied directly to the relative permeability instead of the mobility term. Moreover, elevations were calculated for each phase by assuming that the saturation in the matrix and the fracture

was the same throughout the gridblock. The following expression was proposed to compute the elevation:

$$D_{\alpha p} = \left(\frac{S_{\alpha p} - S_{\alpha pi}}{1 - S_{or\alpha p} - S_{\alpha pi}} \right) L_z \quad \text{.....2.10}$$

where α stands for fluid phase (water or gas) and p represents the porous system (matrix or fracture).

Thomas *et al.*[29] included pseudorelative permeability and pseudocapillary pressure curves to account for gravity effects in the flow terms but did not give details on how they were obtained. However, application examples of pseudofuntion curves are provided elsewhere.[41,42]

Finally, the most important modification to the single-phase model consisted of defining new shape factors for fluid exchange. For the general case of an anisotropic, rectangular matrix blocks, Gilman and Kazemi[8] presented the following expression for the shape factor:

$$\sigma = \frac{4}{k_m} \left(\frac{k_x}{L_x^2} + \frac{k_y}{L_y^2} + \frac{k_z}{L_z^2} \right) \quad \text{.....2.11}$$

Because this type of shape factor does not accurately account for nonlinear pressure gradients within the matrix, additional approaches have been proposed to incorporate them (see Table 2.1). For instance, Thomas *et al.*[29] performed a numerical simulation study to compute the shape factor for fluid exchange by matching single-block experiments with 3D dual-porosity model results. They found an excellent agreement between the numerical results for water/oil imbibition by setting σL^2 equal to 25, and for gas/oil gravity drainage by setting σL^2 equal to 2.

To include nonlinear pressure gradients in the matrix, Coats[30] proposed a model in which the effects on the exchange function owing to viscous gradients in the fracture are ignored. Without presenting the derivation, the following shape factor was recommended:

$$\sigma = 8\left(\frac{1}{L_x^2}+\frac{1}{L_y^2}+\frac{1}{L_z^2}\right) \quad \text{.....2.12}$$

The fluid exchange model proposed by Duguid and Lee[35] was extended to multiphase flow conditions by Evans.[23] The basic modification consisted of using effective permeability instead of absolute reservoir permeability. In his model formulation, capillary effects were considered but gravity effects were not taken into account.

2.2.2.2 Subdomain Methods

Subdomain methods are based on a matrix-block subdivision scheme (see **Fig 2.3)** that allows the computation of pressure and saturation distributions within the matrix blocks. To calculate intra-matrix flow, these methods apply single-porosity flow equations that consider gravity, viscous, and capillary effects within the matrix subdomains. Finally, these equations are combined with single-porosity fracture equations to calculate the interporosity flow rate. Even though these methods theoretically should yield a more accurate fluid exchange estimation and are available in commercial simulators,[43] their application to full field simulation studies its limited because the large number of computational nodes that are required prohibits their use.

The first attempt to apply this technique was the multiple interacting continua (MINC) introduced by Pruess and Narasimhan.[44] In the MINC model, a matrix block is divided into several computational volume elements whose block interfaces are parallel to the nearest fracture. The division of the porous matrix block gave rise to a model of nested

elements as shown in **Fig. 2.3a**. Gilman[45] also proposed a nested-block model. In addition, he also proposed a stacked-block model, which represents a system where the primary flow path is offered by horizontal fractures (**Fig. 2.3b**). The nested model proposed by Gilman requires shape factors to account for flow between the matrix subdomain in contact with the fracture, while the MINC model does not. Beckner *et al.*[46] combined Gilman's nested and stacked models. In the lateral direction, subdomains are the same as in the MINC method, which reduces a two-dimensional problem to one-dimension. In the vertical direction, the stacked model is adapted to account for fluid segregation owing to gravity. A representation of a typical gridblock and a half-matrix block used in this model is shown in **Fig. 2.3c**.

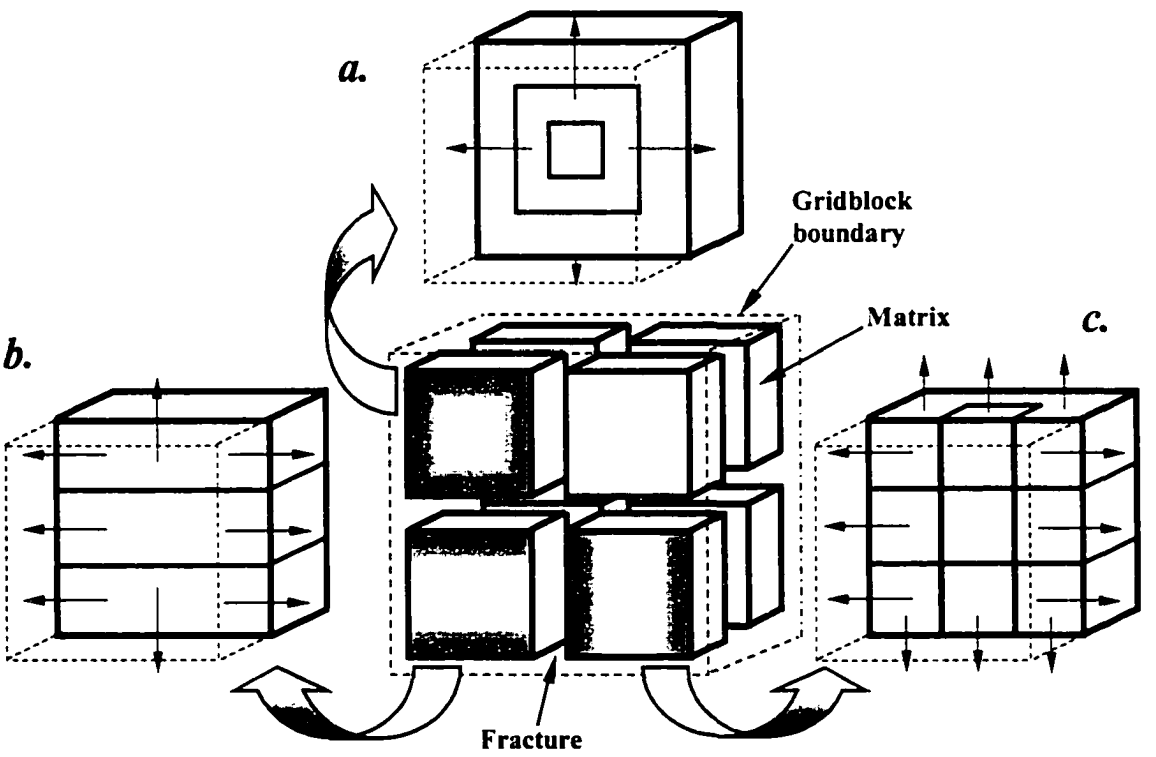

Fig. 2.3 – Dual-porosity modeling with subdomain methods: (*a*) Nested-block model, (*b*) stacked-block model, and (*c*) Beckner *at al.* model (From Penuela *et al.*[47])

2.2.2.3 Empirical Parameter Methods

For the estimation of the interporosity flow rate, de Swaan[48] used an empirical matrix/fracture transfer function based on an exponential model first proposed by Aronofsky *et al.*,[37] who approximated the cumulative oil recovery, R, by an exponential form as:

$$R = R_{\infty}\left(1 - e^{-\lambda t}\right) \quad \text{..... 2.13}$$

where R_{∞} is the ultimate cumulative oil recovery from the imbibition process and λ is a fitting parameter. Based on the recovery curve described by Eq. 2.13, de Swaan[48] expressed the interporosity water flow rate per fracture length using the principle of superposition to account for the variation of water saturation in the fractures as follows:

$$\hat{q} = \lambda R_{\infty} \int_{0}^{t} e^{-\lambda(t-\tau)} \frac{\partial S_{wf}}{\partial \tau} d\tau \quad \text{..... 2.14}$$

Using a similar approach, Kazemi *et al.*[49] concluded that the exponent constant was just a fitting parameter of the oil recovery curve and could not adequately include the saturation dependence of the capillary pressure and relative permeability as well as the interaction of viscous, capillary and gravity forces. Multi-parameter exponential functions for fitting cumulative oil recovery have been used based on a physical interpretation of the imbibition processes. Civan[50,51] worked with two-parameter exponential functions and Gupta and Civan[52] and Civan and Rasmussen[53] showed that three-parameter exponential functions were sufficient and described the behavior of triple-porosity reservoirs accurately.

Reis and Cil[15,54] provided a comparison of analytical models for capillary imbibition and reported the strengths and weakness of each. In spite of the significant attention paid

to quantifying interporosity flow in fractured reservoirs during the past four decades, a rigorous interporosity flow rate expression is still unavailable for implementation in commercial simulators.

2.3 Modeling of Pressure Transient and Saturation Gradient Effects

The aforementioned approaches based on shape factors for computing the interporosity flow rate are usually implemented in current numerical simulators based on a discretization scheme that assigns representative values of pressure and saturation to a fixed position, located at the matrix-block center. To illustrate this point, assume a simulation gridblock is selected where water fronts in fractures flow contacting new matrix/fracture interface area as shown in **Fig. 2.4**. Common discretization schemes using finite-difference approximations would compute an average value of water saturation and would locate it at the center of the simulation gridblock.

Because this discretization scheme implies uniformly distributed water phase within the simulation gridblock, to assign the average saturation at the grid-block center is equivalent to locating the average water saturation at the center of each matrix block within the simulation gridblock. However, physical processes do not necessarily happen at the matrix-block center. In addition, the average value of the water saturation is not located at the center of the matrix block, but instead, shifts from near the interface to the matrix-block center over time as seen in Fig. 2.4. To compensate for the inconsistencies resulting from discretization, correction schemes are needed for proper representation of the physical processes.

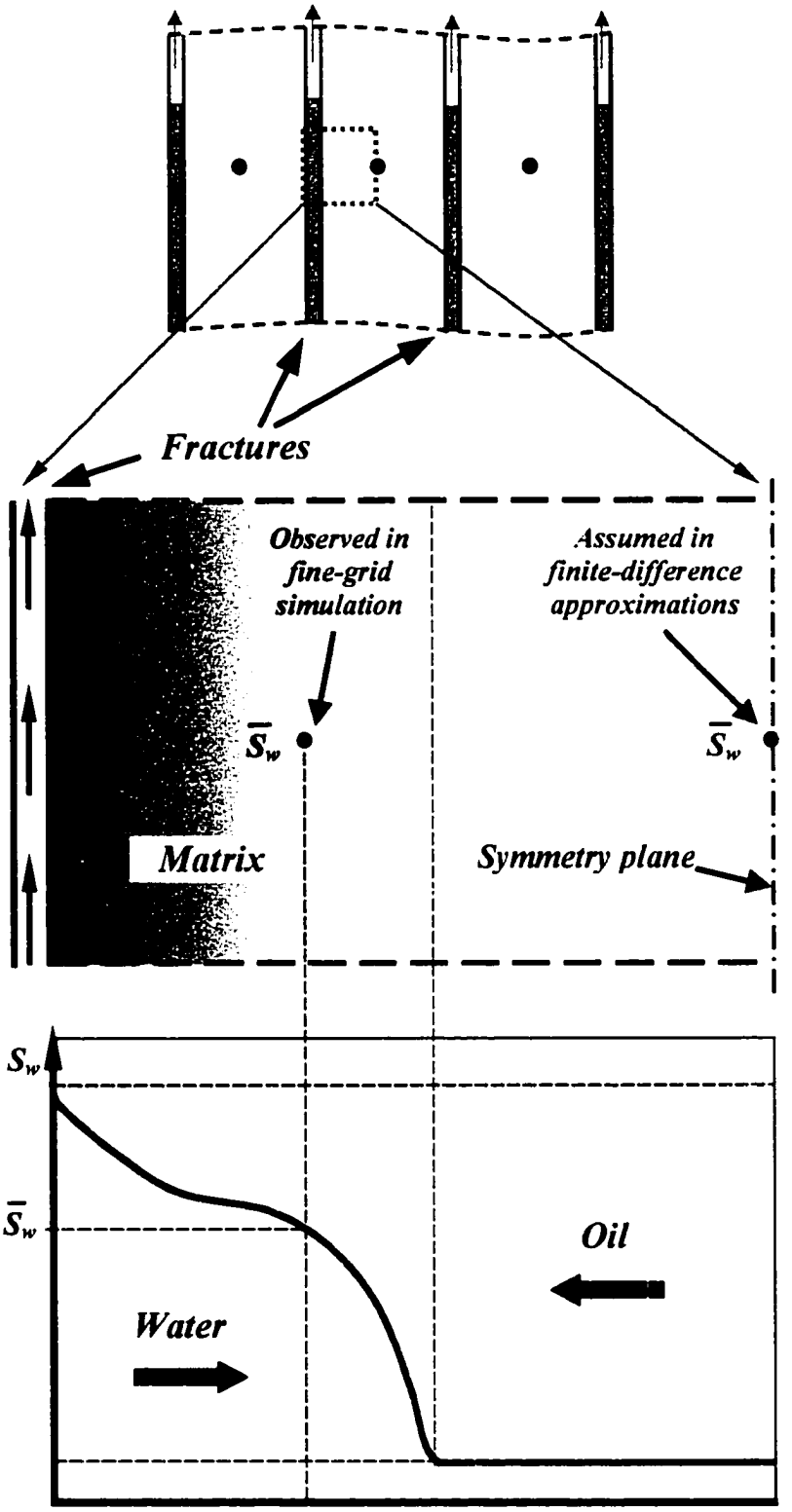

Fig. 2.4 – Finite-difference approximation using average water saturation located at the matrix-block center. In reality, this value moves from the matrix/fracture interface to the matrix-block center.

For single-phase interporosity flow, Najurieta[26] showed that de Swaan's analytical model results[25] were equivalent to numerical solutions provided by Kazemi,[18] which accounted for pressure transient effects by assuming nonsteady-state flow at the matrix/fracture interface. However, the approximate solutions presented by Najurieta oversimplify matrix geometries to strata and blocks. Similarly, Kazemi's model assumes horizontal fractures,[18] which is more applicable to multi-layered reservoirs than naturally fractured reservoirs.

For multiphase fluids, the pseudocapillary-pressure approach has been used to account for the nonuniform saturation within the matrix block.[29,42,55] However, this approach presents some difficulties because when the operating conditions are changed, a new set of dynamic pseudofunctions needs to be calculated.

An alternative technique to consider both pressure transient and saturation gradient effects on the interporosity flow is the subdomain approach.[44-46] However, the large number of computational nodes prevents this approach from being a viable alternative for full reservoir studies.

The procedure developed in this study is intended for implementation in existing simulators without significantly increasing computational work while representing pressure transient and saturation gradient effects on the interporosity flow as accurately as possible. In the following chapter, the conceptual model that is the basis for the proposed procedure is presented.

CHAPTER 3

CONCEPTUAL MODEL

The description of an appropriate conceptual model is the first step before the development of numerical models. A conceptual model that provides an interpretation of flow through a naturally fractured porous media is presented in this chapter before describing a new modeling approach for interporosity flow in naturally fractured reservoirs. However, it is not possible to represent all natural fracture network patterns and their fluid flow with a single model presented here. Therefore, examples of reservoirs where the proposed model is most likely applicable are also presented. Consequently, this is an essential chapter describing the considerations and applicability of the main contributions of this study, the details of which are given in subsequent chapters.

3.1 Model Abstraction

The necessity of specifying a conceptual model arises from the fact that all petroleum reservoirs to some degree are naturally fractured[2,5] and the inability of a single model to accurately simulate all possible types of fractured formations. Therefore, the first step is to define the type of fractured rock to be represented through the conceptual model.

The natural fractures in hydrocarbon-bearing formations may be classified into three broad groups referred to A, B, and C, considering the storage capacities of the matrix and

fracture systems.[2] Group A reservoir rocks are characterized by matrix blocks with large storage capacity and highly conductive fractures with small storage capacities. Matrix porosity may be well interconnected, allowing flow into the wellbore. Reservoirs may be simulated with a dual-porosity/dual-permeability model because matrix permeability can be significant. When the matrix permeability is low, dual-porosity models may be used for reservoir simulation.

Group B reservoirs have about equal storage capacity in the matrix and the fractures. When the matrix is a good reservoir rock (group B-I), a dual-porosity model may be used. For practical purposes, reservoirs where the porous matrix is not a good reservoir rock (group B-II) are equivalent to reservoirs from group C because almost all the storage capacity is owing to the fractures. In group C reservoirs, the fractures are both the storage and the flow path for hydrocarbons.

The present study focuses on group A and B reservoirs, according to the classification proposed by Aguilera,[2] where interporosity flow estimation is needed.

In the following, the conceptual model characteristics for single-phase and multiphase flow conditions are presented.

3.1.1 Single-Phase Flow

Consider a fractured rock sample in a single-phase fluid flow experiment where a pressure difference is applied in a certain direction as shown in **Fig. 3.1**. This rock sample is large enough to contain a representative number of distributed open fractures. As a consequence of the anisotropic nature of the fractured rock, the fluid velocity vectors are not necessarily parallel to the pressure gradient direction. Instead, they tend to align with

the main flow channels formed by the interconnected open fractures. Because the flow velocity vector is proportional to the pressure gradient and the proportionality factor involves the permeability tensor, the flow velocity may have a different direction than the pressure gradient in a fractured media.[56,57]

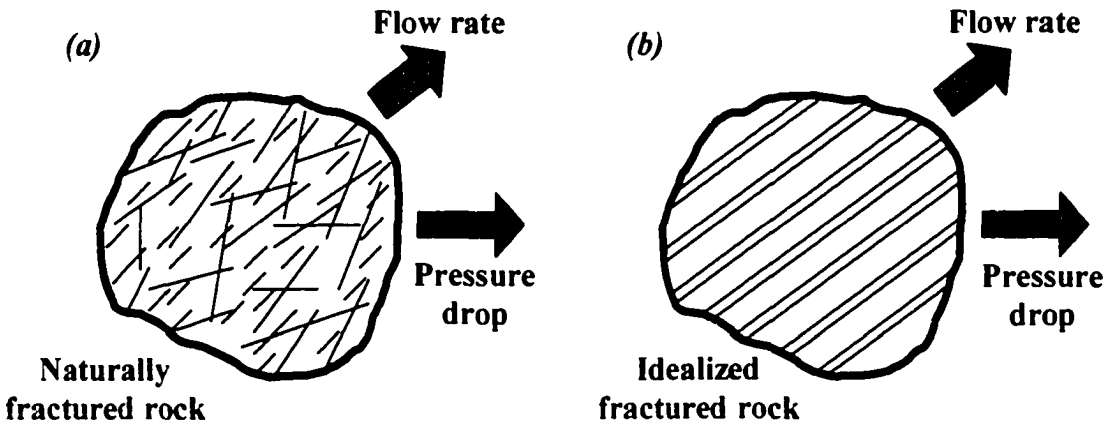

Fig. 3.1 – Representation of (*a*) naturally fractured and (*b*) idealized fractured rock sample in a flow experiment. Fluid flows in preferential paths conformed by interconnected fractures can be mathematically described by permeability tensors (After Penuela *et al.*[47])

Consequently, if the network of randomly distributed fractures is represented by a set of parallel and continuous open fractures such that the same flow velocity direction, flow rate and pressure gradients are maintained, the same permeability tensor for the mathematical description of the system would be obtained from the flow experiment. This representation of the fractured rock considers the matrix blocks as slabs of finite lateral extent where 1D interporosity flow occurs, as illustrated in **Fig. 3.2**. In this illustration, a set of interconnected fractures is substituted by an equivalent fracture with the same conducting capacity. Fluid flow in the surrounding matrix blocks is assumed to be primarily 1D flow.

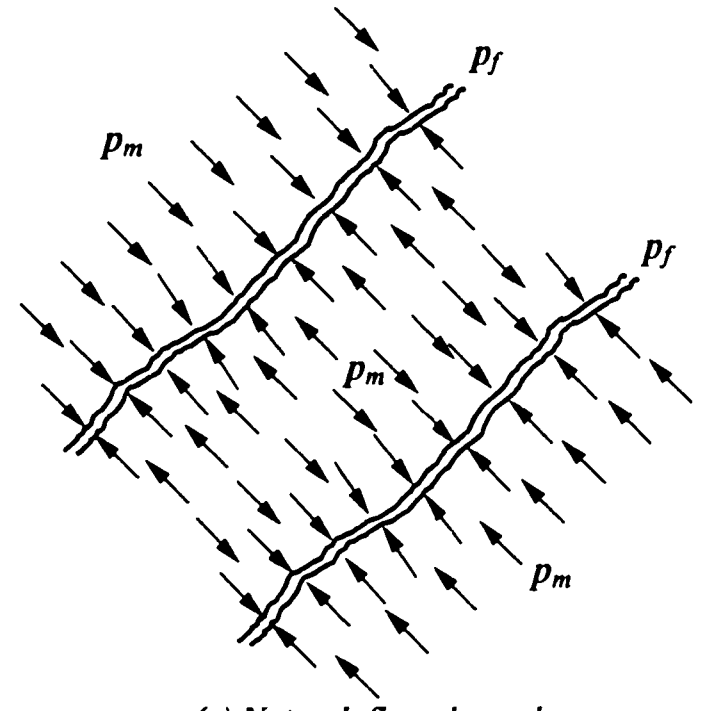

(a) Natural flow channels

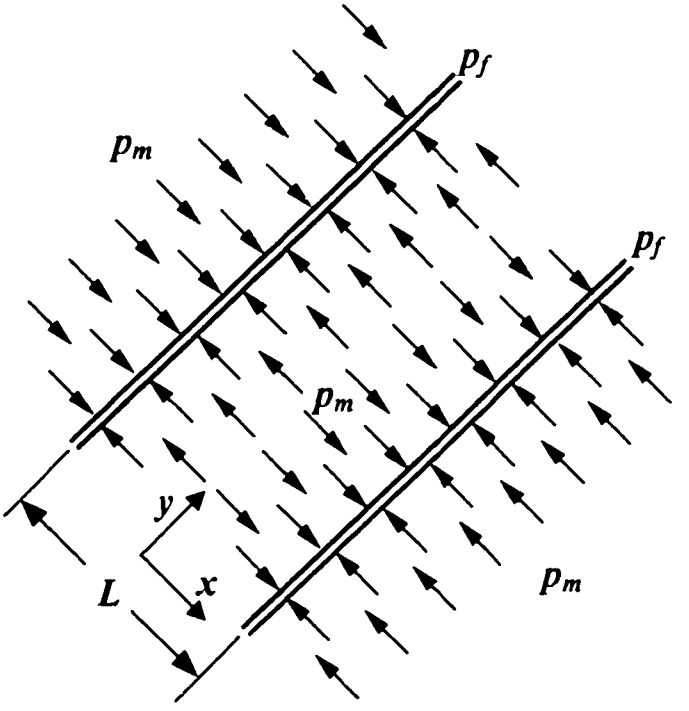

(b) Idealized flow channels

Fig. 3.2 – One-dimensional flow towards flow channels in (*a*) natural and (*b*) idealized matrix/fracture system (From Penuela *et al.*[27])

This conceptualization of a fractured media implies that once the main flow paths have been established through the primary flow channels (interconnected macro- and micro-fractures) in a rock, fluids in the matrix portion principally flow towards these flow channels. All matrix "blocks" within a control volume do not have uniform pressure gradients in all directions. Instead they tend to develop fluid flow perpendicular to the main flow channels rather than parallel to them. The traditional idealization of fractured media as a sugar-cube model is based on the assumption that the pressure gradient is the same in all directions within each matrix block in a gridblock as illustrated in **Fig. 3.3**.

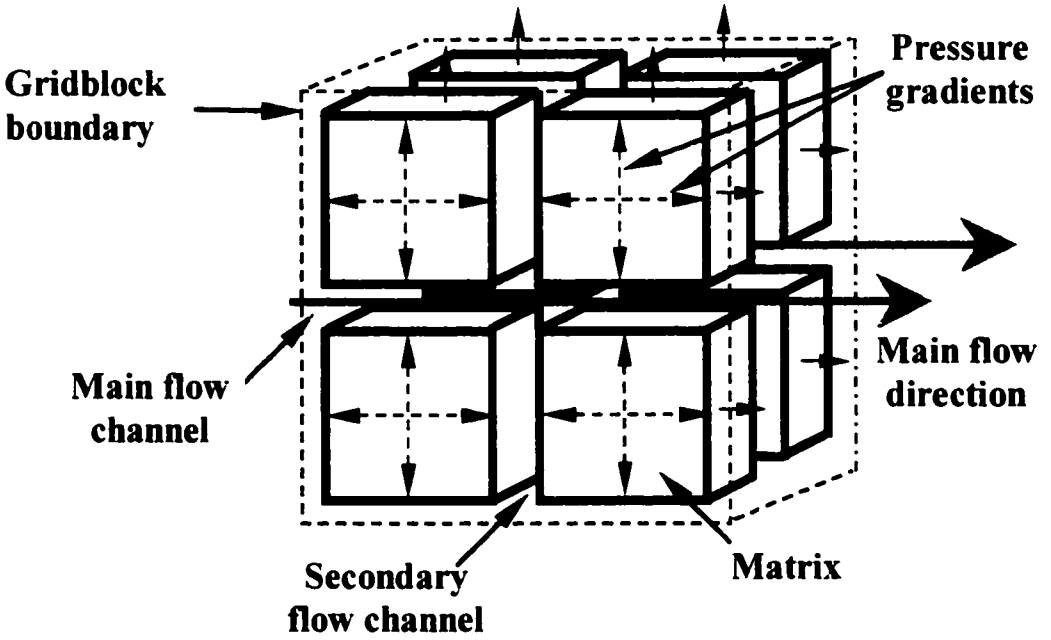

Fig. 3.3 – Sugar-cube idealization assumes equal pressure gradients perpendicular and parallel to main flow channels composed of interconnected open fractures.

This same assumption has been implicitly adopted in multiphase models that rely on the extension of the single-phase models when using geometric shape factors. The proposed model assumes that the pressure gradient is not the same in all directions

because the flow is normal to the flow conduits. However, this is not a limitation because the model can also handle the dual-permeability multi-dimensional flow (see Chapter 4).

3.1.2 Multiphase Flow

Similarly, consider a two-phase flow experiment where the water-wet rock sample shown in Fig. 3.1 is initially saturated with oil. Water flows along the fractures, which limit the matrix blocks as illustrated in **Fig. 3.4**. The water front may rapidly propagate along the high conductivity channel displacing the small oil volume contained within the fractures. This allows water to completely contact the oil-bearing matrix surface. Countercurrent imbibition then occurs. Water and oil flow through the same matrix/fracture interface but in opposite directions.[14] In other situations, the flow of injected water down the fracture will not be sufficiently fast enough and some cocurrent imbibition may occur.[13,58] Another situation can appear if water is injected at a very high pressure so that water will imbibe and oil will flow in the same direction (cocurrent imbibition) owing to the viscous pressure gradient. However, the proposed conceptual model for two-phase interporosity flow is based on the assumption of one-dimensional imbibition.

Water displaces oil from the matrix owing to capillary forces. This almost instantaneously increases the oil-phase pressure and reduces the water-phase pressure throughout the matrix block.[14] These two capillary-created pressure gradients have opposite signs, one driving water into the matrix and the other driving oil into the fracture. As more water is imbibed into the matrix, oil saturation is reduced. Although there is low oil saturation at the matrix/fracture interface, it is not necessarily equal to its residual value. These low saturations allow oil droplets to flow continuously to the

fracture generally through the wider regions of the pore space adjacent to the fracture. It will be shown in Chapter 6 that the value of the relative permeability to oil at the matrix/fracture interface is an important parameter that can control the imbibition process.

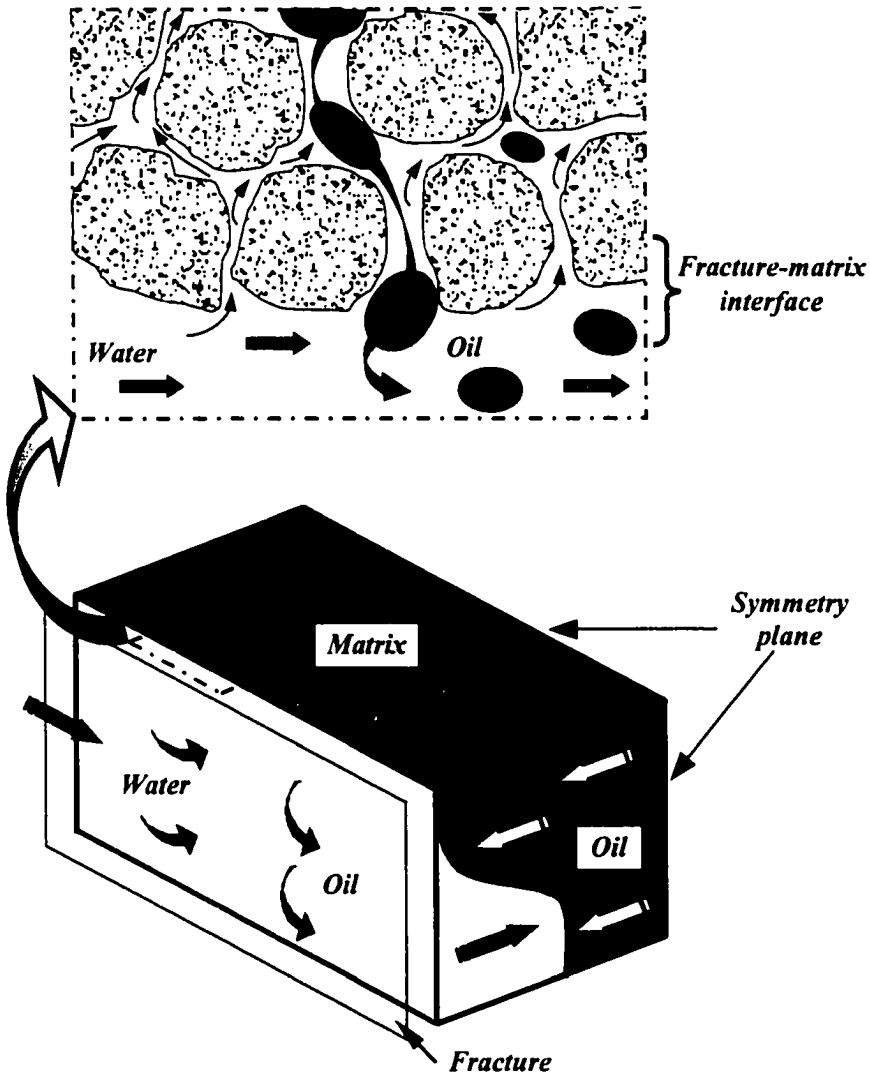

Fig. 3.4 – Countercurrent imbibition: One-dimensional flow of water into a water-wet matrix block reduces oil saturation to a critical value at the matrix/fracture interface. However, this reduced oil saturation allows oil droplets to flow into the fracture (From Penuela *et al.*[47])

As in the single-phase flow conceptualization, matrix "blocks" within a control volume do not have uniform pressure and saturation gradients in all directions. Instead they are prone to develop fluid flow perpendicular to the main flow conduits rather than parallel to them. Once the main flow paths have been established through the fracture sets in a rock, oil in the matrix portion will mainly flow towards the fractures. Reis and Cil[15] have suggested the use of 1D flow models for thin fractured formations where gravity segregation is minimal.

3.2 Model Applicability

In the literature, several reservoir and outcrop studies provide field cases where the proposed model would adequately represent anisotropy effects owing to naturally occurring fractures. In these cases, the conceptual model may be used by numerical simulators to more accurately predict hydrocarbon recovery through pressure depletion and waterflooding.

There are numerous reservoirs that contain fractures with a preferred orientation, which causes the effective medium to be anisotropic.[2,59] A study of the past and present state of stresses provides insight about the mechanisms that formed, modified and currently maintain these fractures as primary flow paths. It has been found that large differential stresses reduce the tendency of fractures to intersect, causing fracture traces to extend linearly and overlap for long distances.[6] This fracture pattern will yield fluid flow that can be described by permeability tensors (see Fig. 3.1b and 3.2).

When the differential regional stress is small, fractures tend to interact and connect, developing a fracture network with a pattern difficult to describe with simple geometry

(Fig. 3.1a) such as a set of cubes or slabs. However, geological information about the genesis of fractures and the present state of stresses indicate which fractures or parts of fracture systems are hydraulically important. When shorter and discontinuous fractures intersect longer and more continuous fractures, the shorter fracture set was created after the longer set. If a fracture crosses the other, the older set was closed at the time the younger set formed.[6]

Similarly, the state of stress may be used to infer fractures characteristics because the stresses can be a controlling factor during fracture formation. It is recognized that fractures that parallel the maximum compressive stress tend to be open while those perpendicular to this direction tend to be closed. Perez *et al.*[60,61] applied this principle to identify which fracture sets were likely to be open. In their study, the maximum horizontal stress in the field was first estimated from borehole ellipticity measurements, and fracture strike was obtained from Formation MicroScanner (FMS) logs. With the preliminary estimate of fracture orientation, they designed a seismic survey to perform an amplitude-variation-with-offset (AVO) analysis of 2D and 3D *P*-wave data. They found that conclusions from the AVO analysis were consistent with the results obtained previously from borehole measurements and *P-S* converted wave studies.[62] In **Fig. 3.5** a map view of the fracture orientation obtained from *P-S* data validated through AVO analysis is shown.

Assume that a map similar to Fig. 3.5 is available for a particular reservoir study. Once fractures that are hydraulically significant conductors have been identified, characterized and mapped, they need to be represented in a numerical simulator. If an equivalent continuum simulation model is used, the volume-averaged behavior of many

fractures needs to be determined. In the case of fracture orientation, which is required for permeability tensor estimation,[59,63] a parallel Cartesian grid may be overlaid on this map to encompass a set of parallel fractures as illustrated in **Fig. 3.6**. The resultant permeability tensor may be then computed by multiplying a normalized permeability tensor obtained from the fracture orientation and a permeability scalar, which is function of fracture density and interconnectivity. These tensors then are numerically calibrated by history matching well tests in the region under investigation. The reader is referred to Avila *et al.*[63] for details of this technique.

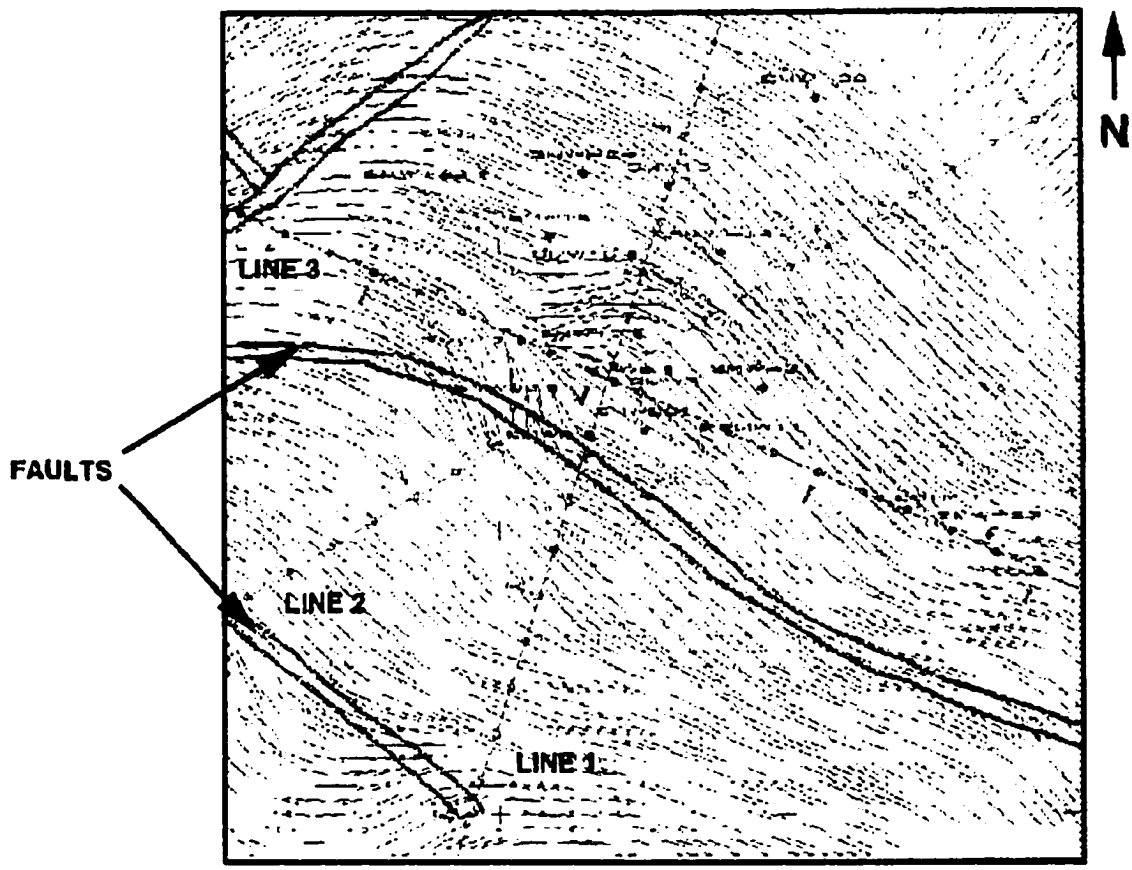

Fig. 3.5 – When open natural fractures are present in sets of local parallel rock discontinuities, a single permeability tensor needs to be computed at each point in the reservoir for the discrete network simulation model (From Perez *et al.*[60])

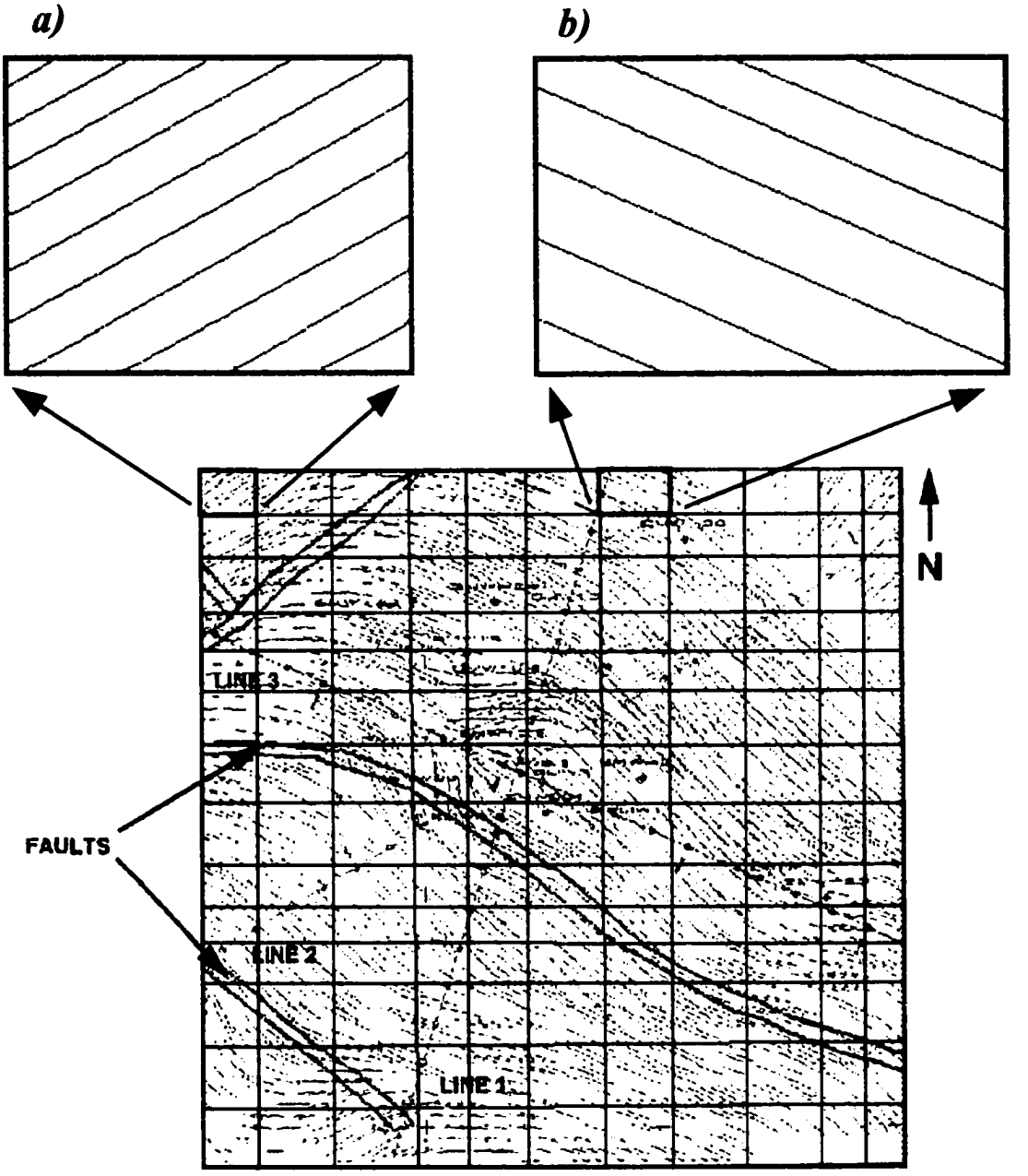

Fig. 3.6 – After identifying representative rock volumes (gridblocks), volume-averaged rock properties may be computed for the equivalent continuum simulation model. A single permeability tensor needs to be calculated in each gridblock using the average fracture orientation and fracture conductivity. For instance, even though fractures in gridblocks (*a*) and (*b*) may have the same absolute permeability, each gridblock needs a different permeability tensor because fractures have different orientation.

3.3 Interporosity Flow Modeling in Linear Matrix/Fracture Systems

The basic conclusion from the previous discussion is that bilinear flow modeling may be sufficient to represent the complexity presented by some naturally fractured reservoirs. One linear flow is along the highly conductive flow channels and the other perpendicular to them. Linear flow in the fracture system may be modeled with the diffusivity equation expressed by Eq. 2.1. In subsequent chapters, a new approach is presented and validated for single-phase, miscible and immiscible two-phase systems for 1D interporosity flow.

An important characteristic of the proposed conceptual model is that it can be incorporated in either a deterministic or stochastic framework. An example of the implementation of the present interporosity flow model in a dual-porosity, dual-permeability reservoir simulator is provided in Chapter 7, where a simulation run with the proposed model is compared with traditional model results.

CHAPTER 4

FLOW CORRECTION FACTOR IN SINGLE-PHASE SYSTEMS

An interporosity flow rate model using a variable shape factor for a single-phase system is derived in this chapter. The variable shape factor is introduced as a time-dependent flow correction factor that accounts for the pressure transient effects in the interporosity flow rate. Derivation details of the analytic expression for the flow correction factor are presented in Appendix A.

Dual-porosity model simulation of naturally fractured reservoirs typically assumes there are two continua, matrix and fractures, within each gridblock. The flow equations are written for each system with a matrix/fracture transfer function to relate the loss or gain of matrix fluids to or from the fracture. For single-phase fluid flowing through an interconnected fracture system, the following governing equation applies:[17]

$$\nabla \cdot \left[\frac{\bar{\bar{k}}_f}{\mu_f B_f} \left(\nabla p_f - \rho_f g \nabla D \right) \right] = \frac{\partial}{\partial t} \left(\frac{\phi_f}{B_f} \right) - \tilde{q} \qquad \text{4.1}$$

where the fluid transfer rate per unit volume of rock, $\tilde{q}$, is commonly calculated as a function of the pressure difference between the matrix and fracture systems, matrix flow capacity, and matrix geometry considered through a constant shape factor. For the matrix system, Eq. 4.1 is applied using matrix rock and fluid properties and a fluid transfer rate with opposite sign.

4.1 Flow Correction Factor Derivation

In fractured reservoirs that may be represented by the conceptual model described in Chapter 3, the interporosity flow is one-dimensional. Assume that the flow rate at the matrix/fracture interface may be computed by means of Darcy's law as follows:

$$q = -A\frac{k_m}{\mu}\frac{\partial \Phi}{\partial x} \quad \text{.....4.2}$$

where k_m is the absolute permeability at the matrix/fracture interface, μ is the average fluid viscosity and Φ is the flow potential. The total fracture surface area, A, is calculated depending on the geometry of the fracture. For fractures with surfaces that can be approximately represented as parallel plates, the total fracture area available for interporosity flow is given by:

$$A = 2\frac{\phi_f}{w_f}V \quad \text{.....4.3}$$

where ϕ_f is the average fracture porosity computed in the control volume V, and w_f is the average fracture width (aperture).

Neglecting gravity effects for simplification, Eq. 4.2 can be approximated in a finite difference form as:

$$q = -A\frac{k_m}{\mu}\frac{\Delta p}{\Delta x} \quad \text{.....4.4.}$$

Consider that the pressure drop, Δp, responsible for the interporosity flow rate, q, can be calculated as the difference between the matrix and fracture fluid average pressures. Further, assume that the two average pressure values are separated by a distance equal to

half the fracture spacing. Therefore, it is necessary to introduce a flow correction factor, F_c, into Eq. 4.4 as follows in order to correct the errors caused by these assumptions:

$$q = F_c A \frac{k_m}{\mu} \frac{\left(\overline{p}_m - p_f\right)}{\frac{L}{2}} \quad \text{.....4.5.}$$

This flow correction factor is similar to the shape factor used in interporosity flow calculations for current dual-porosity modeling. While F_c is dependent on the flow geometry as are the shape factors, it is independent of the matrix block size. In addition, F_c varies with time, and for single-phase fluids its value converges to the steady-state shape factor value reported in previous studies.

To illustrate this point, numerical experiments were performed on a cubic shape matrix block in contact with a fracture along one side. Because of symmetry, only half of the matrix-fracture system was simulated as described in **Fig. 4.1**.

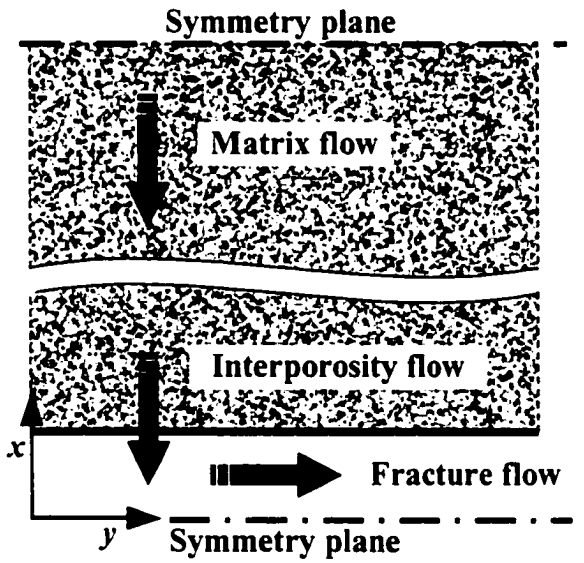

Fig. 4.1 – Representation of the numerically-modeled idealized fracture-matrix system (From Penuela *et al.*[27])

Reservoir rock and fluid data are similar to those described by Lim and Aziz.[31] **Table 4.1** presents data used to obtain both numerical and analytical solutions to this 1D flow problem. **Figure 4.2** shows the 20×1×1 grid and reports x-direction gridblock sizes employed for the numerical simulation ($\Delta y = \Delta z = 10$ ft).

TABLE 4.1 – DATA USED IN NUMERICAL EXPERIMENTS OF A SINGLE-PHASE FLUID (FROM PENUELA *ET AL.*[27])

Matrix porosity, ϕ_m, *fraction*	0.0005
Matrix permeability, k_m, md	0.001
Total compressibility, c_t, psi^{-1}	3.5×10^{-6}
Fluid viscosity, μ, cp	1.0
Initial pressure, p_i, psia	1000
Fracture pressure, p_f, psia	500
Fracture spacing, L, ft	10
Half fracture surface area, A_o, ft^2	100

Pressure profiles inside the matrix block for different times are plotted in **Fig. 4.3**. The average matrix fluid pressure has been indicated as a dotted horizontal line that intersects with the pressure curve from which the volume-weighted average pressure value was computed. **Figure 4.4** shows the average matrix pressure and the location of this value as a function of time. It is observed from Figs. 4.3 and 4.4 that the distance between the location of the average pressure, Δx, increases from zero at the fracture surface up to a steady-state value that is less than the assumed half fracture spacing. Therefore, the purpose of F_c in the interporosity flow rate (Eq. 4.5) is to correct for the actual location of the average pressure in the matrix.

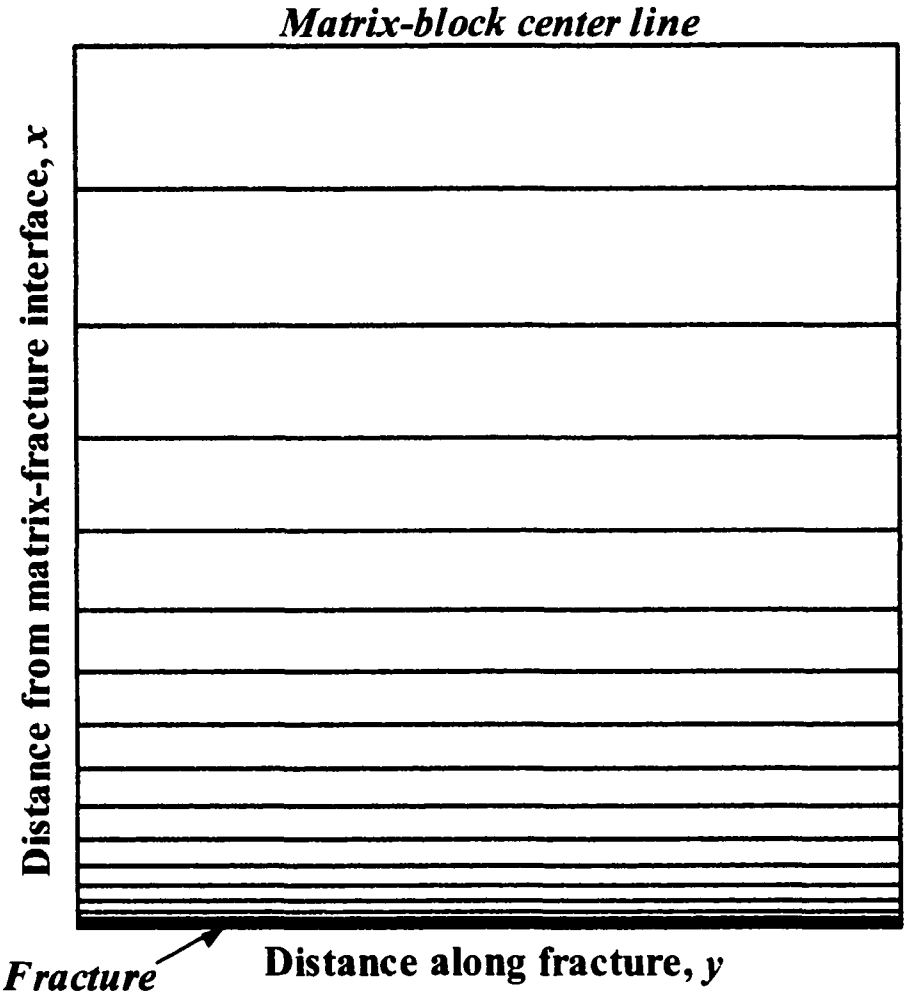

Fig. 4.2 – Schematic grid system discretization of one-half matrix block into gridblocks for numerical solution. The fracture is the first gridblock. Gridblock Δx values are 0.002, 0.004, 0.007, 0.012, 0.02, 0.04, 0.06, 0.09, 0.12, 0.15, 0.18, 0.21, 0.25, 0.3, 0.36, 0.44, 0.53, 0.64, 0.77, 0.815 ft (From Penuela *et al.*[27]).

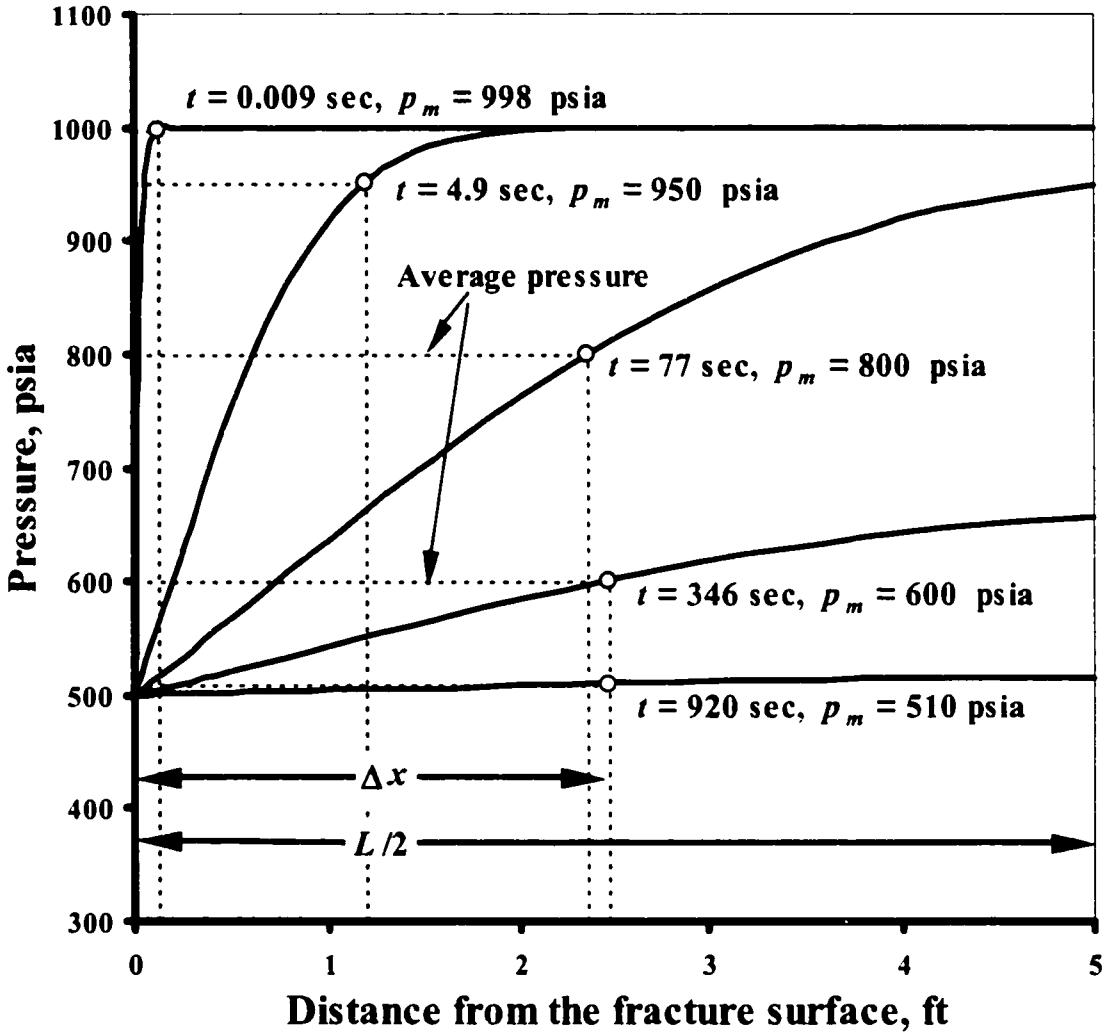

Fig. 4.3 – Pressure profiles and average pressure locations for 1D numerical simulation with properties given in Table 4.1 (From Penuela *et al.*[27])

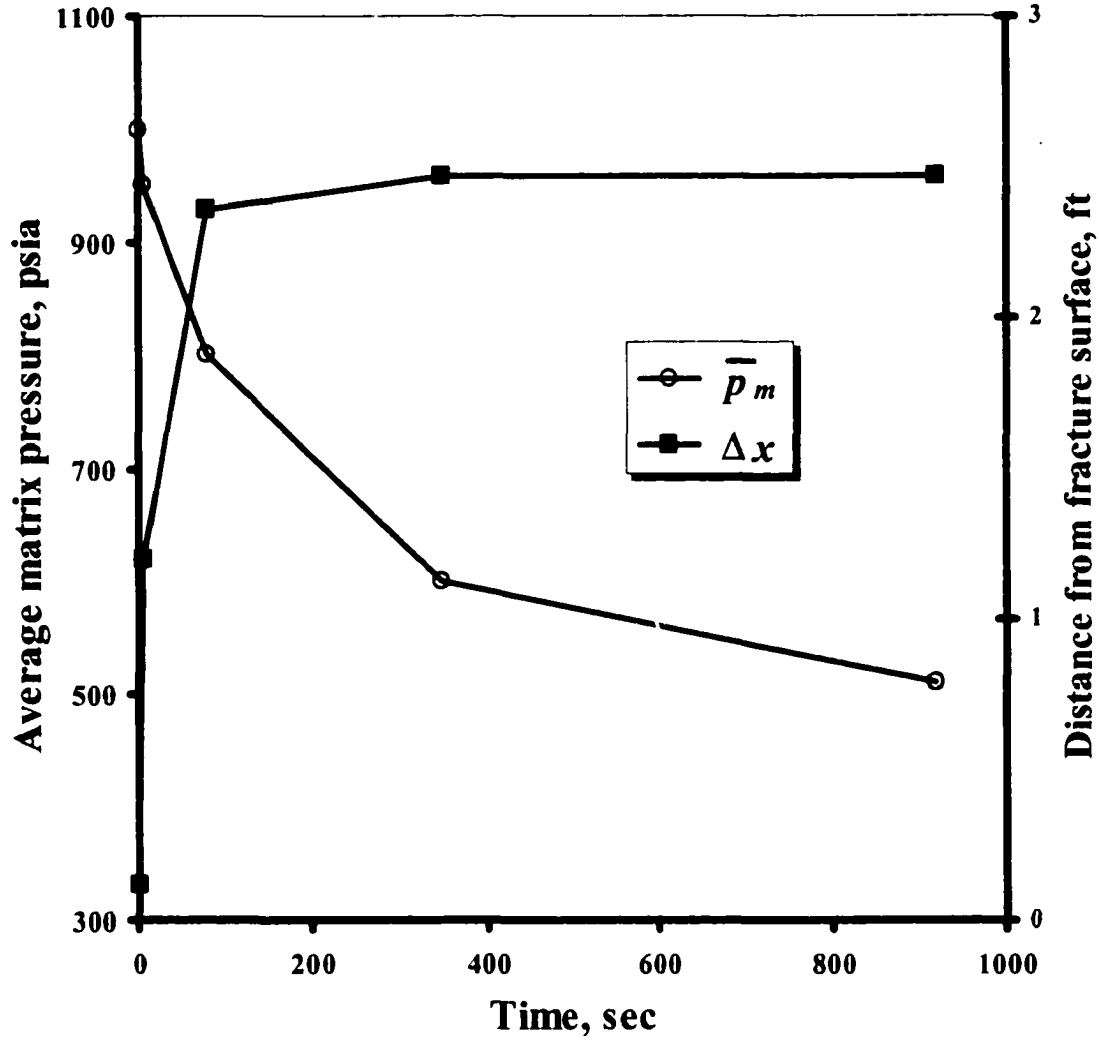

Fig. 4.4 – Average matrix pressure and its location on the pressure profile curve (Fig. 4.3) as functions of time. Note the distance converges to a steady-state value (From Penuela *et al.*[27])

The analytical solution (see Appendix A) of the average pressure difference and interporosity flow rate in this 1D flow problem were used to compute F_c, shown in **Fig. 4.5**.

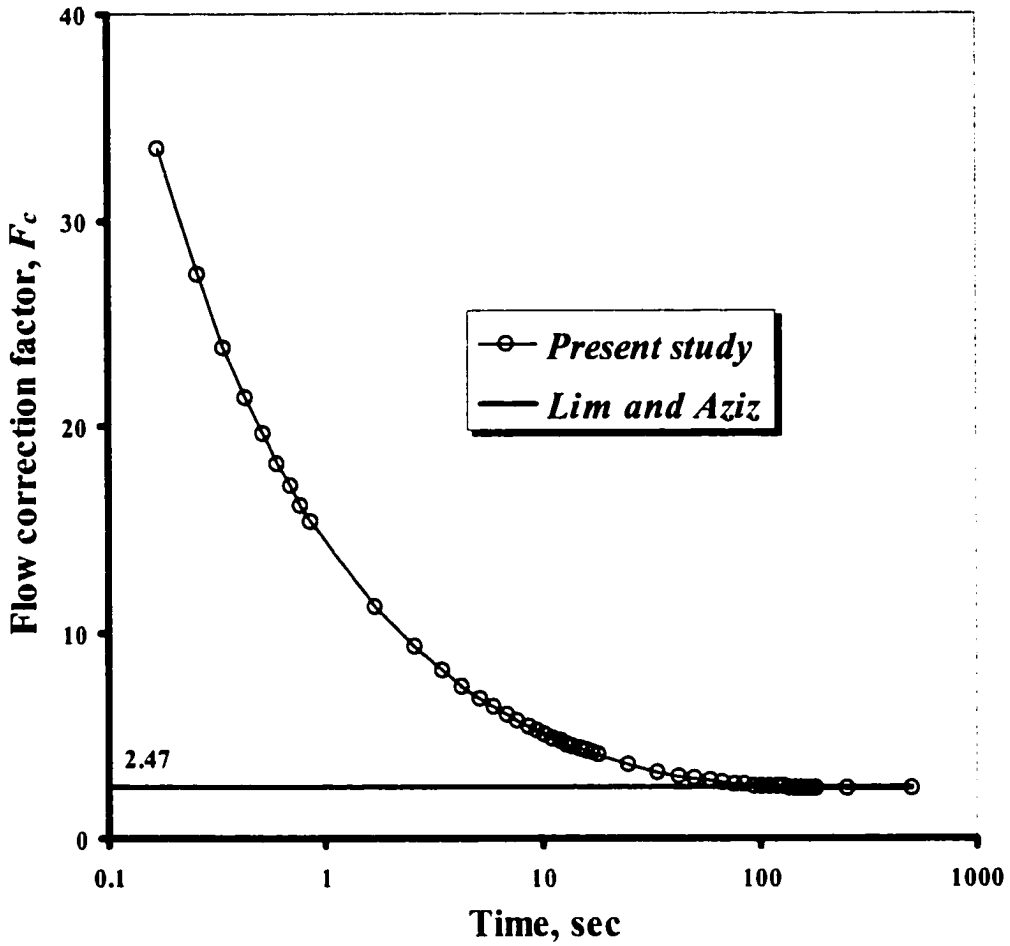

Fig. 4.5 – Comparison of flow correction factors computed from the analytic solution and from the constant shape factor reported by Lim and Aziz[31] (From Penuela *et al.*[27])

Convergence to the shape factor obtained by Lim and Aziz[31] for one set of parallel fractures was observed. Thus, these numerical studies indicate:

$$\lim_{t \to \infty} \frac{4F_c(t)}{L^2} = \sigma \qquad \text{4.6}$$

where L is the fracture spacing for one set of parallel fractures and σ is the corresponding shape factor for that matrix geometry.

The input data presented in Table 4.1 were used along with several values for matrix permeability and block size to determine their effect on F_c (**Fig. 4.6**). Rapid convergence of F_c to the steady-state value is observed in small blocks with high matrix permeability. As block size increases (larger fracture spacing) and matrix permeability (or fluid mobility) decreases, time dependency of F_c becomes important.

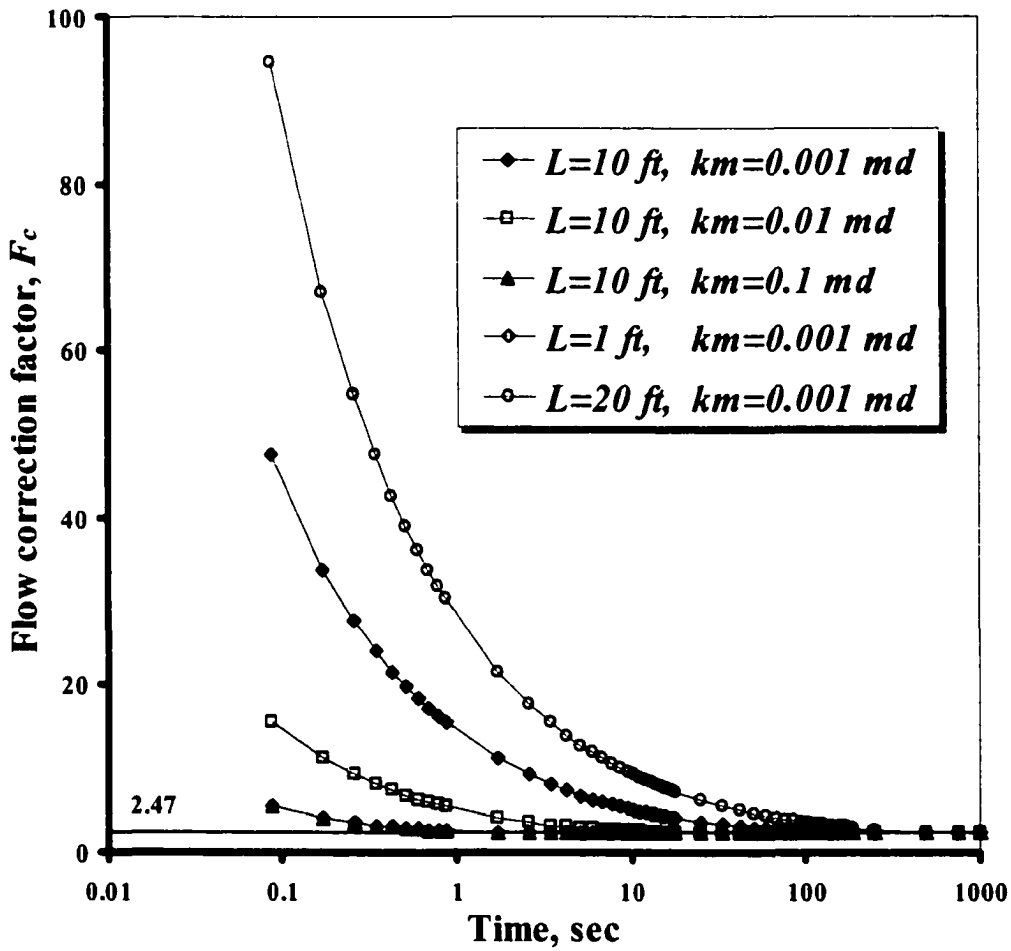

Fig. 4.6 – Variation of flow correction factor for different fracture spacing and average matrix permeability (From Penuela *et al.*[27])

A generalized curve for F_c that reflects this time dependency is obtained by defining a convenient dimensionless time as follows:

$$t_D = \frac{k_m}{\phi_m \mu c_t L^2} t \quad \text{.....4.7.}$$

The data obtained for Fig. 4.6 was replotted using the t_D definition given by Eq. 4.7 and a single curve was obtained (**Fig. 4.7**). An equation of the form:

$$F_c = C_1 \left(1 + \frac{C_2}{t_D}\right)^{C_3} \quad \text{.....4.8}$$

was used to fit this curve. The asymptotic behavior should be the analytical result of Lim and Aziz, thus, C_1 was taken to be equal to 2.47. The remaining constant values C_2 = 0.0133 and C_3 = 0.5 were obtained by regression analysis (**Fig. 4.8**) with a coefficient of regression R^2=0.9992. The solid line curve in Figs. 4.6 through 4.8 is the Eq. 4.8 correlation.

4.2 Parametric Study

A parametric study was carried out to investigate the applicability of the present approach in multi-dimensional flow in dual-permeability media.

The proposed interporosity flow equation, Eq. 4.5, indicates that the main driving force for fluid flow is the matrix pressure gradient. This pressure gradient may or may not be uniform depending on either the matrix geometry or the permeability ratio (or heterogeneity degree[64]):

$$\omega_K = \frac{k_m}{k_f} \quad \text{.....4.9.}$$

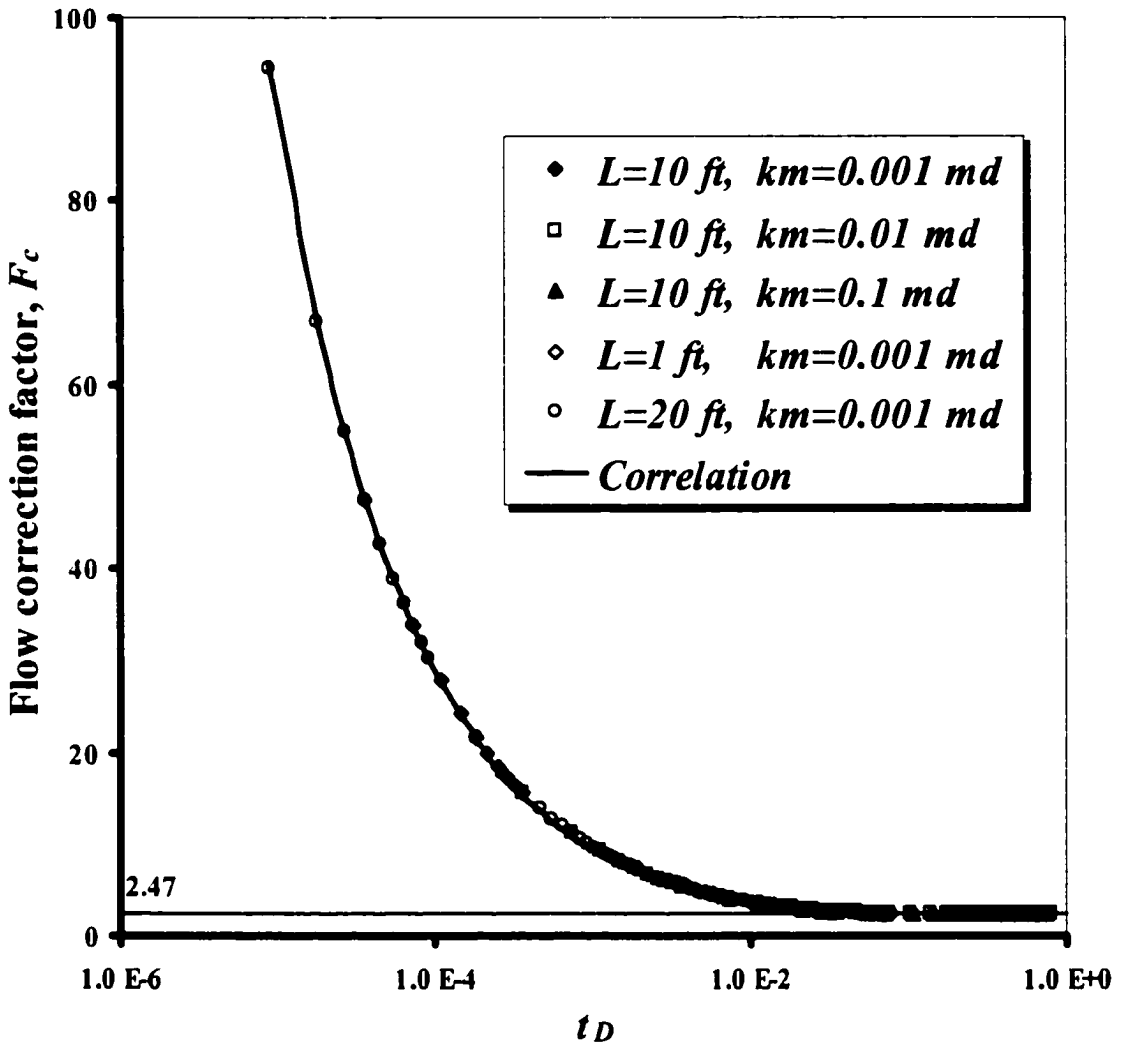

Fig. 4.7 – Flow correction factor curve as function of dimensionless time. The steady-state F_c approaches to a constant value computed from Lim and Aziz (From Penuela *et al.*[27])

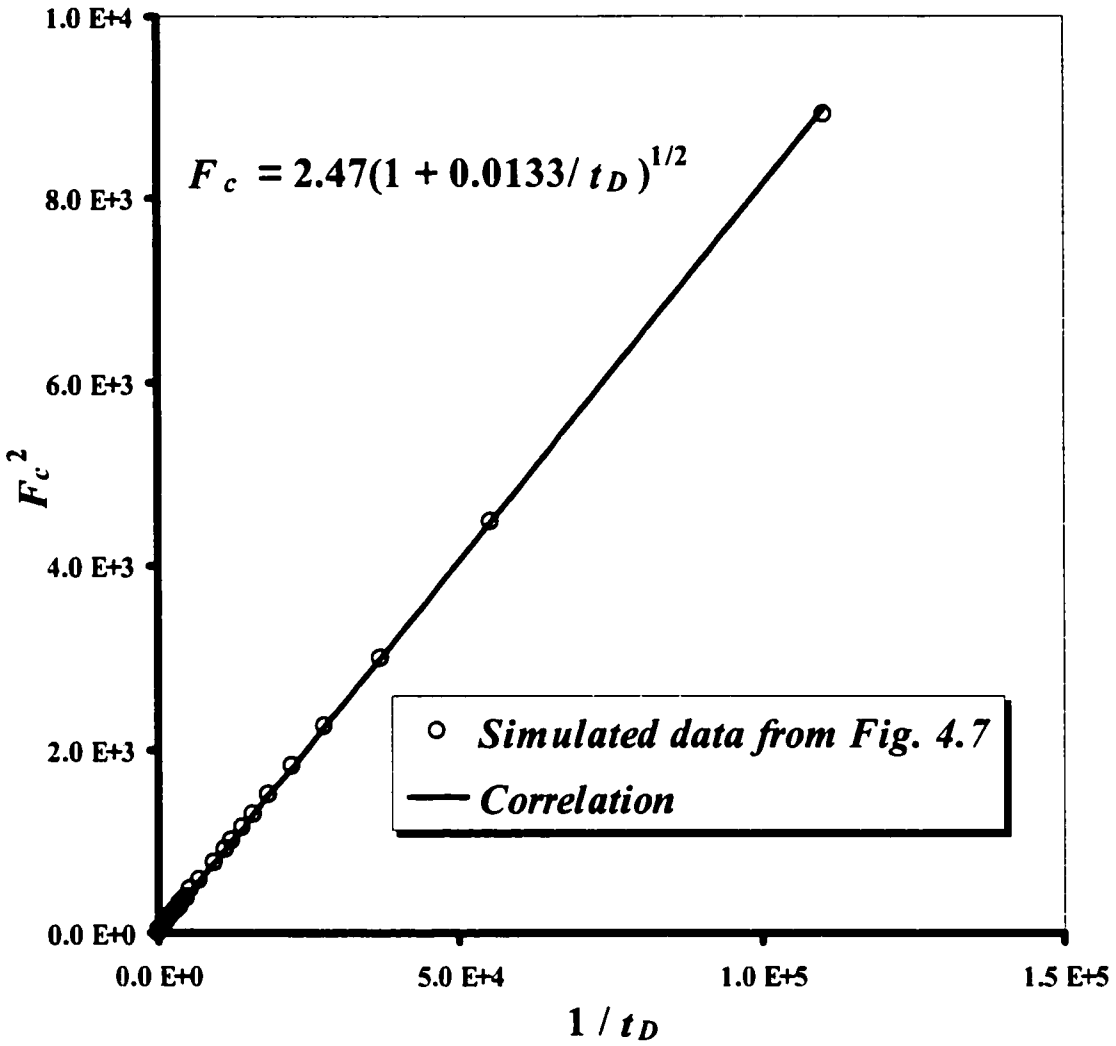

Fig. 4.8 – Generalized correlation for the flow correction factor (After Penuela *et al.*[27])

Figure 4.9 depicts fluid velocity vectors in the matrix for different pressure gradients. **Figure 4.9a** represents the matrix flow in a dual-porosity model. The inherent assumption is that the fracture is highly conductive compared with the matrix (the system has a very low permeability ratio,[64] $\omega_K << 1$) and 1D flow perpendicular to the fracture surface is observed.

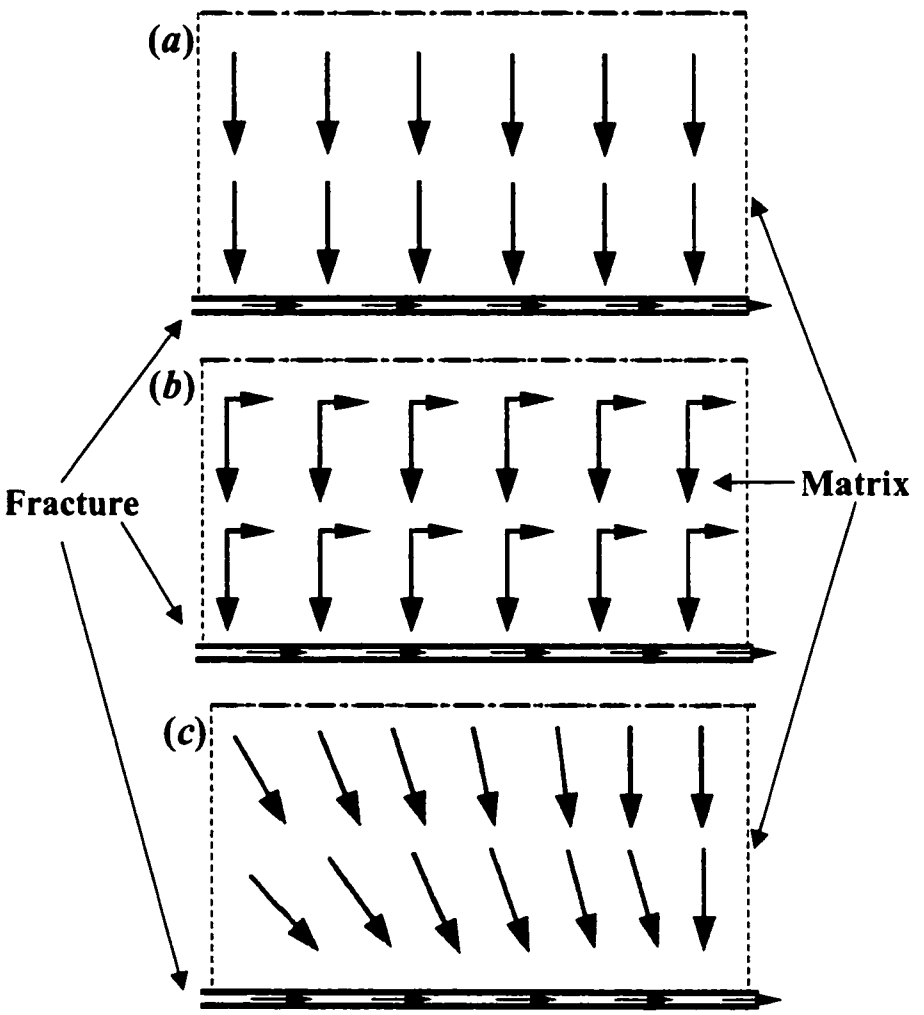

Fig. 4.9 – Different types of matrix flow. Case (*a*): Dual-porosity model. Case (*b*): Dual-permeability model. Case (c): Fluid velocity vectors observed at high permeability ratio (From Penuela *et al.*[27])

Figure 4.9b shows behavior observed in typical cases of dual-permeability media because either the matrix is also fluid conductive or the fracture has low fluid conductivity. This case shows 2D flow where the main velocity vector components are perpendicular to the fracture surface. **Figure 4.9c** is a special case of the dual-permeability media flow pattern shown in Fig. 4.9b. Note that the velocity vectors display a 2D flow behavior with principal components parallel to the fracture. This regime was observed in a few of the parametric studies described below.

To investigate the effect of ω_K on the flow correction factor, a parametric study was performed using the fluid and rock data reported by Thomas *et al.*[29] and summarized in **Table 4.2**.

TABLE 4.2 – DATA USED IN THE PARAMETRIC STUDY (AFTER PENUELA *ET AL.*[27])

Matrix porosity, ϕ_m, *fraction*	0.003
Matrix permeability, k_m, md	1.0
Matrix compressibility, c_m, psi^{-1}	3.5×10^{-6}
Fracture compressibility, c_f, psi^{-1}	3.5×10^{-6}
Connate water saturation, S_{wc}, %	20
Oil density, ρ_o, lb/ft^3	51.14
Oil viscosity at p_b, μ_o, cp	0.21
Slope of μ_o above p_b, $d\mu_o/dp$, cp/psi	1.72×10^{-5}
Oil formation volume factor at p_b, B_o, RB/STB	1.8540
Slope of B_o above p_b, dB_o/dp, RB/STB/psi	-4.0×10^{-5}
Initial pressure, p_i, psia	5575
Fracture pressure, p_f, psia	5565
Bubble point pressure, p_b, psia	5560
Fracture spacing, L, ft	10
Half fracture surface area, A_σ, ft^2	100

Values shown in **Table 4.3** for fracture porosity and fracture permeability were calculated assuming the parallel plate model to achieve different permeability ratios. A 2D numerical simulation was performed using a modified version of the BOAST-VHS program.[65] The grid chosen was 20×20×1 which was equally divided in the y-direction (Δy=0.5 ft) and had dimensions in the x-direction as indicated in Fig. 4.2. Because of symmetry, only half of the cubic fracture-matrix system was modeled. To simulate the fracture, gridblock properties from Table 4.3 were used in blocks, indexed (1,1) to (1,20). The single-phase flow across the fracture was simulated by placing a fictitious well at block (1,1) with a constant fluid injection rate and a well at block (1,20) producing fluid at constant bottomhole pressure ($p_{wf}= p_f$). The interporosity rate was calculated as the rate difference between the injection and production ports.

TABLE 4.3 – FRACTURE PROPERTIES USED IN THE PARAMETRIC STUDY (AFTER PENUELA *ET AL.*[27])

Fracture width	Bulk properties		Gridblock properties		Permeability ratio
w_f ft	ϕ_f %	k_f Darcys	ϕ_2 %	k_2 Darcys	ω_K
0.000108	0.00108	0.01	2.71	2.5	0.1
0.000503	0.00503	1	12.58	250	0.001
0.002336	0.02336	100	58.40	25000	0.00001

Numerical solutions were compared with the analytic solution (Eq. A-8), which represents the ideal behavior of a dual-porosity medium where the fracture is infinitely conductive ($\omega_K \approx 0$). The effects of having different values for ω_K are shown in **Figs. 4.10-4.12**. **Figure 4.10** shows pressure differences between the fracture and average

matrix pressure as a function of dimensionless time (Eq. 4.7). The average matrix pressure was calculated as the arithmetic mean of the block pressures for all blocks except for those indexed by (1,1) through (1,20).

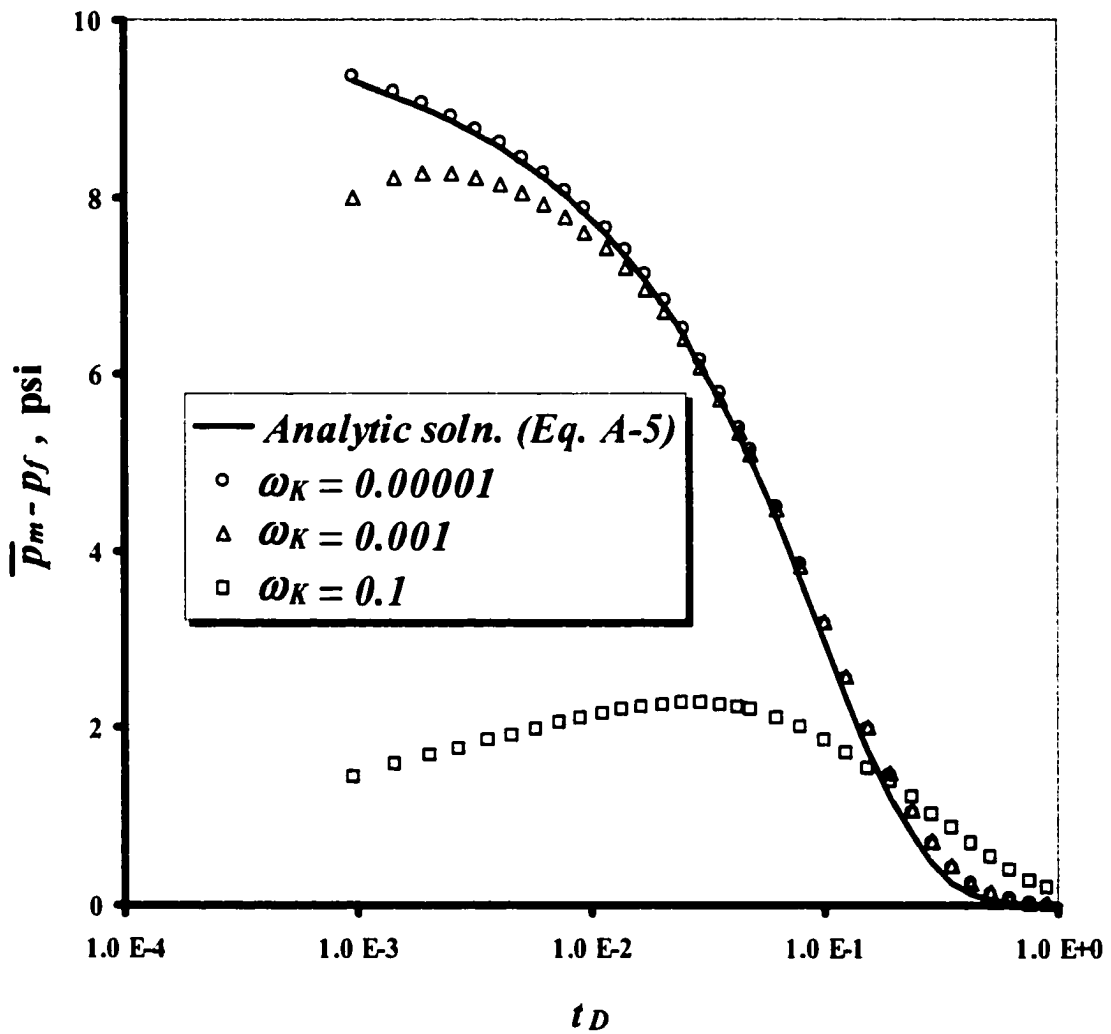

Fig. 4.10 – Pressure differences at different permeability ratios. Analytic solution represents an ideal dual-porosity system (From Penuela *et al.*[27])

At low fracture permeability, the fracture is not able to function as a high conductivity channel and consequently 2D flow occurs in the matrix. This is the case represented by **Fig. 4.9c** and is also shown in **Fig. 4.11**. At high ω_K, the initial pressure difference increases while fluids fill the fracture (fracture pressurization). Fluids are then produced simultaneously from the matrix and the fracture. **Figure 4.12** shows that small values of the permeability ratio lead to large values of the interporosity flow rate while large values for ω_K lead to smaller interporosity flow rates. The limiting case is $\omega_K = 1$, where matrix and fracture have the same fluid conductive capacity. In this specific case, the average pressures in both media would be the same and thus the interporosity flow rate would drop to zero. Even though the assumption of 1D flow is violated and interporosity flow rate is reduced at high ω_K, the flow correction factor shows small changes (**Fig. 4.13**). Therefore, the interporosity flow equation is applicable to both dual-porosity and dual-permeability situations.

4.3 Discussion

The interporosity flow equation developed in this work offers several advantages. The first advantage is related to the physical meaning expressed in the proposed interporosity flow equation. Assume that fracture surfaces can be approximated by parallel plates. Hence, the fluid transfer rate per unit volume of rock can be calculated by substituting Eq. 10 into Eq. 12 to obtain the following equation:

$$\tilde{q} = 4F_c \frac{\phi_f}{w_f} \frac{k_m}{\mu} \frac{\left(\overline{p}_m - p_f\right)}{L} \qquad \text{.....4.10.}$$

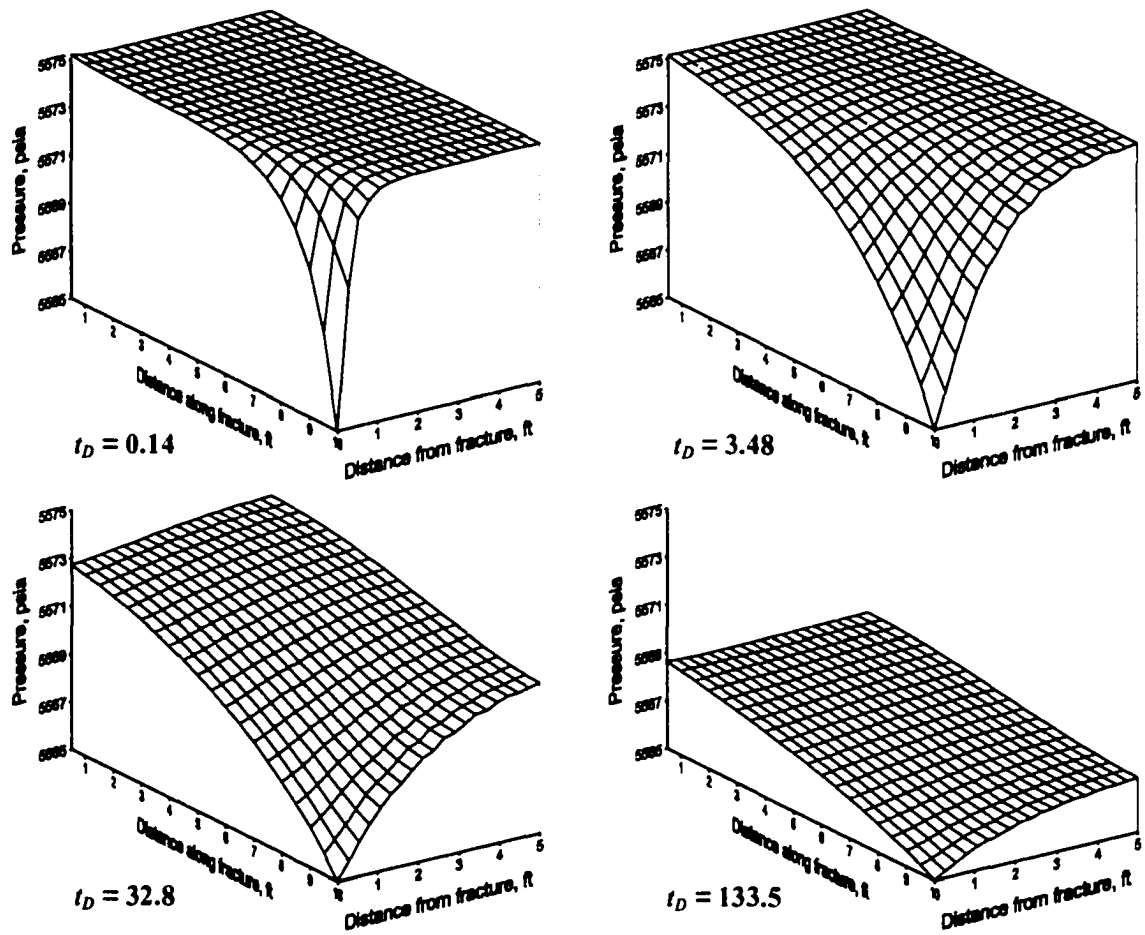

Fig. 4.11 Two-dimensional flow experienced at high permeability ratio. This pressure distribution corresponds to ω_K=0.1 (From Penuela *et al.*[27])

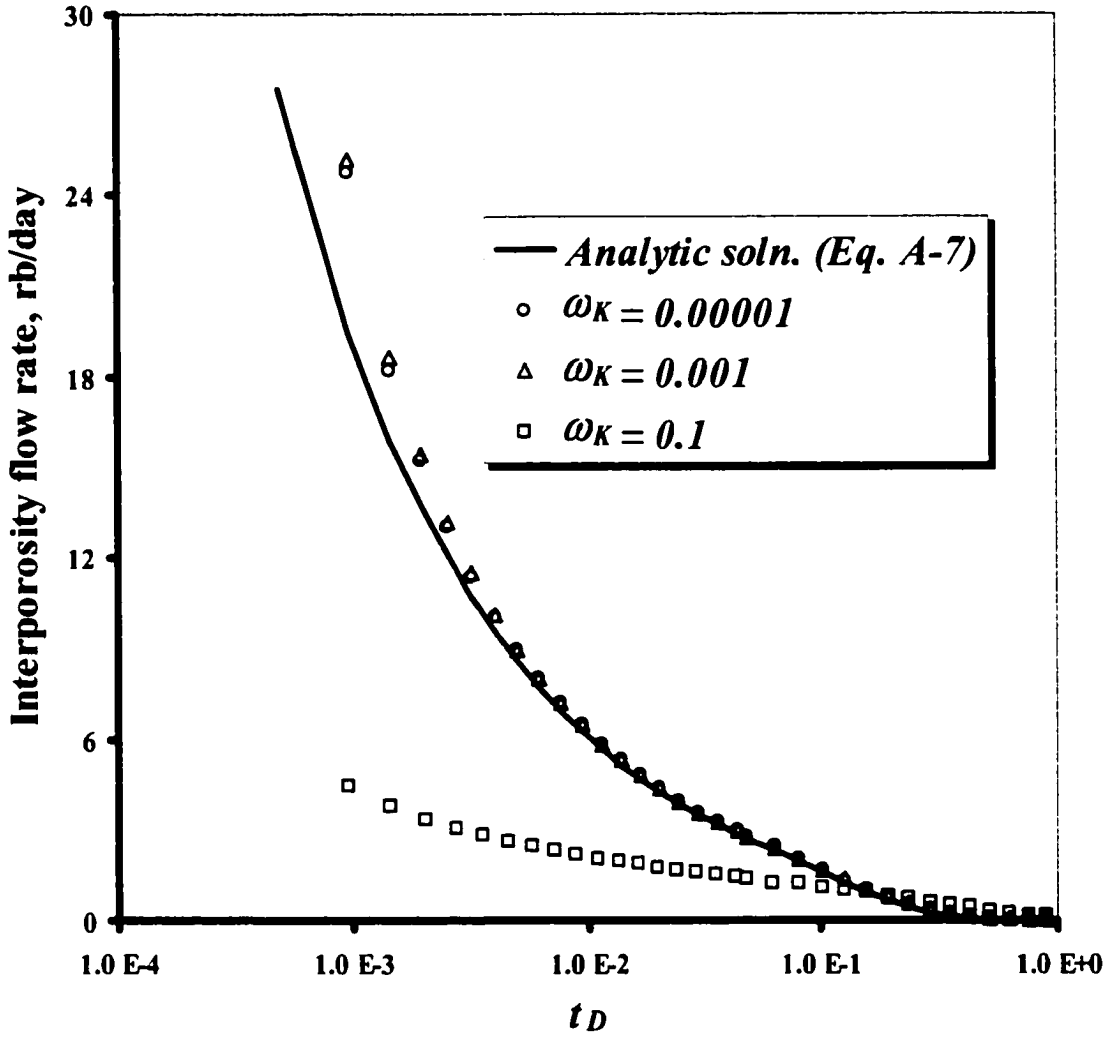

Fig. 4.12 – Effect of permeability ratio on interporosity flow rate. At high ω_K, fluid flows almost equally into matrix and fracture; therefore the interporosity flow rate is reduced (From Penuela *et al.*[27])

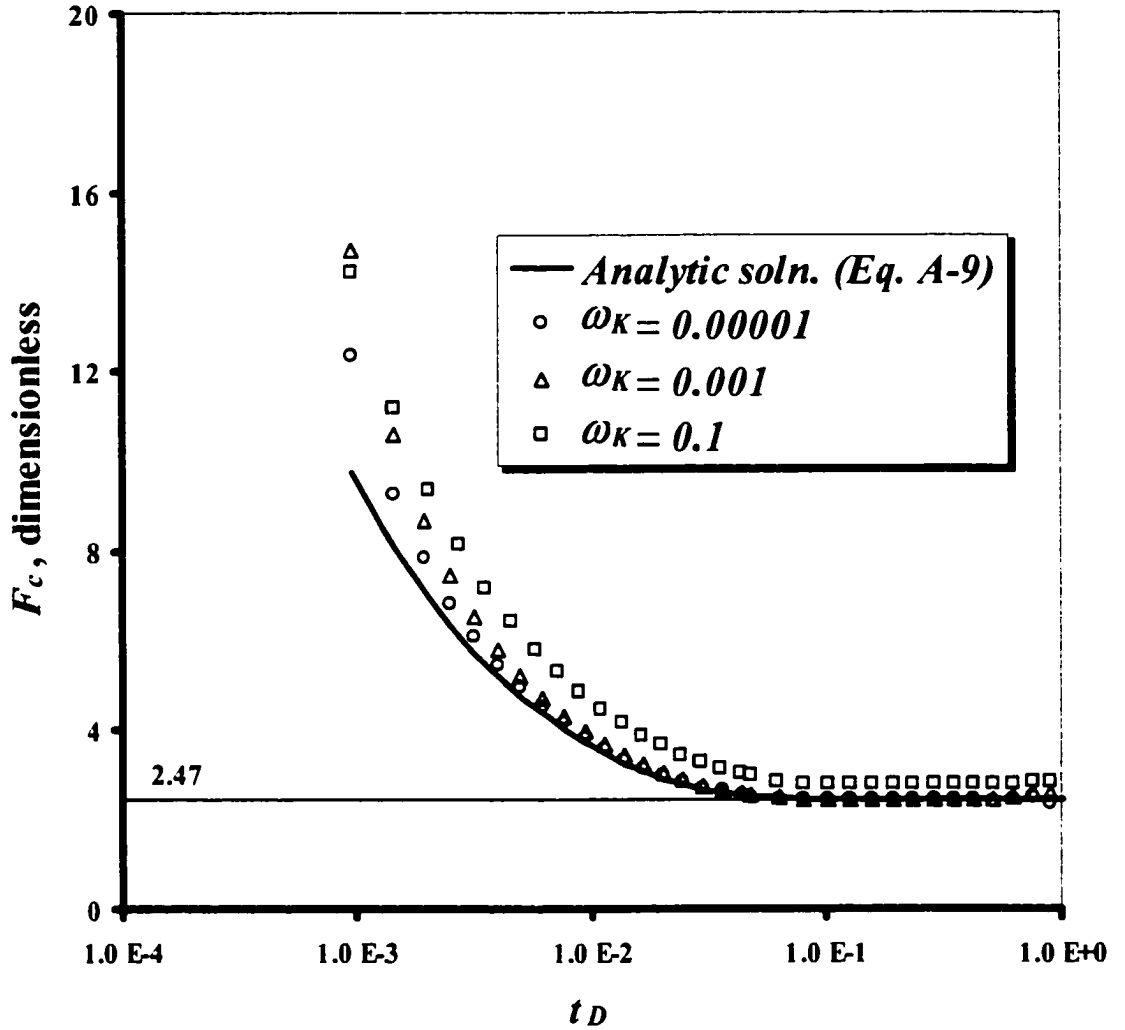

Fig. 4.13 – Effect of permeability ratio on flow correction factor (From Penuela *et al.*[27])

The interporosity flow rate computed from Eq. 4.10 is not only a function of matrix geometry and petrophysical properties expressed in Eqs. 2.2 through 2.5, but also considers fracture characteristics, such as fracture porosity and width. In previous works, the shape factor given by Eq. 2.8 considered only the fracture geometry for the estimation of the interporosity flow rate. To see the significance of using the fracture surface area, consider **Fig. 4.14**, which shows two gridblocks containing two parallel fractures in the same rock volume.

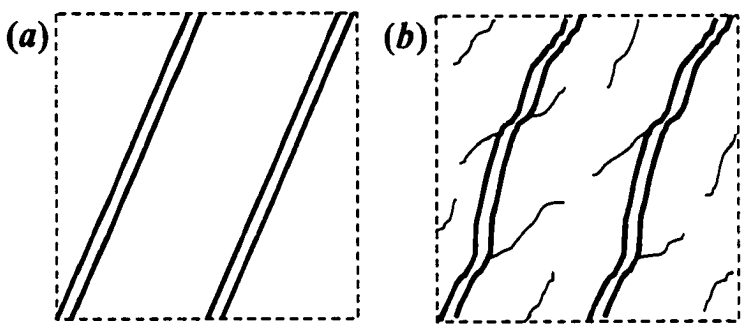

Fig. 4.14 – Two simulation gridblocks containing a pair of parallel fractures in the same rock volume. In Case (*b*), fluids would be produced faster from the matrix than in Case (*a*) because of a larger fracture surface area assuming negligible stress effects on the interporosity flow (From Penuela *et al.*[27])

In case *a*, the interporosity flow rate estimation is the same regardless whether Eq. 2.2 or Eq. 4.10 is used. On the other hand for case *b*, the interporosity flow rate computed from Eq. 4.10 is higher than case *a* because the fracture surface area is higher for the same gridblock volume. Equation 4.10 would predict twice the rate for a system that has twice the fracture porosity, while Eq. 2.2 would predict the same rate for both systems. The same conclusion is achieved regardless of the type of fluid present in the matrix block.

Implementation of Eq. 4.5 to compute single-phase fluid transfer is straightforward because the same variables are available in a dual-permeability, dual-porosity simulator. However, during the derivation of the flow correction factor expressed by Eq. 4.7 it was assumed that the pressure gradient observed in the matrix is the result of a constant pressure kept at the matrix/fracture interface. Since in a real situation the pressure in the fracture does not change instantaneously to reach a constant value, fracture pressure variation effects on the flow correction factor are considered by means of the superposition principle as shown in Chapter 7.

The correlation generated for the flow correction factor for single-phase systems may be extended to gas-condensate systems by defining an appropriate dimensionless time. The validity of this approach will be shown in Chapter 5.

CHAPTER 5

FLOW CORRECTION FACTOR IN GAS-CONDENSATE SYSTEMS

In this chapter, the applicability of the flow correction factor correlation given by Eq. 4.8 for gas-condensate systems is shown by introducing an appropriate dimensionless time. Derivation details of the analytic expression for the flow correction factor for computing the interporosity molar flow rate are presented in Appendix B.

Gas production from a naturally fractured gas-condensate reservoir is impaired by retrograde condensation. This phenomenon occurs when the local pressure is reduced below the dew point. Flow of gas from the matrix to the fracture is affected by the presence of the liquid phase, which reduces the relative permeability to the gas phase. Matrix pressure gradients are also affected by the presence of saturation gradients resulting from the condensation of liquids from the fracture-matrix interface to the block center as pressures drop below the dew point pressure. However, the gas-condensate fluid problem becomes identical to the single-phase fluid problem when pseudofunctions to account for the multiphase effects observed below the dew point pressure of the gas. Appendix B shows the theoretical equivalence between the single-phase and gas-condensate fluid formulations and the corresponding solutions for interporosity flow. In the following, the flow correction factor will be derived using pseudofunctions that reduce the gas-condensate problem to a single-phase problem.

5.1 Flow Correction Factor Derivation

Darcy's law is applied to estimate the interporosity flow rate. The reduction of effective permeability to the gas phase in the presence of the liquid phase is described by means of the relative permeability to the gas. Neglecting gravity and capillary pressure effects, the interporosity molar flow rate can be calculated from the following expression:

$$q_t = -Ak_m\left(\rho_g \frac{k_{rg}}{\mu_g} + \rho_o \frac{k_{ro}}{\mu_o}\right)\frac{\partial p}{\partial x} \quad \text{.....5.1.}$$

The pseudopressure function defined by Jones and Ravaghan[66] may be used to write Eq. 5.1 as follows:

$$q_t = -Ak_m \frac{\partial p_p}{\partial x} \quad \text{.....5.2,}$$

where

$$p_p = \int_{p_{ref}}^{p}\left(\rho_o \frac{k_{ro}}{\mu_o} + \rho_g \frac{k_{rg}}{\mu_g}\right)dp \quad \text{.....5.3.}$$

The pressure gradient expressed in terms of the pseudofunctions in Eq. 5.2 may be substituted by the difference in the matrix and fracture average pseudopressures, whose locations in the matrix block are separated by a distance $L/2$, if a flow correction factor is introduced into Eq. 5.2 as follows:

$$q_t = F_c A k_m \frac{\left(\overline{p}_p - p_{pf}\right)}{\frac{L}{2}} \quad \text{.....5.4.}$$

The flow correction factor, F_c, is defined by the Eq. 4.8 correlation with the following dimensionless time:

$$t_D = \frac{k_m}{\phi_m L^2} t_p \quad \text{..... 5.5}$$

where t_p is an appropriate pseudotime function.

The use of pseudotime functions effectively simplifies the complex flow problems. Lee and Holditch[67] used a pseudotime function for well testing in gas wells using type curves developed for slightly compressible liquids in a homogenous reservoir. They theoretically analyzed the conditions under which their pseudofunction linearizes the flow equation for single-phase gas. For gas-condensate systems, Penuela and Civan[68,69] applied the following pseudotime function, which accounts for multiphase flow effects:

$$t_p = \int_{t_{mf}}^{t} \left[\frac{\partial \left(\rho_o S_o + \rho_g S_g \right)}{\partial p_p} \right]^{-1} dt \quad \text{..... 5.6}$$

where the pseudopressure function was defined by Eq 5.3. As indicated in Appendix B, the pseudotime function given by Eq. 5.6 can be used along with Eqs. 4.8 and 5.5 to compute the total molar rate of interporosity fluid transfer in a matrix block that contains a gas-condensate fluid.

This approach was verified by using a compositional simulator whose formulation is described by Penuela.[70] The simulator is a semi-implicit, non-Newton-Raphson, equation of state (EOS)-based compositional, 1D radial reservoir model, which was modified to handle 1D linear flow. Numerical experiments were performed on a cubic shape matrix block (L = 10 ft) in contact with a fracture along one side. Because of symmetry, only half of the matrix-fracture system was simulated using the 20×1×1 grid shown in Fig. 4.2. Matrix permeability and porosity were respectively k = 0.001 md and ϕ = 0.05%. Initial matrix pressure was set at the dew point pressure of the gas (p_{dew} = 6750 psia) and

fracture pressure was kept constant at p_f = 6250 psia. Mixture 2 for the fluid and set 2 for the relative permeability from Penuela[70] are used. The fluid system is represented by means of a mixture of five pseudo-components with parameters described in **Table 5.1**.

TABLE 5.1 – PSEUDO-COMPONENT PROPERTIES FOR FLUID USED IN COMPOSITIONAL SIMULATION (AFTER PENUELA[70])

Mixture 2		Pseudo-component				
		pC_1	pC_2	pC_3	pC_4	pC_5
Initial mole fraction, %		10.931	74.064	7.870	2.583	4.552
Molecular weight, *lb/lb-mole*		44.01	16.28	32.97	68.19	131.85
Critical pressure, *psia*		1071	663	687.7	503.6	375
Critical temperature, *°R*		547.91	341.03	573.97	811.14	1450
Critical volume, *ft³/lb-mass*		0.026	0.085	0.068	0.055	0.010
Acentric factor, *dimensionless*		0.2250	0.0110	0.1091	0.2289	0.4000
Shift factor, *dimensionless*		-0.26	-0.1555	-0.0971	-0.0507	0.0710
Parachor, *dimensionless*		78	76.3	116.8	216.4	381.1
Binary interaction coefficients, *dimensionless*	pC_1	0	--	--	--	--
	pC_2	0.1	0	--	--	--
	pC_3	0.12	0.1	0	--	--
	pC_4	0.1	0.1	0	0	--
	pC_5	-0.02	0	0	0	0

The relative permeabilities were represented using Corey-type functions with coefficients interpolated between the immiscible and miscible limits depending on the capillary number evaluated at the matrix/fracture interface. The end-points and exponents of the relative permeability curves for the immiscible limit are given in **Table 5.2**, and for the miscible limit, linear relative permeabilities of saturation are assumed. For additional

information regarding rock-fluid description and flow modeling, the reader is referred to Penuela.[70]

TABLE 5.2 – PARAMETERS FOR RELATIVE PERMEABILITY (AFTER PENUELA[70])

Parameter	Oil phase	Gas phase
End-point relative permeability, *fraction*	1	1
Residual saturation, *fraction*	0.048	0.15
Exponent of the Corey function, *dimensionless*	2	2.12

Simulator output data were used to compute the flow correction factor, F_c, as a function of dimensionless time. To further test this approach, several values of absolute permeability and block length were used. One single F_c curve was obtained as observed in **Fig. 5.1**. Some deviations were observed during initial simulation because of fluid compressibility effects that are not properly captured by the implementation of Eq. 5.6 and the assumptions under which this equation was derived as indicated in Appendix B.

5.2 Implementation

Implementation of Eq. 4.5 to compute single-phase fluid transfer is straightforward because the same variables are available in a dual-permeability, dual-porosity simulator. However, the implementation of Eq. 5.4 in current compositional simulators to estimate the interporosity molar rate requires the computation of the average pseudopressure function as defined by the following double integral:

$$\overline{p}_p = \frac{1}{L}\int_{-L/2}^{L/2}\int_{p_{ref}}^{p}\left(\rho_o\frac{k_{ro}}{\mu_o}+\rho_g\frac{k_{rg}}{\mu_g}\right)dp\,dx \qquad \text{5.7.}$$

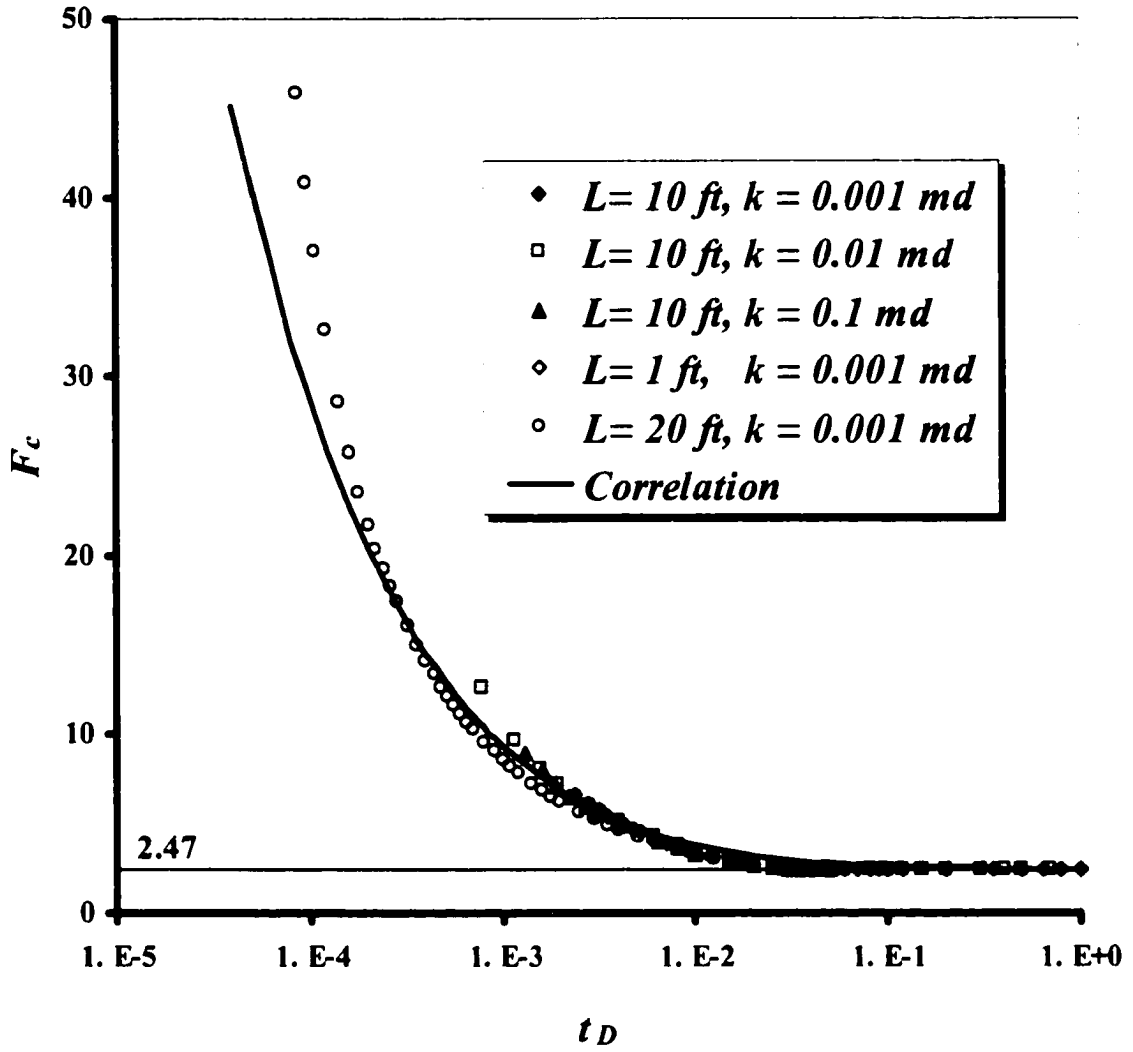

Fig. 5.1 – Flow correction factor computed from compositional simulation. Dimensionless time effectively reduces to one single F_c curve data generated for different size matrix block and absolute permeability (From Penuela *et al.*[27])

The pressure distribution inside each matrix block in a gridblock will not be available. Instead, the average pressure in a gridblock is computed at every timestep. To overcome this difficulty, the average pressure may be used to compute the pseudopressure function if Eq. 24 is approximated by the following expression:

$$\bar{p}_p \approx \int_{p_{ref}}^{\bar{p}} f(\bar{p})\, d\bar{p} \qquad \text{5.8}$$

where $f(p)$ is approximated as follows:

$$f(\bar{p}) = \frac{1}{L}\int_{-\frac{L}{2}}^{\frac{L}{2}} \left(\rho_o \frac{k_{ro}}{\mu_o} + \rho_g \frac{k_{rg}}{\mu_g} \right) dx \approx \bar{\rho}_o \frac{\bar{k}_{ro}}{\bar{\mu}_o} + \bar{\rho}_g \frac{\bar{k}_{rg}}{\bar{\mu}_g} \qquad \text{5.9.}$$

The average values needed in Eq. 5.9 should be readily available from the compositional simulator at the end of every timestep to explicitly compute the interporosity flow rate. Performance of this approximation is shown in **Fig. 5.2** where the average pseudopressure function computed from Eq. 5.7 is also plotted using fluid data for mixture 2 given by Penuela.[70] Although the approximation introduces some errors, they are reasonably insignificant and Eq. 5.7 may be used to compute the average pseudopressure function from the average matrix pressure and fluid composition available at the end of each timestep in the compositional simulator.

Application to cocurrent two-phase flow may be simulated by Eq. 5.4 with an appropriate dimensionless time and if capillary forces can be neglected. This conclusion can be drawn from similarities between the governing equations of gas-condensate systems (see Appendix B) and two-phase fluid systems. However, in cocurrent flow in water-wet systems capillary pressure plays an important role that may not be neglected.[13]

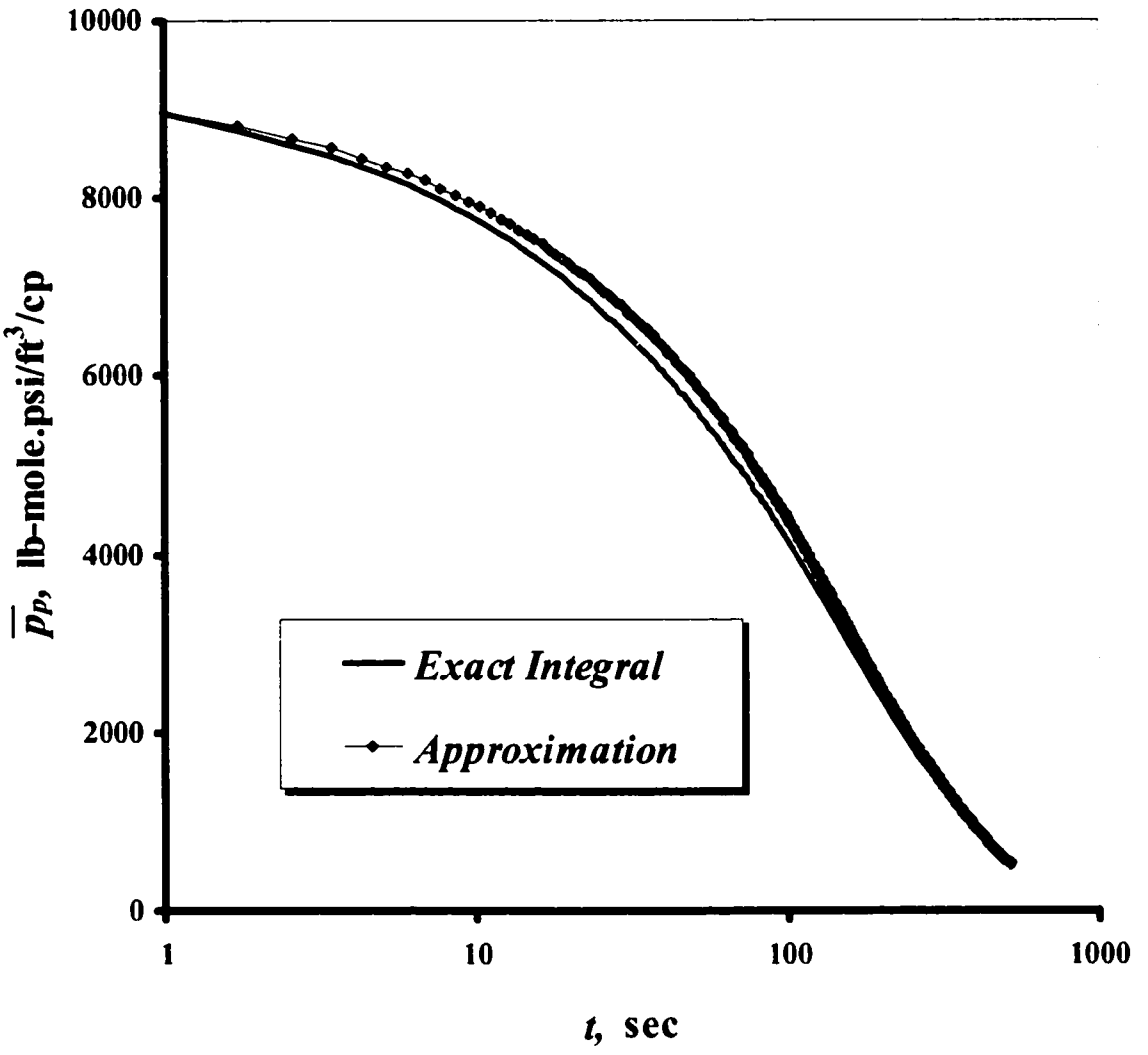

Fig. 5.2 – The average pseudopressure may be computed from an approximate integral that uses the average values of fluid mobility, which are functions of the average matrix pressure and fluid composition already available in the compositional simulator (From Penuela *et al.*[27])

The importance of capillary pressure effects can be better observed in counter-current flow, which may be the most important energy source for imbibition in a water wet system. The water front moving slowly towards the matrix block center would generate corresponding pressure gradients that also move slowly, and would therefore create high flow correction factors that are strongly time-dependent. Transient effects of pressure and saturation gradients on the flow correction factor for countercurrent flow will be described in the following chapter.

CHAPTER 6

FLOW CORRECTION FACTOR IN IMMISCIBLE TWO-PHASE SYSTEMS

In this chapter, model formulation for the interporosity flow rate in an immiscible two-phase system is presented. The model considers a time-dependent flow correction factor to be used in the flow equations for phase α in the fracture system given by:

$$\nabla \cdot \left[\frac{\bar{\bar{k}}_f k_{r\alpha f}}{\mu_{\alpha f} B_{\alpha f}} \left(\nabla p_{\alpha f} - \rho_{\alpha f} g \nabla D \right) \right] = \frac{\partial}{\partial t} \left(\phi_f \frac{S_{\alpha f}}{B_{\alpha f}} \right) - \tilde{q}_\alpha \quad \text{..... 6.1}$$

where $\tilde{q}_\alpha$ is the interporosity flow rate per unit volume of rock. The subscript α denotes an immiscible fluid phase, such as water or oil. A similar set of equations may be defined for multiphase fluid flow in the matrix media in the dual-porosity and dual-permeability model.

6.1 Flow Correction Factor Derivation

The single-phase approach presented in Chapter 4 is extended by assuming that the multiphase Darcy's law can be used to compute the interporosity flow rate from the following expression:

$$q_o = -Ak_m \frac{k_{ro}}{\mu_o} \frac{\partial p_o}{\partial x} \quad \text{.....6.2}$$

where k_m is the average absolute permeability in the matrix block, μ_o is the average oil viscosity, p_o is the pressure of the oil phase in the matrix, and A is the total fracture surface area, which is calculated from the fracture geometry. A finite-difference approximation of Eq. 6.2 may be written in the following form:

$$q_o = -Ak_m \frac{k_{ro}}{\mu_o} \frac{\Delta p_o}{\Delta x} \quad \text{.....6.3.}$$

It is further assumed that the pressure drop, Δp_o, responsible for the interporosity flow rate, q_o, may be calculated as the difference between the average oil-phase pressures computed in the matrix and fracture, and where these two average values of pressure are separated by a distance equal to half fracture spacing. A flow correction factor, F_c, is introduced in order to correct for the deviations due to the previous assumptions. Consequently, Eq. 6.3 can be written as:

$$q_o = F_c A k_m \frac{k_{ro}}{\mu_o} \frac{\left(\overline{p}_{om} - p_{of}\right)}{\frac{L}{2}} \quad \text{.....6.4.}$$

When a single-phase fluid flows from the matrix to the fracture due to fluid expansion, the flow correction factor depends on the shape of the matrix block and not on its dimensions. This is contrary to constant shape factors, which depend both on the shape and the block dimensions. Another important characteristic is that F_c varies also with time and converges to the steady-state shape factor value reported in previous studies as shown in Chapter 4. Bourbiaux *et al.*[22] indicated that numerical simulation would improve if transient imbibition is considered. They suggested to replace the constant

shape factor by a shape factor that varies as a function of the average water saturation by assuming a simple piston-type movement of the water front into the matrix. However, since this solution is oversimplified and is coarse for capillary imbibition,[22] a more rigorous approach using fine-grid simulation is presented in the following.

To determine the flow correction factor based on Eq. 6.4, numerical experiments were performed on a cubic matrix block in contact with a fracture along one of its sides. Because of symmetry, only half of the matrix/fracture system was simulated. Reservoir rock and fluid data are similar to those described by Pooladi-Darvish and Firoozabadi.[14] **Table 6.1** presents data used to obtain numerical solutions to this 1D flow problem using a modified version of BOAST-VHS program[65] with 100 gridblocks.

TABLE 6.1 – DATA USED IN NUMERICAL EXPERIMENTS (FROM PENUELA *ET AL.*[47])

Matrix porosity, ϕ_m, fraction	0.3
Matrix permeability, k_m, md	20
Matrix compressibility, c_f, psi^{-1}	3.5×10^{-6}
Water viscosity, μ_w, cp	1.0
Oil viscosity, μ_o, cp	1.0
Initial pressure, p_i, psi	0
Fracture pressure, p_f, psi	0
Fracture spacing, L, ft	1.3123
Half fracture surface area, A_o, ft^2	0.4305
Oil rel. perm. exponent, n_o	4
Water rel. perm. exponent, n_w	4
Oil rel. perm. end-point, k_{ro}^*	0.75
Water rel. perm. end-point, k_{rw}^*	0.20
Capillary pressure constant, p_c^*, psi	1.45

The imbibition relative permeability and capillary pressure functions are expressed by:[14]

$$k_{ro} = k_{ro}^{*}(1 - S_{wD})^{n_o} \quad \text{..... 6.5,}$$

$$k_{rw} = k_{rw}^{*} S_{wD}^{\ n_w} \quad \text{..... 6.6,}$$

$$p_c = -p_c^{*} \ln(S_{wD}) \quad \text{..... 6.7,}$$

where normalized water saturation is defined as follows:

$$S_{wD} = \frac{S_w - S_{iw}}{1 - S_{or} - S_{iw}} \quad \text{..... 6.8,}$$

in which S_w, S_{iw}, and S_{or} denote the water saturation, connate water saturation and residual oil saturation, respectively. The oil-phase pressure profiles in the matrix block for different times are shown in **Fig. 6.1**. The average pressure over the matrix has been indicated as a dotted horizontal line intersecting with the oil-phase pressure curve from which the average pressure value was computed. The location of this intersection measured from the matrix/fracture interface represents the distance Δx in Eq. 6.3. It is observed from Fig. 6.1 that the distance to the location of the average matrix pressure, Δx, increases from zero at the fracture up to a steady-state value that is less than the assumed half fracture spacing. Therefore, Eq. 6.4 needs a shape factor F_c to correct for the actual location of the average pressure inside the matrix block.

Solving Eq. 6.4 for F_c gives an expression that can be evaluated using appropriate average values for oil viscosity, oil relative permeability and matrix block pressures computed from the fine grid simulations.

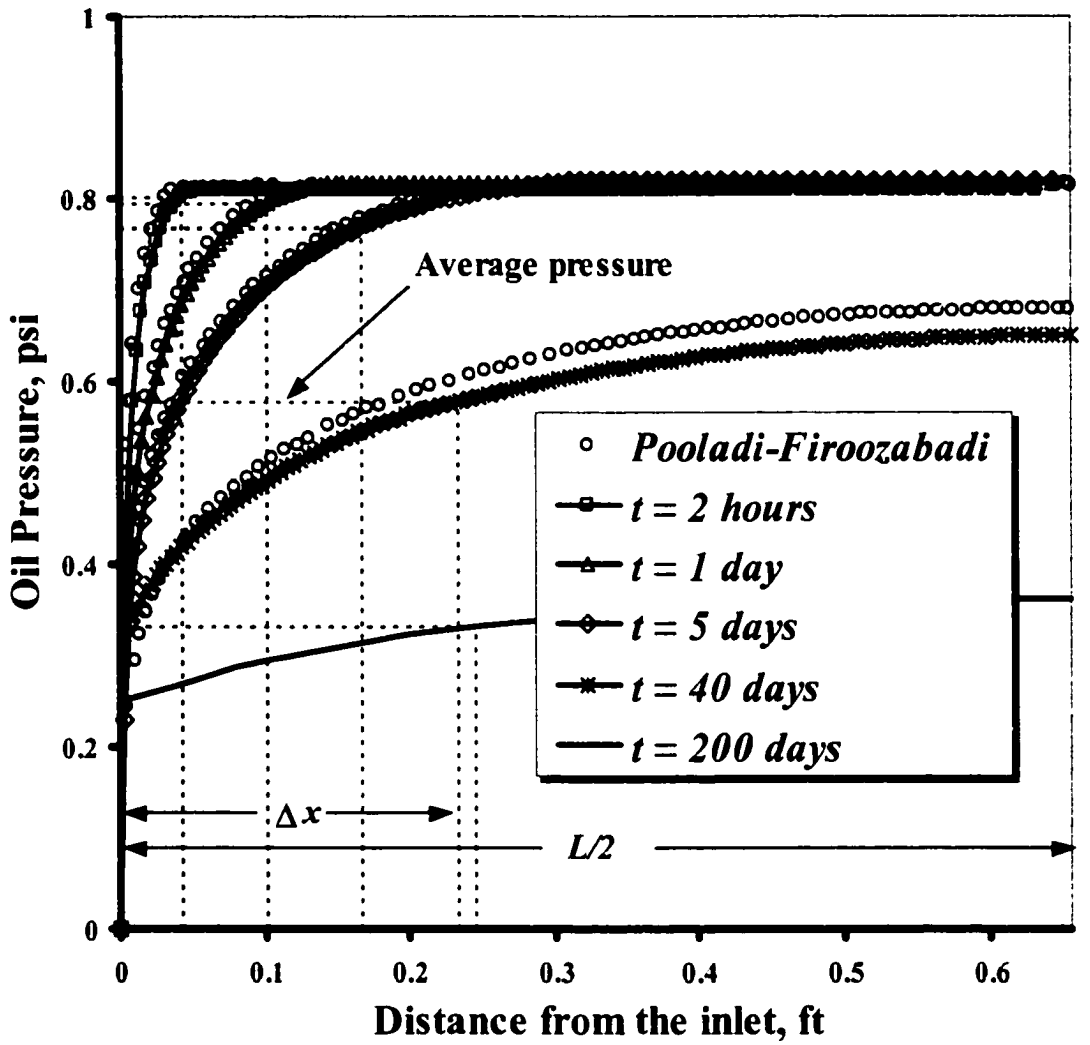

Fig. 6.1 – Location of the average oil-phase pressure in the matrix moves slowly to a point that is not the assumed *L/2* (From Penuela *et al.*[47])

However, a difficulty arises because the k_{ro} value is not the relative permeability to oil calculated at the average water saturation in the matrix. Instead, it is a critical relative permeability, k_{ro}^{o}, which is close to the end-point value ($k_{ro}^{o} = k_{ro}(S_w^{o} \approx 1-S_{or})$). This k_{ro}^{o} is small but high enough to allow oil to flow into the fracture across the matrix/fracture interface as illustrated in Fig. 3.4. In general, it is difficult to measure relative permeability near the end-points required for determination of interporosity flow rate at the interface. In addition, fine-grid simulation is not practical to estimate its value. This problem was also noted by McWhoter and Sunada[71] in numerical simulations of drainage experiments.

This numerical difficulty can be circumvented by studying the physics of the imbibition process at the matrix/fracture interface. Once water is in contact with the matrix (Fig. 3.4), water imbibes into the matrix and displaces oil, reducing its saturation to a residual value. However, the same capillary forces responsible of the water-phase pressure gradient may generate an oil-phase pressure gradient to move oil from matrix to fracture. Oil droplets in the matrix/fracture interface region coalesce forming a continuous mobile phase that carries oil to the fracture against the continuous water phase that is imbibing (see Fig. 1 by Civan and Rasmussen[53]). This critical mobile oil saturation ($S_o^{o} \approx S_{or}$) is rapidly achieved, remains almost constant and controls the exchange of fluids between the matrix and the fracture. Physically, it makes sense that there is some relationship between the relative permeability to water and the relative permeability to oil. Higher water relative permeabilities mean that the amount of connected oil, as expressed by the oil relative permeability, will be smaller (with the reverse also being true). A relationship between the relative permeability to oil at high water saturation in

counter-current imbibition has not been extensively studied. For convenience, a general power law for saturation is assumed as follows:

$$k_{ro}^{o} = \beta\, k_{rw}^{\bullet} \left(S_o^o\right)^{\gamma} \quad \text{.....6.9.}$$

where β and γ are constants. It is further assumed that the saturation at the interface remains constant and the relative permeability to oil is simply a linear function of the end-point relative permeability to water. Therefore, Eq. 6.9 can be written as follows:

$$k_{ro}^{o} = \left[\beta\left(S_o^o\right)^{\gamma}\right] k_{rw}^{\bullet} = a k_{rw}^{\bullet} \quad \text{.....6.10}$$

where a is a constant to be determinated from experiments. Substitution of Eq. 6.10 into Eq. 6.4 yields the following expression for the product $a\,F_c$:

$$a\,F_c = \frac{q_o \mu_o L}{2 A k_m k_{rw}^{\bullet} \left(\overline{p}_m - p_f\right)} \quad \text{.....6.11.}$$

Input data presented in Table 6.1 was used along with several values for matrix absolute permeability and block size assumed to investigate their effect on the product $a\,F_c$ as shown in **Fig. 6.2**. A single curve (**Fig. 6.3**) was obtained when numerical data were plotted using the t_D definition given by:

$$t_D = \frac{k_m t}{\phi_m \mu_w L^2} \left[k_{rw} \frac{dp_c}{dS_w} \right]_{S_w^{\bullet}} \quad \text{.....6.12.}$$

There are two flow periods clearly observed in Fig. 6.3. The initial flow period is characterized by a water front moving toward the matrix block center contacting an oil phase that moves in the opposite direction. As illustrated in **Fig. 6.4**, the second flow period starts after the water front reaches the block center and cannot continue moving toward the next fracture.

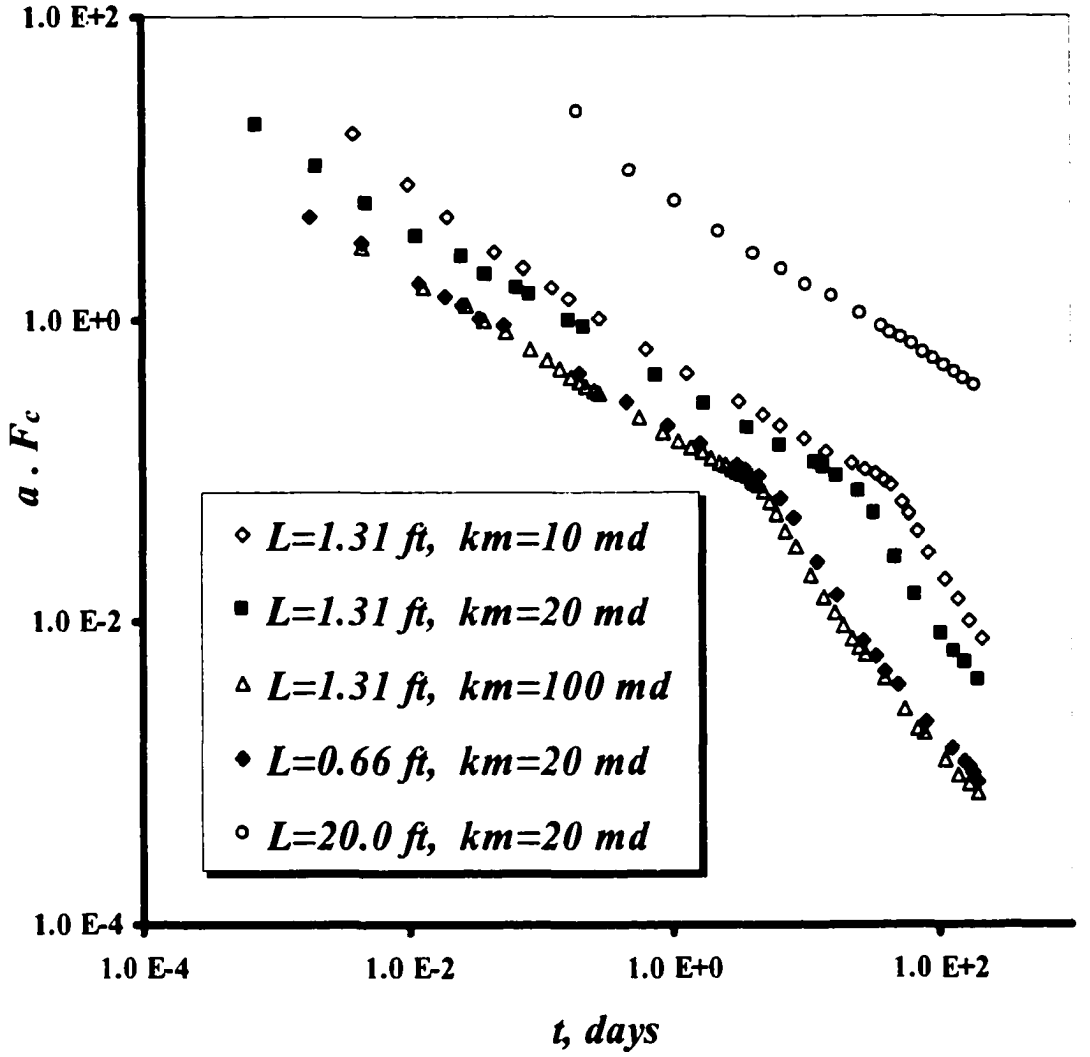

Fig. 6.2 – Plot of $a.F_c$ vs. t_D generated by the fine-grid simulation of countercurrent imbibition in a water-wet rock using the Table 6.1 data.

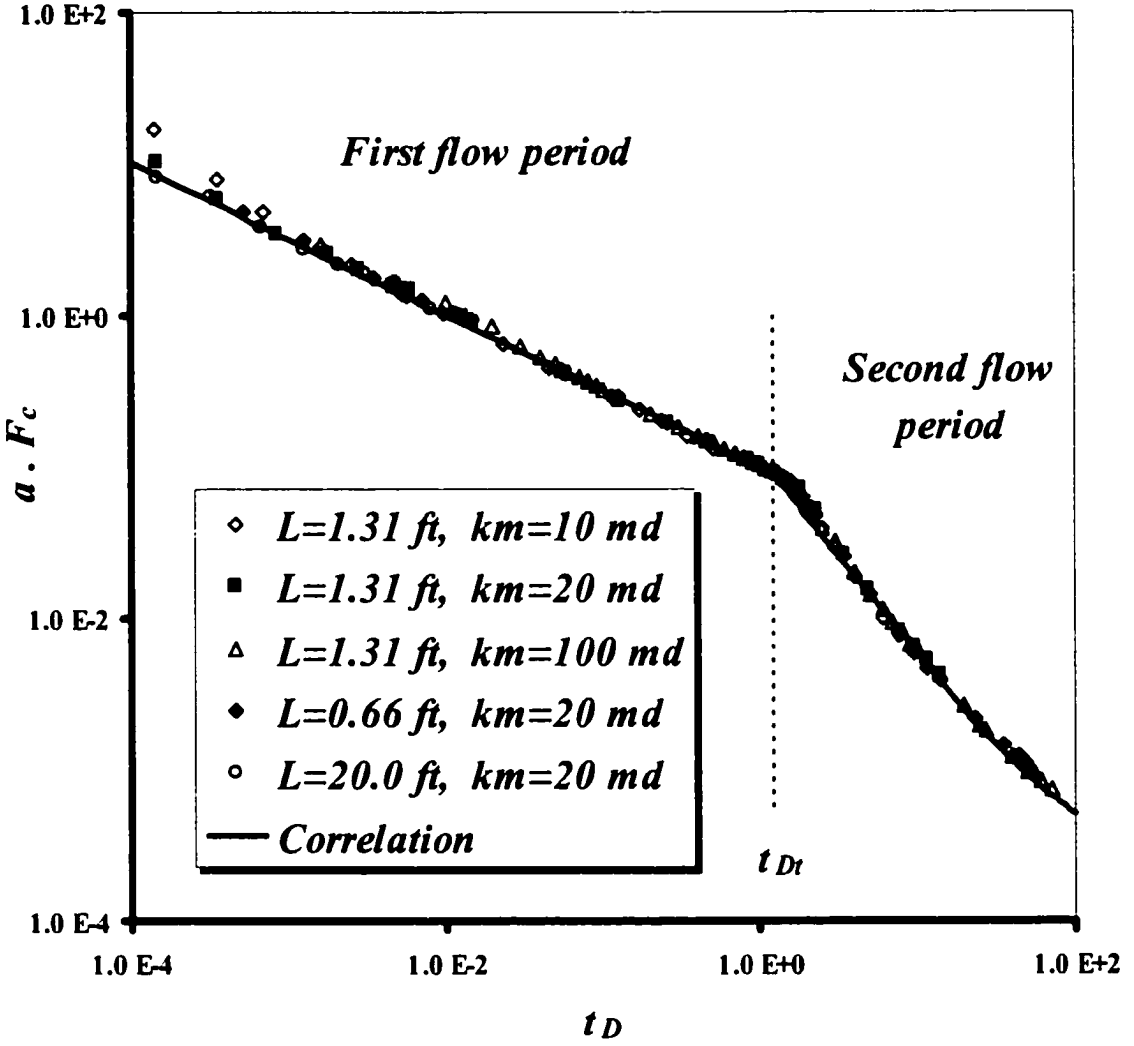

Fig. 6.3 – Two flow periods are observed in the curve $a.F_c$ vs. t_D. The dimensionless time at which the second flow period starts is approximately t_{Dt} = 1.21, which corresponds to t = 17 days in a matrix rock of average matrix permeability of k_m = 20 md and fracture spacing of L = 1.31 ft (From Penuela *et al.*[47])

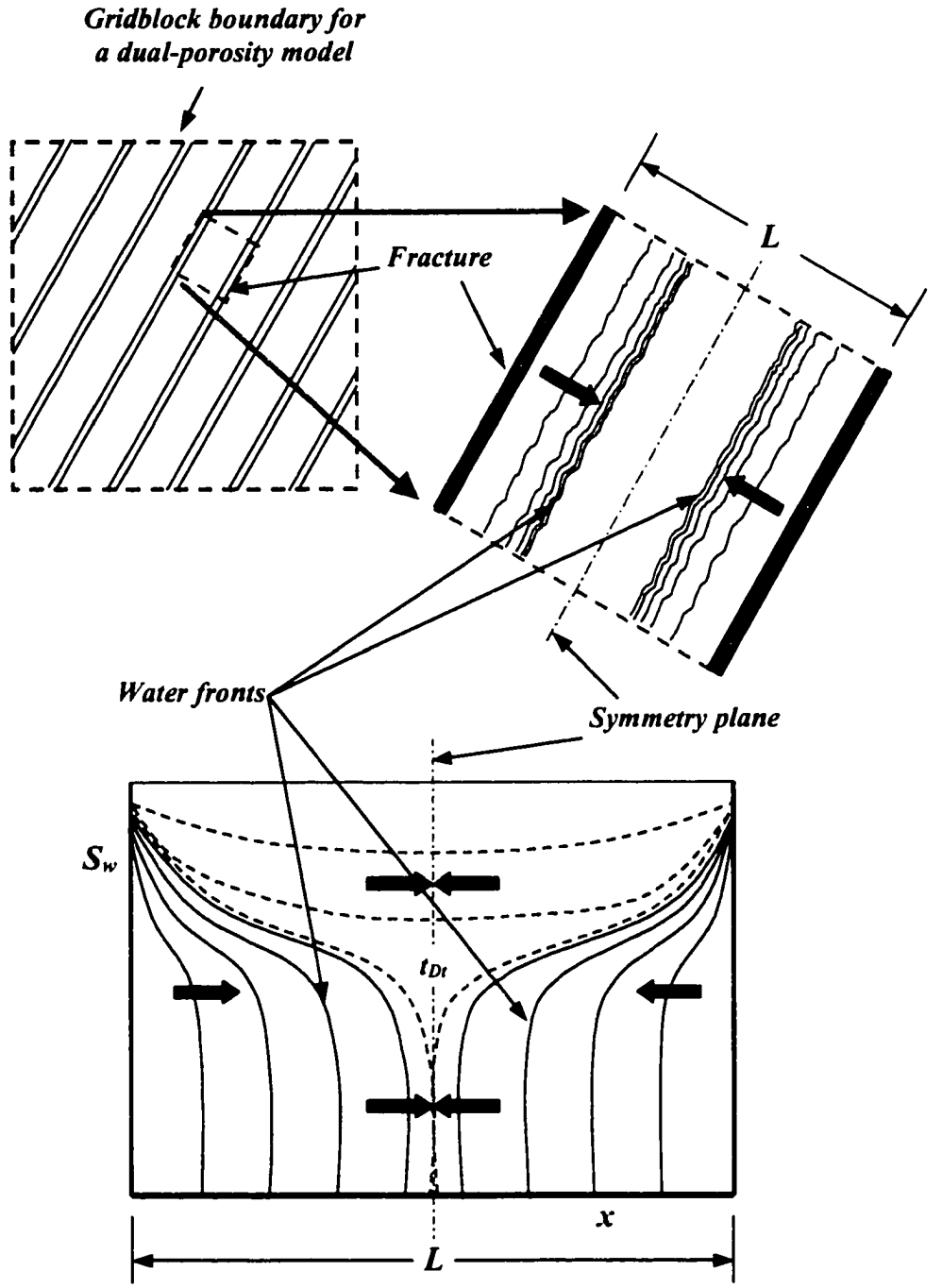

Fig. 6.4 – Flow periods observed in the $a.F_c$-curve shown in Fig. 6.3 have a physical interpretation. First flow period corresponds to a water front that moves freely from the fracture through the matrix as if it were an infinite media. Second period reflects the interference produced by the encounter of water fronts at the matrix-block center (From Penuela *et al.*[47])

The interference produced by the intersecting water fronts at the block center generates an additional average pressure drop and a different interporosity flow rate decline (**Fig. 6.5**). These two flow periods have been observed by other researchers both in numerical and laboratory experiments. For example, Reis and Cil[15,54] grouped existing analytical models for capillary imbibition into early-time and late-time models depending on the flow period that applies.

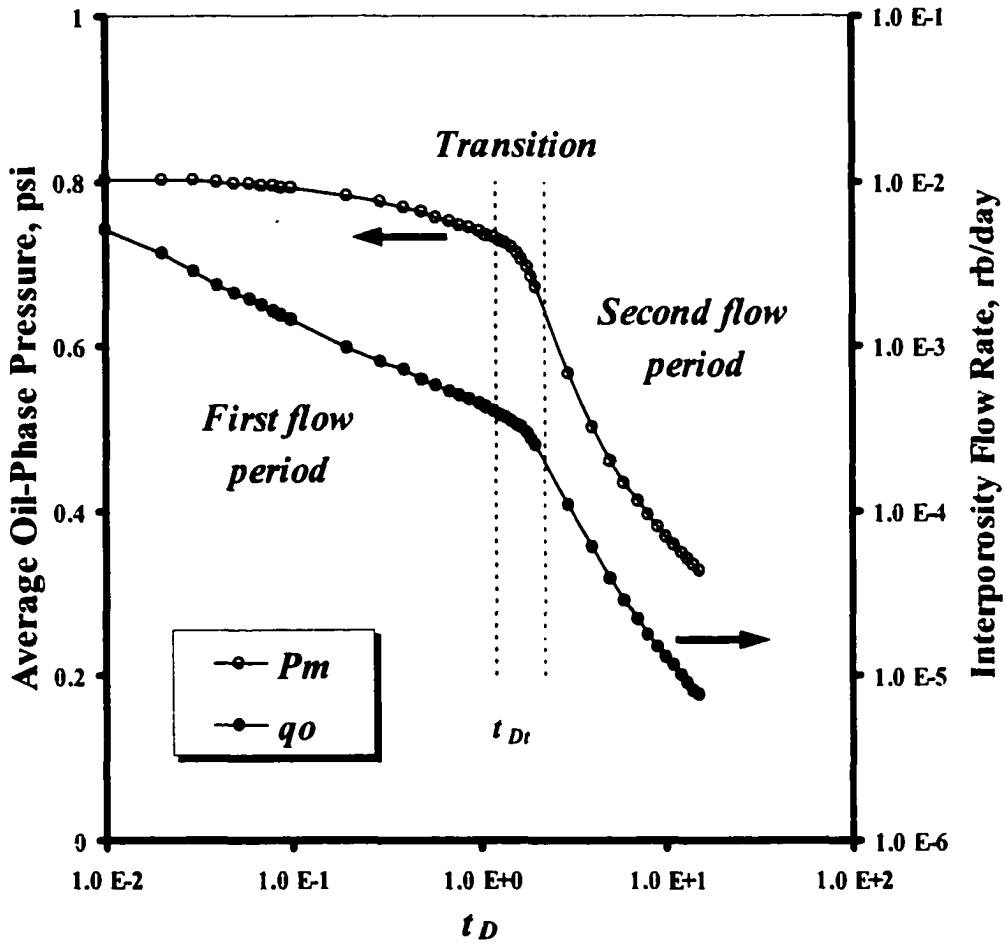

Fig. 6.5 – The interference caused at the matrix-block center produces an additional average pressure drop in the matrix and a different flow rate decline during the second flow period (From Penuela *et al.*[47])

Based on data shown in Fig. 6.3, using the relation of Eq. 4.6, and assuming $a = 10^{-4}$, the following generalized correlation for F_c was obtained by regression analysis (see **Figs. 6.6** and **6.7**):

$$F_c = f_{kn}\left(\frac{1}{t_D} + \frac{1\times10^{-5}}{t_D^2}\right)^{1.2}, \quad t_D < t_{Dt} \qquad \text{.....6.13,}$$

and

$$F_c = 2.47\left(1 + \frac{4.73\times10^{2}}{t_D^{3/4}}\right), \quad t_D \geq t_{Dt} \qquad \text{.....6.14.}$$

It will be seen later in the parametric study that the parameter f_{kn} and the dimensionless transition time, t_{Dt}, are functions of the end-point relative permeability to water, $k_{rw}^{\bullet}$, and the exponent of relative permeability to oil, n_o. For $k_{rw}^{\bullet} = 0.2$ and $n_o = 4$, $f_{kn} = 1000$ and $t_{Dt} = 1.21$ are required. The correlation given by Eqs. 6.13 and 6.14 is shown in Fig. 6.3. The 2.47 value in Eq. 6.14 is the analytical value obtained by Lim and Aziz[31] for a set of parallel fractures and is the value that was obtained for single-phase matrix-fracture simulations.

6.2 Parametric Study

In the following, a parametric study that investigates the effects of using different relative permeability and capillary pressure relationships on the flow correction factor is presented. This parametric study is based on numerical simulation using input data given in Table 6.1. Values of exponents and end-points for relative permeability and capillary pressure curves to be used in Eqs. 6.5-6.7 are given in **Table 6.2**.

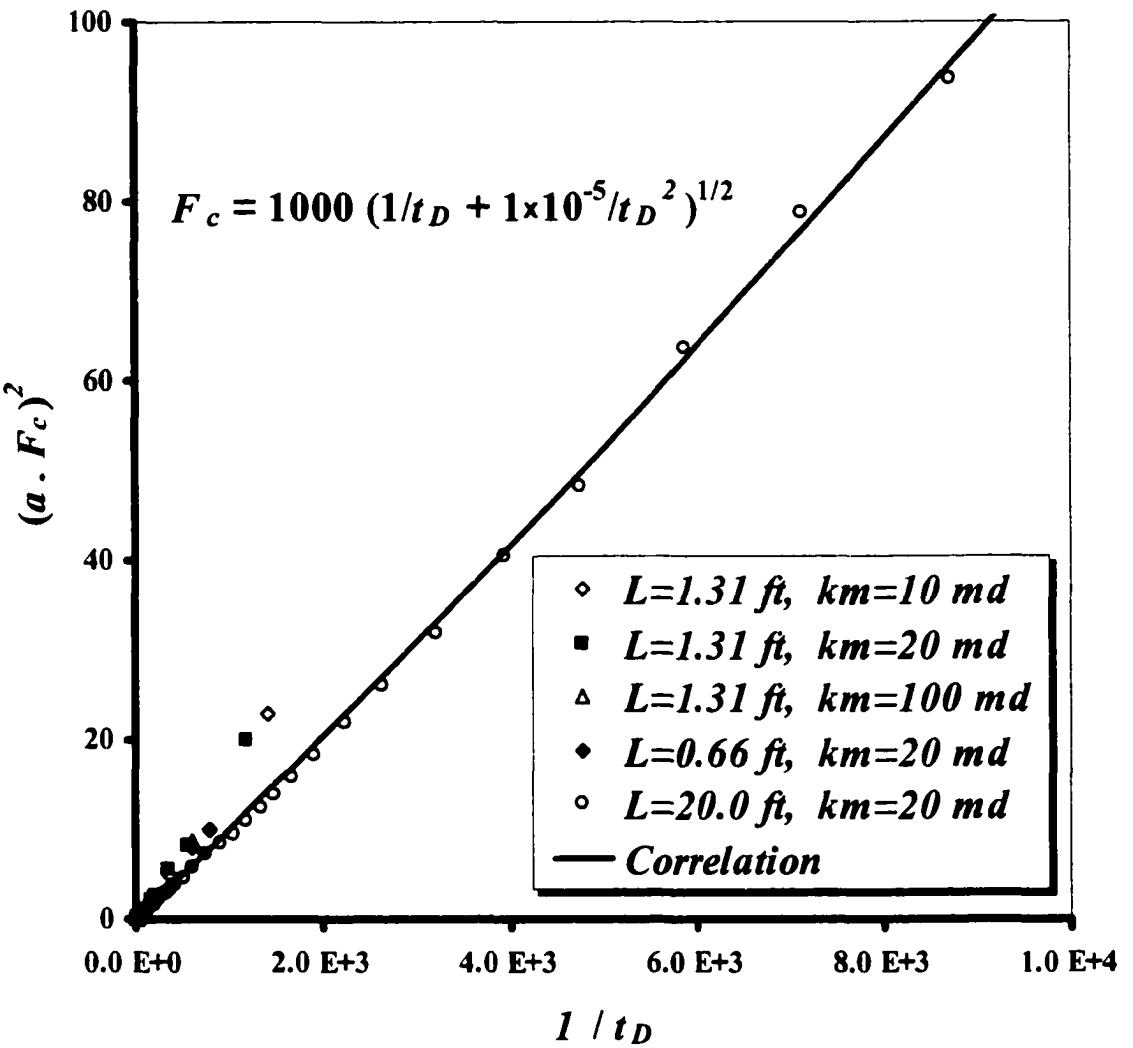

Fig. 6.6 – Regression analysis for data points corresponding to the first flow period. k_{rw}^* = 0.2 and n_o = 4 were used in numerical simulation (From Penuela *et al.*[47])

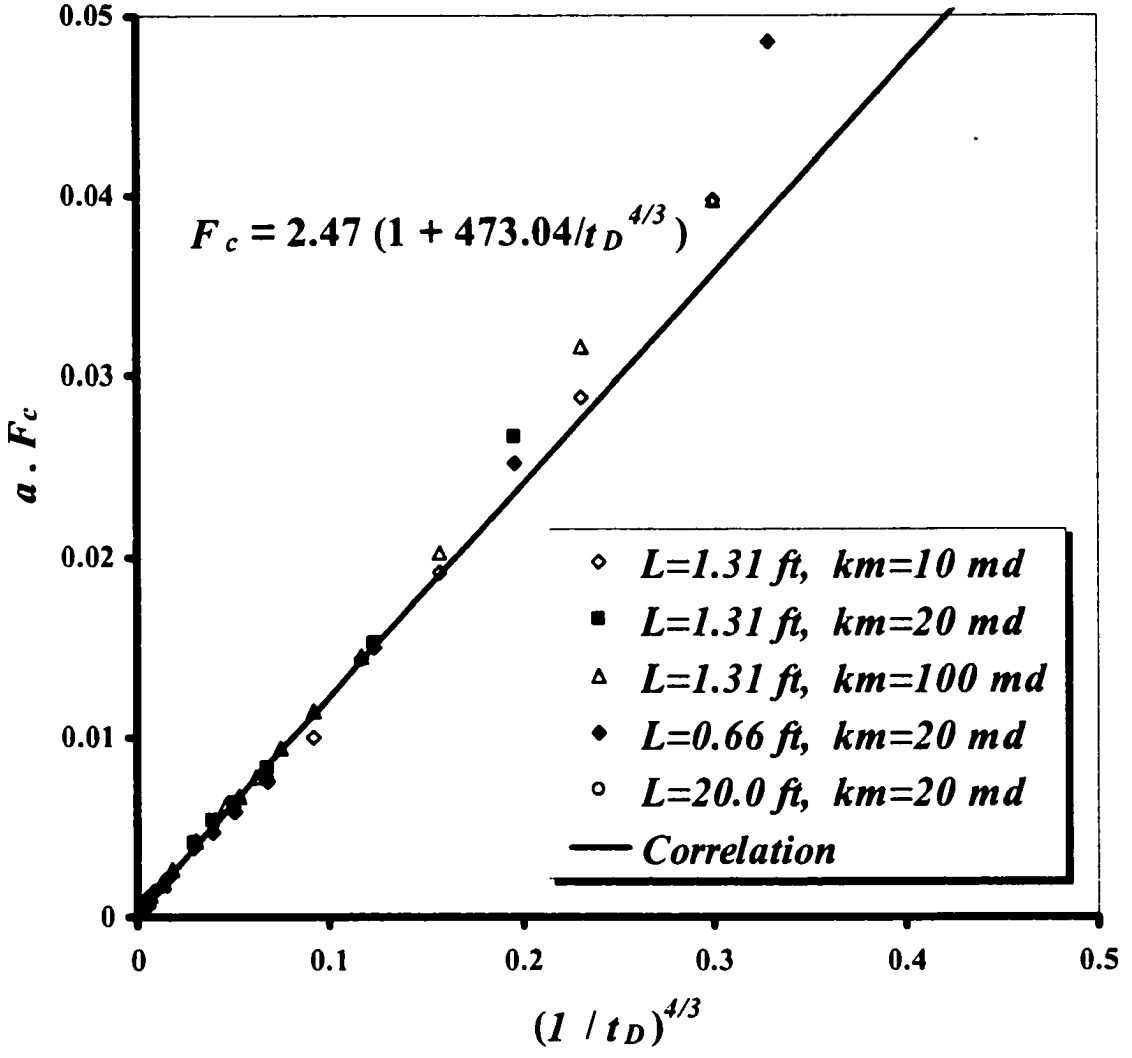

Fig. 6.7 – Regression analysis for data points corresponding to the second flow period. $k_{rw}^* = 0.2$ and $n_o = 4$ were used in numerical simulation (From Penuela *et al.*[47])

TABLE 6.2 – DATA USED IN THE PARAMETRIC STUDY (FROM PENUELA *ET AL.*[47])

Oil rel. perm. exponent, n_o	2, 3, 4
Water rel. perm. exponent, n_w	2, 3, 4
Oil rel. perm. end-point, k_{ro}^*	0.5, 0.75, 1
Water rel. perm. end-point, k_{rw}^*	0.20, 0.5, 1
Capillary pressure constant, p_c^*	0.7, 1.45, 3

6.2.1 Relative Permeability

Variation of end-points and exponents in Eqs. 6.5 and 6.6 indicated that k_{rw}^* and n_o yield a set of curves that need to be correlated, while different k_{ro}^* and n_w values yield F_c curves that collapse into one single curve described by Eqs. 6.13 and 6.14. As observed in **Fig. 6.8**, variation of k_{rw}^* yields a set of parallel F_c curves that merge into one during the second flow period. Variation of n_o as shown in **Fig. 6.9** yields a set of F_c curves that are almost parallel at all times. Data shown in Figs. 6.8 and 6.9 can be correlated with Eq. 6.13, where the parameter f_{kn} is a function of k_{rw}^* and n_o according to the following expression:

$$f_{kn} = 125.1(10 - n_o)\left(k_{rw}^{*\,2} - 2.03k_{rw}^* + 1.70\right) \quad \text{.....6.15}$$

The dimensionless transition time t_{Dt} is also a function of k_{rw}^* and n_o. The following expression can be used to compute t_{Dt}:

$$t_{Dt} = 9.67\left(\frac{k_{rw}^* + 0.41}{8.86 - n_o}\right) \quad \text{.....6.16.}$$

For the second flow period, the correlation given by Eq. 6.14 applies. In the process of deriving Eqs. 6.15 and 6.16, it was found that the flow parameter a is a function n_o according to the following expression:

$$a = \frac{0.0004}{n_o} \quad \text{.....6.17.}$$

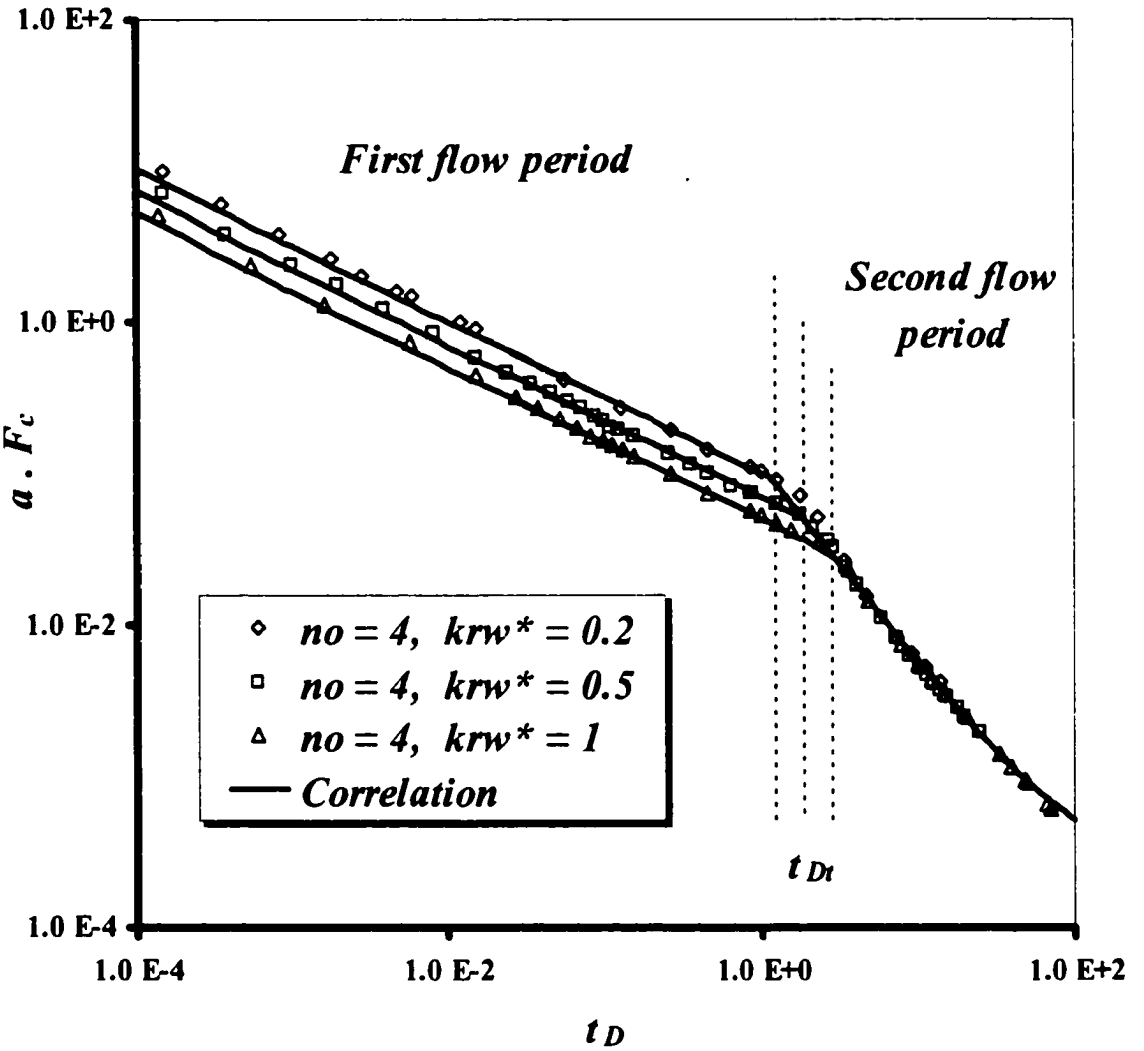

Fig. 6.8 – The end-point relative permeability to water influences the flow correction factor during the first flow period. For the second flow period only a single curve is needed for F_c as function of t_D (From Penuela *et al.*[47])

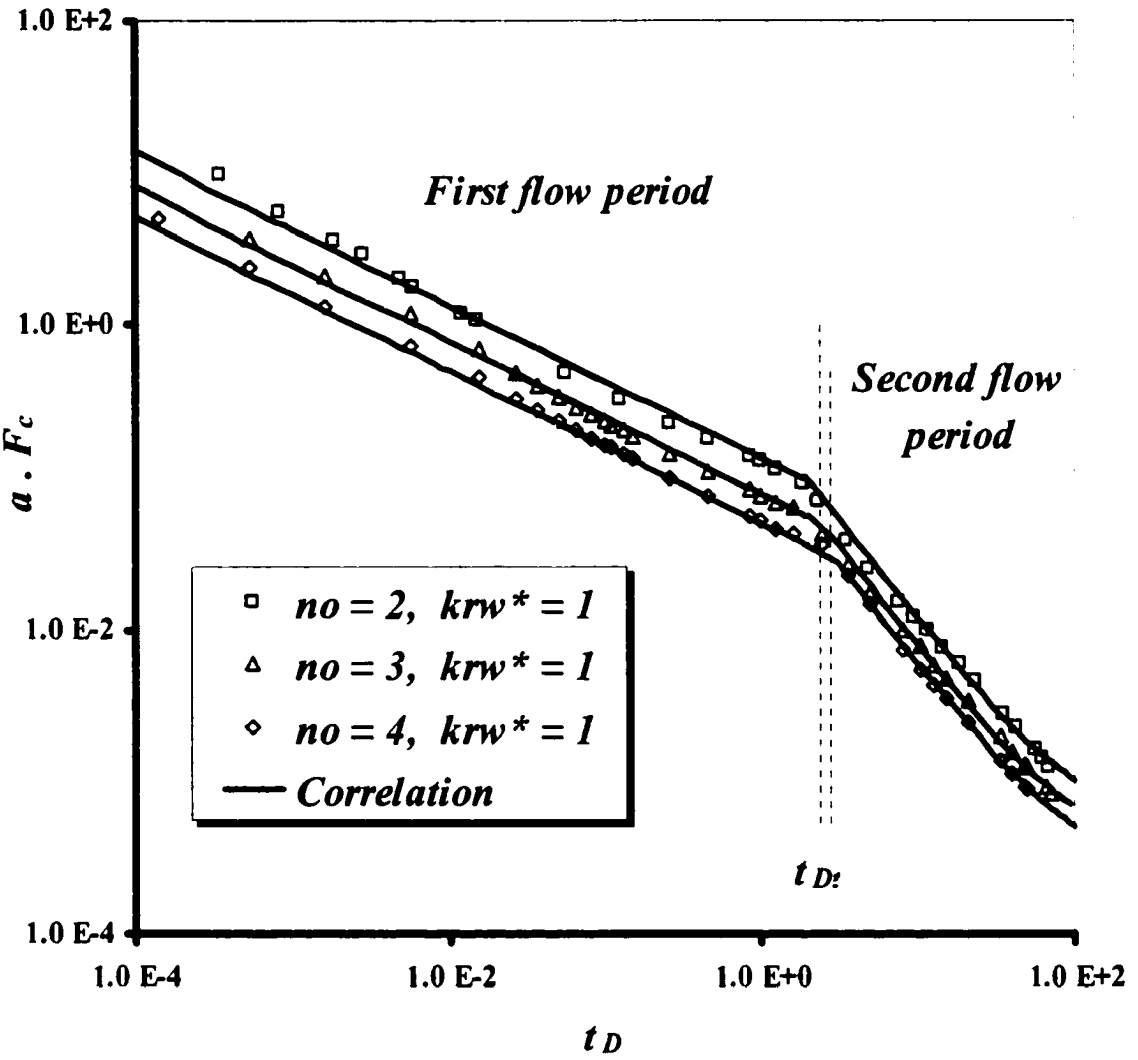

Fig. 6.9 – The exponent of relative permeability to oil influences the flow correction factor during both flow periods. A correlation is developed by writing the flow parameter a as a function of n_o (From Penuela *et al.*[47])

The physical interpretation of Eqs. 6.13-6.14 is based on the ability of the water phase to go across the matrix/fracture interface and the effect of interference at the block center. For the same n_o, low k_{rw}^* values generate low interporosity flow rates that have water fronts that move slower than those with high k_{rw}^* values. The average pressure associated with this water front slowly moves to a steady-state distance from the fracture, keeping the correction factors high for a longer period of time. Once the water fronts reach the matrix block center, a period of transition occurs and interference due to merging of responses from both sides of the block affect interporosity flow rate independent of k_{rw}^*. Therefore, the same correction factor is observed for different k_{rw}^* at $t_D > t_{Dt}$ (see Fig. 6.8). The effect of n_o on F_c is not easily seen in Fig. 6.9 since n_o is involved in the definitions of both a and F_c. However, since high n_o values generate low relative permeability to oil (Eq. 6.11), one can conclude that high n_o values generate high F_c values.

The physical meaning of Eq. 6.16 is better understood after substitution of the t_D definition into Eq. 6.16, where it can be seen that for a constant n_o, the higher k_{rw}^* the faster the second period is reached.

Variation of k_{ro}^* does not influence F_c as much as k_{rw}^*. A single F_c-curve was obtained for three different numerical values of k_{ro}^* (see Table 6.2). This result indicates that the definitions of F_c and t_D are appropriate to scale the imbibition process. It also indicates that the intuitive equation for the relative permeability to oil at the matrix/fracture interface, k_{ro}^o, given by Eq. 6.9 seems to capture the physics of the process. Similarly, variation of n_w does not influence F_c as much as n_o and one single curve was obtained for three different exponent values indicated in Table 6.2. The main effect of lower n_w is to

produce longer transition periods. However, the average F_c curve can be still represented by Eqs. 6.13-6.17.

6.2.2 Capillary Pressure

Several values for p_c^* were assumed (Table 6.2) and used along with data shown in Table 6.1. Numerical experiments showed that one single curve for F_c was obtained for different values of p_c^*. This result indicates that the effect of capillary pressure is properly considered in the dimensionless time, which uses the derivative of capillary pressure with respect to saturation evaluated at the matrix/fracture interface ($dp_c/dS_w = p_c^*$ at $S_w = S_w^*$).

6.3 Discussion

In the following, characteristics and the numerical implementation of the interporosity flow rate computed from Eq. 6.4 are discussed.

6.3.1 Time Dependency

The flow correction factor for countercurrent flow has a stronger time-dependency than the flow correction factors for single-phase fluid flow because of the slow motion of a water saturation front driven by capillary forces across the matrix. To illustrate this point, one can write Eq. 6.2 in terms of saturation gradient by applying Darcy's law to the water phase, using the capillary pressure relationship ($p_c = p_o - p_w$) and the condition of imbibition rates ($q_o = -q_w$) to obtain:

$$q_o = -Ak_m \frac{k_{ro}}{\mu_o}\left(1+\frac{k_{ro}}{k_{rw}}\frac{\mu_w}{\mu_o}\right)^{-1}\left(\frac{dp_c}{dS_w}\right)\frac{\partial S_w}{\partial x} \quad \text{.....6.18}$$

For countercurrent two-phase fluid flow, the water front moves from the fracture to the matrix-block center. A long time is required to reach a steady-state situation under this flow condition and its duration depends on the capillary forces involved during imbibition. For single-phase fluid flow, a pressure wave rapidly propagates into the matrix reaching a steady-state condition in a very short period of time.

A comparison of dimensionless time equations used to scale the process during single- and two-phase fluid flows may be done to investigate the forces responsible for the interporosity flow rate in each case. It was shown in Chapter 3 that for the single-phase case, the dimensionless time given by Eq. 4.17 may be used as a scaling function. For two-phase flow, Eq. 6.12 can be used for scaling purposes. This expression is very similar to the equation proposed by Rapoport[72] based on inspectional analysis of the differential equations of water/oil flow through porous media. Pooladi-Darvish and Firoozabadi[14] used Rapoport's equation as a scaling criteria and obtained one single recovery curve for 1D co- and countercurrent imbibition using several values of absolute permeability, fracture spacing, water viscosity, and derivative of the capillary pressure with respect to water saturation at the matrix/fracture interface ($S_w^* = 1-S_{or}$). In this study, Rapoport's equation is modified by adding the relative permeability to the water evaluated at the same interface conditions.

Comparing Eqs. 4.7 and 6.12, one can conclude that the flow correction factor for single-phase flow converges rapidly to a steady-state value at a speed proportional to the inverse of total compressibility while the flow correction factor for two-phase flow slowly converges at a speed proportional to the slope obtained from the capillary pressure curve evaluated at the average water saturation present at the matrix/fracture interface.

6.3.2 Asymptotic Behavior of F_c-Curve

No convergence to a constant a F_c was observed in any simulation runs reported in this study. Even though F_c converges to 2.47 according to Eq. 4.6, the numerical value of a is not always constant and goes to zero during the later stages of imbibition, when S_o^o approaches S_{or}. However, for practical purposes knowledge of S_o^o is not necessary because the energy provided by the capillary forces are so small at the end of the imbibition process that the interporosity rate computed by Eq. 6.4 is very low and the error introduced by F_c assuming constant S_o^o is negligible.

6.3.3 Implementation

The proposed interporosity flow rate equation can be implemented in a dual-porosity, dual-permeability reservoir simulator. Current numerical simulators determine the interporosity flow rate from the following expression:

$$q_o = \sigma V k_m \frac{k_{ro}}{\mu_o}\left(\overline{p}_m - p_f\right) \quad \text{.....6.19}$$

where σ is the constant shape factor and V is the gridblock volume. Modifications of Eq. 6.19 include the substitution of the shape factor by the flow correction factor given by Eqs. 6.13-16. Inclusion of k_{ro} is not estimated from the average saturation in the matrix, but instead, it is computed from Eq. 6.10 and Eq. 6.17, and finally, the substitution of V by the total fracture surface area (computed from the fracture geometry) and fracture spacing, L, according to Eq. 6.4. Most of these variables are readily available in current numerical simulators, such as average pressures, fluid viscosities, fracture spacing, exponents and end-points of relative permeability and capillary pressure curves. Fracture

surface area may be estimated from fracture porosity and its particular geometry. The actual permeability to be used in Eq. 6.4 is the absolute matrix permeability at the matrix/fracture interface, which includes the damage due to mineral crystallization along the surface area that may impair the flow. Laboratory experiments on naturally fractured cores are needed to have an indication of fracture geometry and conditions at the matrix/fracture interface as they control the interporosity rate.

Under the conditions considered in this study, the use of average water saturation to compute the relative permeability needed in the interporosity rate calculation yields unrealistic oil recovery as observed in **Fig. 6.10**. Oil recovery computed from a fine grid simulation of a matrix block is compared with the recovery estimated by using the difference between the fracture pressure and the average matrix pressure and relative permeability to oil from the average water saturation calculated from the same fine grid simulation. Consequently, using the average water saturation overpredicts the mass exchange at the matrix/fracture interface because this value is significantly above the actual interface saturation values. Hence, direct application of the present approach would predict an early water breakthrough because more water is available to flow along the fracture.

The approach described in this chapter matches the fine-grid simulation but cannot be directly implemented in most finite-difference simulators for fractured reservoirs because of the limitations imposed by the assumptions established while deriving the flow correction factor. Initially, the fracture is not entirely filled with water, and therefore, the saturation change with water injection has an effect on the flow correction factor. Moreover, the relative permeability to oil at the matrix/fracture interface before water

completely fills the fracture is higher than the one considered in this study, causing the present approach to underpredict the interporosity flow.

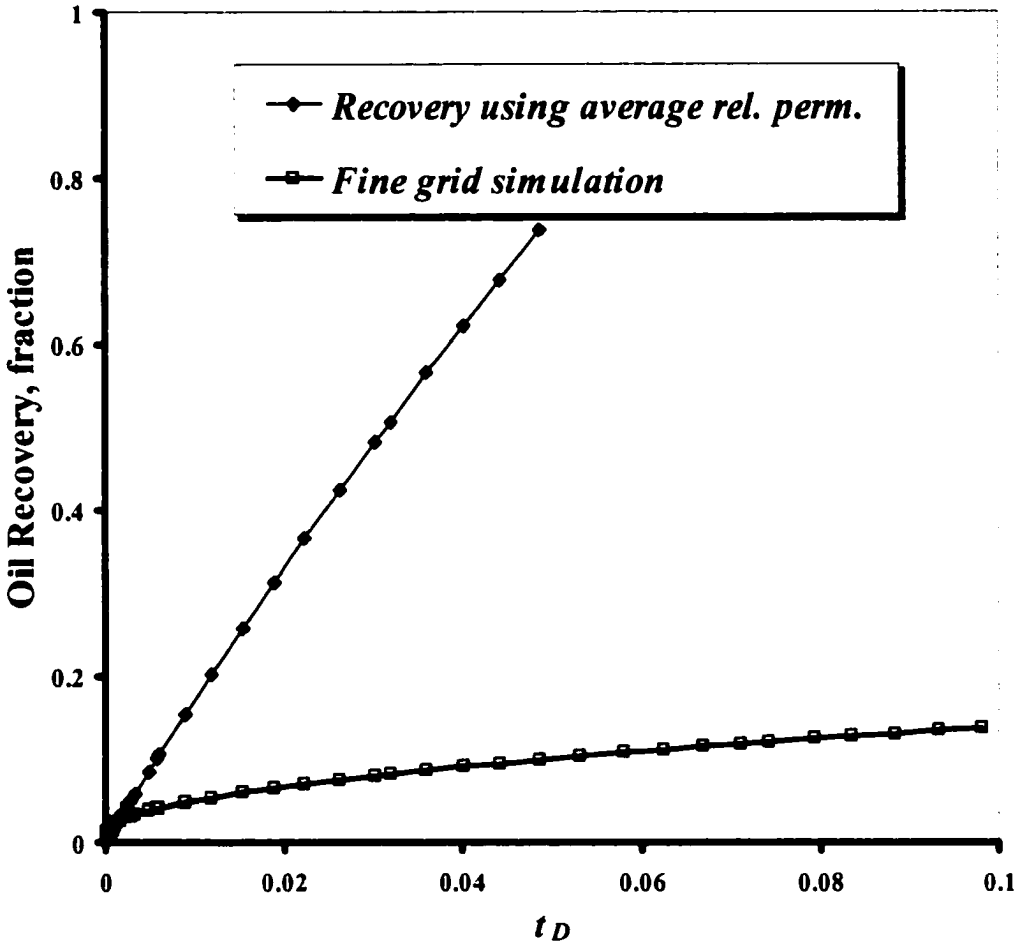

Fig. 6.10 – Oil recovery is overpredicted by using average water saturation in the matrix to estimate the effective oil permeability for the interporosity rate in countercurrent flow. Fine-grid simulation considers a cubic oil-bearing matrix block with L=0.66 ft in contact with a fracture completely saturated with water (From Penuela *et al.*[47])

Another physical effect observed during waterflooding is the cocurrent flow encountered when high pressure in the fracture prevails, making the total flow velocity to be different than zero ($q_o \neq - q_w$). However, once oil phase pressure in the matrix is higher than the pressure in the fracture, oil will flow in the opposite direction to water until the conditions described above in this study apply ($q_o = - q_w$). This limitation of the present approach observed during implementation requires further research on developing flow correction factors involving situations where there is an interaction of viscous, capillary and gravity forces. Thus, an approach to overcome these difficulties during the implementation of flow correction factors in a finite-difference simulator for fractured reservoirs is presented in the following chapter.

CHAPTER 7

IMPLEMENTATION IN A FINITE-DIFFERENCE RESERVOIR SIMULATOR

This chapter provides general information about the definite-difference reservoir simulator that is used to test the time-dependency effects of flow corrections factors on the interporosity flow. In this reservoir simulator, single-phase and immiscible two-phase fluid formulae only are implemented because the simulator formulation assumes a black-oil fluid. However, the approach applied for single-phase fluid systems is readily applicable to gas-condensate systems if appropriate pseudofunctions are used as shown in Chapter 5. After describing the simulator formulation, procedures to implement single-phase and immiscible two-phase flow correction factors for the interporosity flow calculation are presented in this chapter.

7.1 Model Formulation

Model formulation is based on the black-oil fluid model proposed by Evans.[23] It is assumed that the fractured media may be represented by two overlapping continua with distinctive porosity and permeability. The matrix is composed of interconnected porous rock intersected by a second porosity medium denoted as the fracture system. The flow equation for phase α in the matrix system is given by:

$$\nabla\cdot\left[\frac{\bar{\bar{k}}_m k_{r\alpha m}}{\mu_{\alpha m}B_{\alpha m}}(\nabla p_{\alpha m}-\rho_{\alpha m}g\nabla D)\right]=\frac{\partial}{\partial t}\left(\phi_m\frac{S_{\alpha m}}{B_{\alpha m}}\right)+\tilde{q}_\alpha \quad \text{..... 7.1}$$

where $\tilde{q}_\alpha$ is the interporosity flow rate per unit volume of rock. The subscript α represents water, oil and gas phases. In Eq. 7.1, gas solubility into the oil phase has not been indicated for the sake of simplicity. However, in this study, the presence of a gas phase was not considered. Only the oil and water phases are considered in the implementation of the flow correction factors and these factors were derived for interporosity flow of oil and water phases.

The fracture system is assumed to be composed of interconnected fractures that provide the most important pathways to fluid production. This means that only interconnected fractures are considered part of the fracture system; and, therefore, disconnected fractures are considered as part of the matrix system. The flow equation for phase α in the fracture system is given by:

$$\nabla\cdot\left[\frac{\bar{\bar{k}}_f k_{r\alpha f}}{\mu_{\alpha f}B_{\alpha f}}\left(\nabla p_{\alpha f}-\rho_{\alpha f}g\nabla D\right)\right]=\frac{\partial}{\partial t}\left(\phi_f\frac{S_{\alpha f}}{B_{\alpha f}}\right)-\tilde{q}_\alpha \quad \text{..... 7.2.}$$

An important characteristic of fractured media is the inherent anisotropic permeability. Thus, it is very important to use the full permeability tensor in Eq. 7.2 to account for anisotropy.[23,57]

If porous matrix, fracture and fluid properties are known, the system of equations given by Eq. 7.1 and 7.2 can be solved along with the following algebraic auxiliary equations. The phase saturations in the porous matrix and fractures must add to unity:

$$\sum_\alpha S_{\alpha m}=1 \quad \text{..... 7.3,}$$

and,

$$\sum_{\alpha} S_{\alpha f} = 1 \quad \text{..... 7.4.}$$

Two independent capillary pressure relationships for the primary pores and two for the fractures are required as functions of saturation:

$$p_{cowm} = p_{om} - p_{wm} = f(S_{wm}) \quad \text{..... 7.5,}$$

$$p_{cgom} = p_{gm} - p_{om} = f(S_{gm}) \quad \text{..... 7.6,}$$

$$p_{cowf} = p_{of} - p_{wf} = f(S_{wf}) \quad \text{..... 7.7,}$$

$$p_{cgof} = p_{gf} - p_{of} = f(S_{gf}) \quad \text{..... 7.8.}$$

7.2 Reservoir Simulator Development

Finite-difference solutions of Eq. 7.1 through 7.8 were obtained by modifying an existing single-porosity reservoir simulator. A version of BOAST (Black Oil Applied Simulation Tool) was selected for this modification because it is a cost-effective and easy-to-use reservoir simulation tool whose code was available. The source code was modified to model the fracture system and the interporosity flow. BOAST is a three-dimensional, three-phase, finite-difference black-oil simulator developed for use on a personal computer. The BOAST program simulates isothermal, Darcy flow in three dimensions. The simulator assumes that the reservoir fluids can be described by three fluid phases (oil, water, and gas) of constant composition whose properties are functions of pressure only. BOAST can simulate oil and/or gas recovery by fluid expansion, displacement, gravity drainage, and imbibition mechanisms. BOAST employs the implicit pressure -

explicit saturation (IMPES) formulation for solving its system of finite-difference equations. The IMPES method finds the pressure distribution for a given timestep first, then the saturation distribution for the same timestep. BOAST employs the line-successive, over-relaxation (LSOR) iterative solution technique to solve the system of pressure equations.[65]

BOAST-VHS is the version of BOAST that was modified to handle a fractured media using a dual-porosity, dual-permeability model. The original BOAST-VHS code was translated from FORTRAN to Visual Basic® and implemented in the Microsoft® Excel® environment. Several runs were performed until results from both simulators were almost identical. All equations were verified, and errors in the original BOAST-VHS code were found and corrected in the modified version. After writing the equations, modifications were made to handle the fracture system. To accomplish this, the BOAST formulation was compared to the Evan's formulation[23] for a naturally fractured reservoir. It was found that the formulations were similar, and therefore equation discretization would follow a similar process. Terms that contain the non-diagonal part of the fracture permeability tensor and the interporosity flow rate were then added. The partial differential equations were solved using finite-difference approximations in the same way BOAST equations were discretized. The modified version also uses an IMPES solution of the resulting set of linear equations. The simultaneous solution of the pressure equations for the fracture and the matrix is handled using LSOR. Additional information about the source code and model capabilities may be obtained from the Mewbourne School of Petroleum and Geological Engineering at The University of Oklahoma or from the Unites States Department of Energy.[73]

7.3 Interporosity Flow Implementation

In addition to permeability tensors for the fracture system, expressions to compute the interporosity flow rate were implemented in BOAST by initially assuming constant shape factors. Numerical simulation of fractured reservoirs with this model provided a first approach of the interplay between viscous, capillary and gravity forces. In the following, gravity forces are not considered since they may be easily incorporated into the formulation by using flow potentials instead of pressures.

7.3.1 Modeling Fluid Exchange for Waterflooding

Numerical simulation of waterflooding in a naturally fractured formation indicates that several flow stages may appear along a fracture that connects an injector to a producer. A schematic of these stages is presented in **Fig. 7.1** using seven boxes to represent the matrix at any stage. The reader is referred to Appendix C for a description of the input data and simulation output results. Input data for the simulation described in Appendix C is taken from the literature.[29,74]

Arrows in **Fig. 7.1a** qualitatively represent the net flow in this dual-porosity, dual permeability idealization of the fractured media. Forces involved during the recovery process cause fluids to move from high-energy regions to lower ones, such that net fluid flow in Fig. 7.1a is the result of their interaction. Net fluid flow has been qualitatively divided into flow components in **Fig. 7.1b** depending on the forces prevailing during each stage. The appearance of capillary forces is related to the presence of water in the fracture and matrix systems. Typically, capillary pressure in a fracture at a given water saturation is lower than the capillary pressure in the matrix.

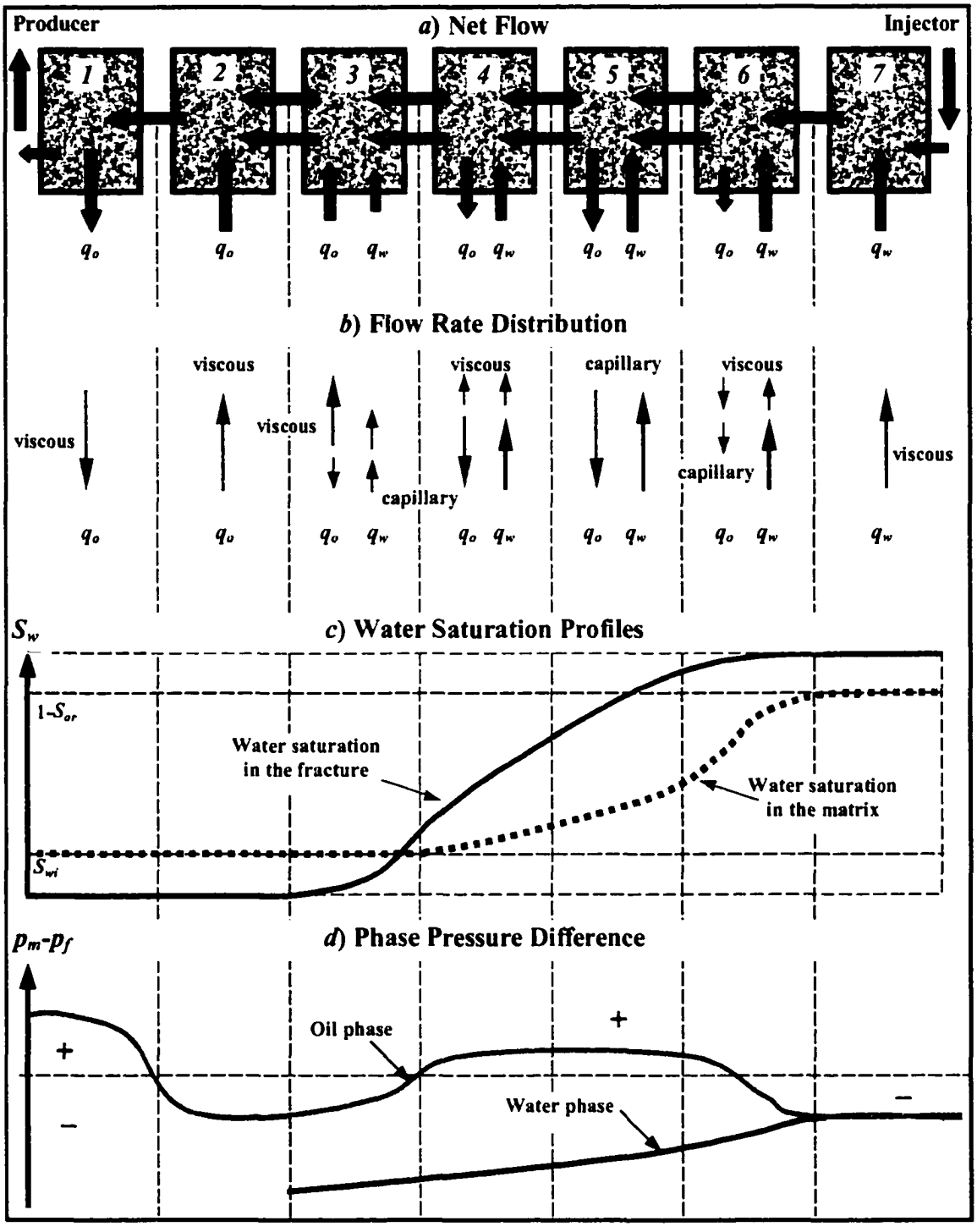

Fig. 7.1 – Seven flow stages may be observed along a fracture during waterflooding. They appear as a result of the interplay of viscous and capillary forces. Initially, oil is produced due to the pressure difference between the matrix and the fracture. Then, oil is produced basically because of capillary forces in the matrix system.

This difference in capillary pressure at the same saturation is even greater when water flows fast enough in the fracture causing the water front in the matrix to stay behind the corresponding water front in the fracture as illustrated in **Fig. 7.1c**. In this case, water velocity in the fracture is not only a function of the injection rate, but also depends on how effective imbibition is. For instance, in a particular situation where strong capillary forces are present, high imbibition rates appear and the water front in the fracture slows down. Once water imbibes into the matrix, oil-phase pressure in the matrix rises, and the consequent positive pressure gradient causes oil to move to the matrix/fracture interface. Phase pressure differences between the matrix pressure and the fracture pressure observed during each stage are presented in **Fig. 7.1d.**

Fluid production causes a pressure drop in the fracture system producing positive pressure gradients in the matrix that cause single-phase interporosity flow to occur during the first stage. At this stage viscous forces control oil recovery from the matrix. Once water is injected, pressure in the fracture system increases causing negative pressure differences between the fracture and the matrix and forcing oil to flow into the matrix (drainage) as represented in stage 2 in Fig. 7.1. As water injection continues, some water imbibes as a result of the combined effect of viscous forces (forced imbibition) and capillary forces (natural imbibition) during stage 3. At this time, viscous forces still dominate the interporosity flow and cocurrent imbibition is observed. Stage 4 represents the case when capillary forces begin to control the interporosity flow and oil phase pressure difference becomes positive. As water saturation increases in the fracture, oil relative permeability approaches a critical value, and capillary forces dominate the

interporosity flow as illustrated in stage 5. Additional information about this flow stage is provided in section 3.1.2, and mathematical modeling is provided in Chapter 6.

Restrictive flow areas at the matrix/fracture interface and the reduction of mobile oil saturation in the matrix causes the interporosity oil rate to decrease in stage 6. At this time, viscous forces begin to dominate as capillary pressure in the matrix approaches the capillary pressure in the fracture. Finally, only water flows along the fracture and across the matrix/fracture interface because of viscous forces at stage 7.

7.3.1.1 Model Formulation

Model formulation is based on a single matrix block in contact with a fracture that is being waterflooded as shown in **Fig. 7.2**. This single matrix block may represent any of the boxes in Fig. 7.1 under a particular flow stage. The interporosity oil rate is given by the sum of oil flow produced across the area that has not been exposed to water and the area where imbibition is taking place. In general, the total oil flow rate is given by:

$$q_o = q_o\big|_{1P} + q_o\big|_{2P} \quad \text{.....7.9}$$

where subscript $1P$ stands for single-phase and $2P$ for two-phase flow regions, respectively. The oil produced from region $1P$ is primarily driven by viscous forces manifested through a pressure gradient, while oil outflow from region $2P$ is the result of capillary forces because of a saturation gradient. Substituting interporosity rate equations Eqs. 4.5 and 6.4 into Eq. 7.9, the following general expression is obtained:

$$q_o = 2F_c\big|_{1P} A_c k_m \left.\frac{k_{ro}}{\mu_o}\right|_{1P} \frac{\left(\overline{p}_{om} - p_{of}\right)}{L} + 2F_c\big|_{2P} A_w k_m \left.\frac{k_{ro}}{\mu_o}\right|_{2P} \frac{\left(\overline{p}_{om} - p_{of}\right)}{L} \quad \text{.....7.10}$$

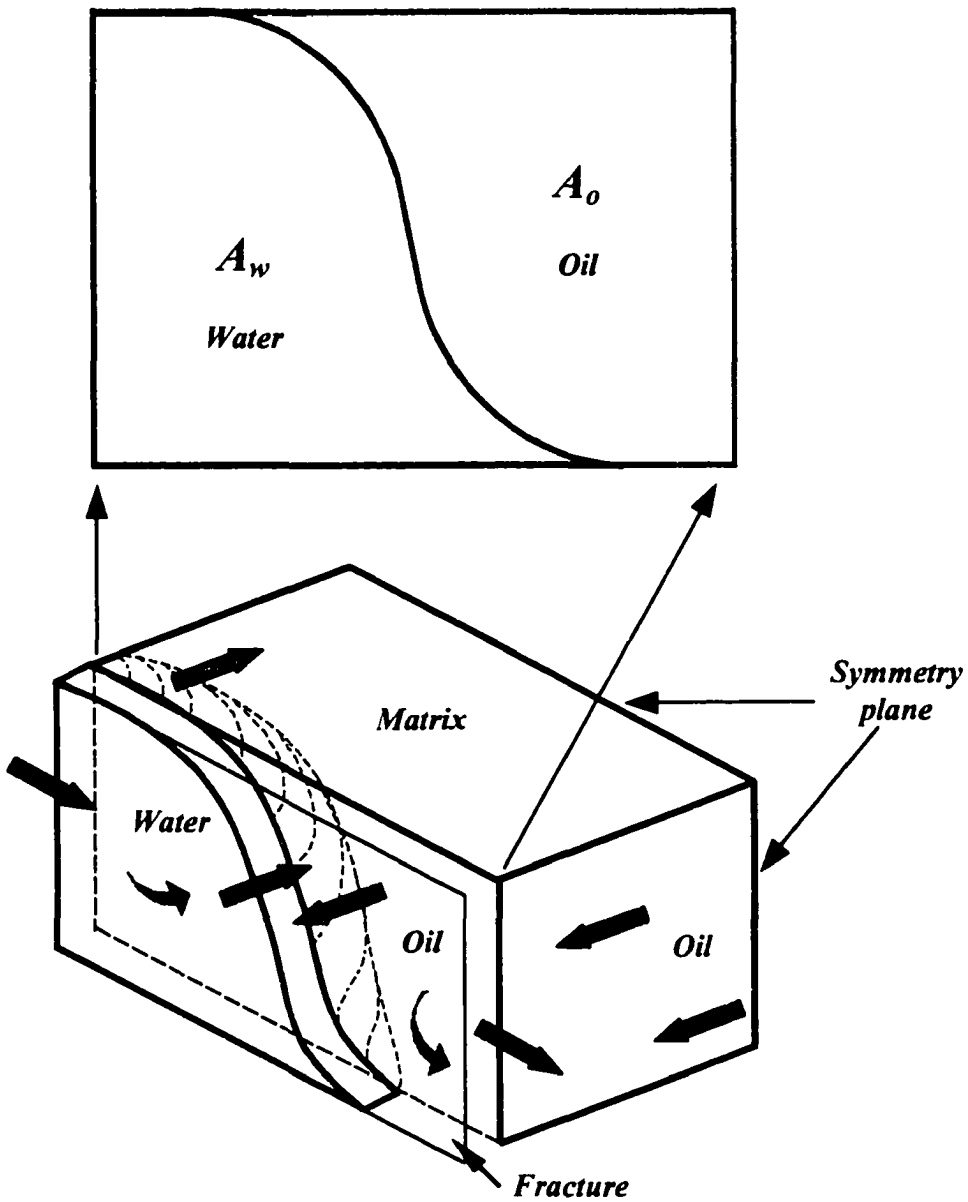

Fig. 7.2 – Water that flows along a fracture contacts matrix surface area causing imbibition to occur. The matrix/fracture interface area for imbibition is proportional to the water saturation in the fracture system. Ahead of water front, oil flows out of the matrix a result of viscous forces active across an area proportional to the oil saturation in the fracture system.

where effective flow areas are computed as linear functions of phase saturation in the fracture as follows:

$$A_o = S_{of} A \quad \text{.....7.11,}$$

and,

$$A_w = S_{wf} A \quad \text{.....7.12.}$$

Note that A_o+A_w would give the total matrix/fracture interface area, A, using the auxiliary expression given by Eq. 7.4. Equations 7.11 and 7.12 assume that fluid flows along fractures with uniform width.

Similarly, interporosity water rate is computed as a result of the interplay between capillary and viscous forces. However, it is assumed in this case that both forces act simultaneously, with capillary forces more predominant at initial stages of imbibition. Once capillary pressures in the matrix and the fracture are equal, viscous forces would control the interporosity water rate. This may be expressed as follows:

$$q_w = 2F_c\big|_{2P} A_w k_m \left.\frac{k_{rw}}{\mu_w}\right|_{2P} \frac{\left(\overline{p}_{wm} - p_{wf}\right)}{L} \quad \text{.....7.13}$$

where effective area for water, A_w, to flow across the interface is given by Eq. 7.12.

7.3.1.2 Single-Phase Flow Correction Factors

A time-dependent flow correction factor when a single-phase fluid flows across the matrix/fracture interface was derived in Chapter 4. The derivation of the correlation assumed a constant pressure at the interface during fluid production from the matrix. This constant pressure at the interface was assumed to be the result of an initial instantaneous

pressure drop in the fracture. However, gradual and slow pressure changes in the fracture may occur when the fractures are not very good fluid conductors and/or oil outflow from the matrix replenishes the fractures fast enough. To consider pressure changes at the interface using results from Chapter 4, the principle of superposition is used. This principle is based on the addition of partial solutions of linear differential equations to provide the complete solution.[75] The application of the superposition principle with Duhamel's theorem was presented by de Swaan[25] in the solution of single-phase well-test problem in fractured media. He computed the interporosity flow rate by using the fluid outflow caused by a unitary pressure drop at the interface. Therefore, the application of the superposition principle to estimate the interporosity flow rate may be written as a convolution as follows:

$$q_o(p_f,t)=\int_0^t q_o(t-\tau)\frac{\partial p_D}{\partial \tau}d\tau \qquad \text{.....7.14}$$

where $q_o(t-\tau)$ is the interporosity oil rate calculated using a constant pressure at the interface. The dimensionless pressure considers the fractional pressure variation with respect to the maximum pressure change that the matrix block will experience and is given as follows:

$$p_D=\frac{p_i-p_f}{p_i-p_{f\max}} \qquad \text{.....7.15}$$

The expression given in Eq. 7.14 is equivalent to the interporosity flow equation used by de Swaan to obtain analytic solutions for determining naturally fractured reservoir properties by well testing in which the fractured formation is considered isotropic and

homogenous. In this study, Eq. 7.14 is used to obtain numerical solutions where the fracture media may be highly anisotropic and heterogeneous.

A numerical simulation test was designed to check the importance of using a time-dependent flow correction factor. Input data for this test are given in **Table 7.1** and output data is shown in **Fig. 7.3**.

TABLE 7.1 – RESERVOIR DATA FOR THE NUMERICAL SIMULATION TEST

Matrix porosity, ϕ_m, *fraction*	0.18
Matrix permeability, k_m, md	0.0167
Matrix compressibility, c_m, psi^{-1}	1.32×10^{-5}
Fracture porosity, ϕ_f, *fraction*	0.02
Fracture permeability, k_f, md	40
Fracture compressibility, c_f, psi^{-1}	1.32×10^{-5}
Fluid viscosity, μ, cp	2
Formation volume factor, B_o, RB/STB	1.23
Initial pressure, p_i, psia	4000
Production rate, Q_o, STB/D	115
Reservoir thickness, h, ft	20
Fracture spacing, L, ft	9.07
Wellbore radius, r_w, ft	0.316

Input data represent the same reservoir used by Warren and Root[17] with total storativity $\phi_m c_m + \phi_f c_f = 2.64\times10^{-6}$ psi^{-1}, interporosity parameter $\lambda = 5\times10^{-6}$, and storativity ratio $\omega = 0.1$. Pressure drawdown in a well located at the center of a cylindrical reservoir was simulated with a 80×80×1 parallel Cartesian grid with the well located at the gridblock labeled (1,1,1). Gridblock sizes logarithmically increase in the x- and y-directions with $\Delta x = \Delta y = 5$ ft at block (1,1,1). A maximum block size of $\Delta x = \Delta y =$

46.7 ft was used at (80,80,1) to complete a square grid system of total side length of 1500 ft. Boundary and gridblock size effects were avoided with this grid configuration for the simulation results presented in Fig. 7.3.

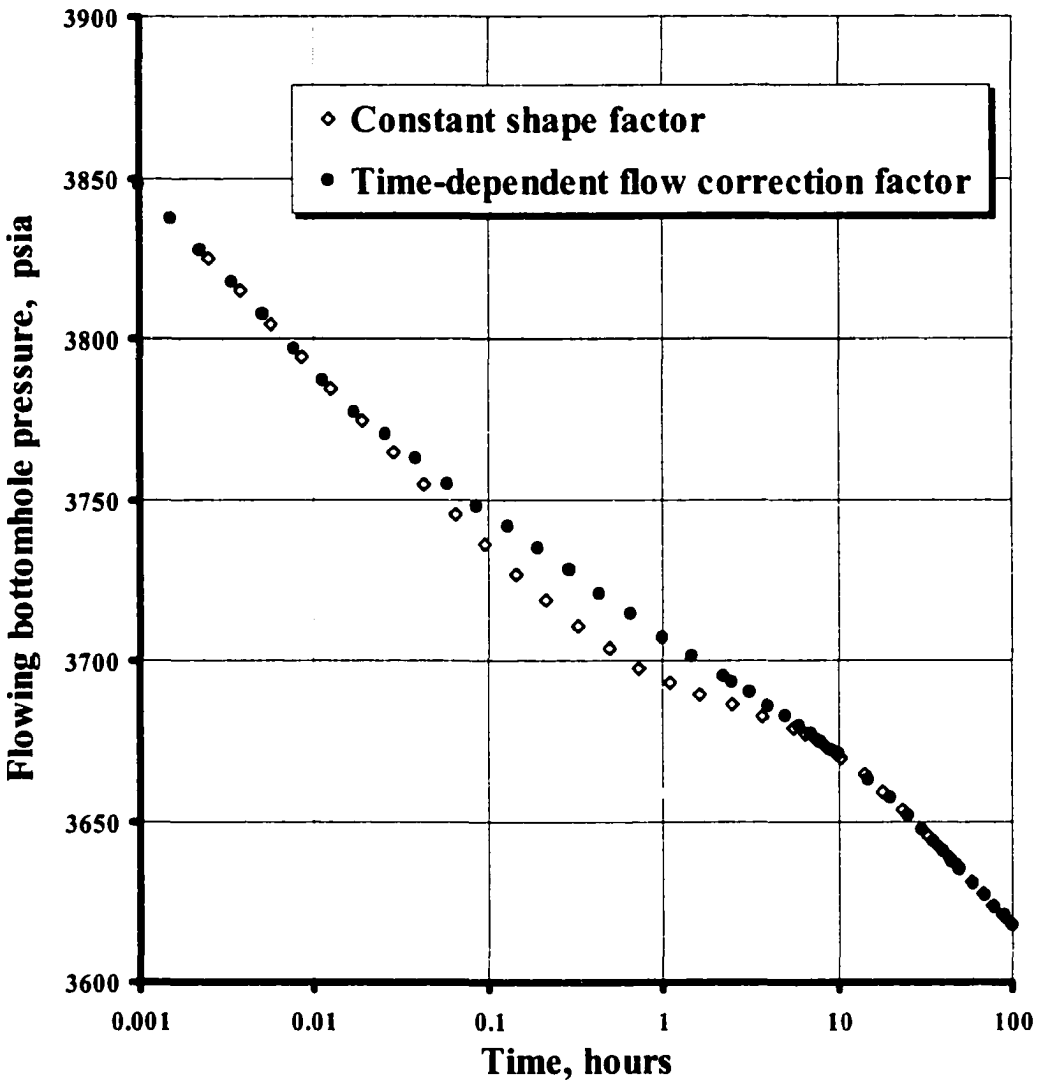

Fig. 7.3 – Pressure drawdown in a naturally fractured reservoir. Time-dependent effects are seen in a well test during the transition between the typical two straight lines. This flow period may or may not be seen during a pressure test depending on the wellbore storage effects. However, for long term numerical simulation, pressure transient effects in the matrix because of a single-phase interporosity flow may be ignored.

Typically, transient effects are not considered important in field scale problems[74] because the impact in the long term reservoir behavior is negligible such as in the case shown in Fig. 7.3. After 10 hours of production, time-dependent effects in the interporosity flow disappear and constant shape factors that consider the steady-state pressure gradient are sufficient. Results presented in Chapter 4 suggest that constant shape factors derived by Lim and Aziz[31] are good approximations. In terms of flow correction factors, F_c = 2.47 is in close agreement with fine grid simulation of 1D interporosity flow.

7.3.1.3 Two-Phase Flow Correction Factors

The use of Eqs. 7.11 and 7.12 accounts for the saturation variation at the matrix/fracture interface, making the results presented in Chapter 6 applicable to the present general model for interporosity flow. However, the flow correction factor for the water phase is not the same as for the oil phase. In the following, the approach used for the oil phase is applied for the water phase in order to compute the appropriate flow correction factor to be used in Eq. 7.13.

The necessity of deriving a flow correction factor for the water phase is concluded from the analysis of numerical simulation results observed in **Figs. 7.4** and **7.5.** Input data for this numerical simulation are given in Table 6.1 and details about the grid system are provided in Chapter 6. In Fig. 7.4, the average oil-phase pressure, for instance at t = 5 days, is indicated by a horizontal line that intersects the pressure curve from which it was computed. The distance from the matrix/fracture interface to the intersection point is Δx.

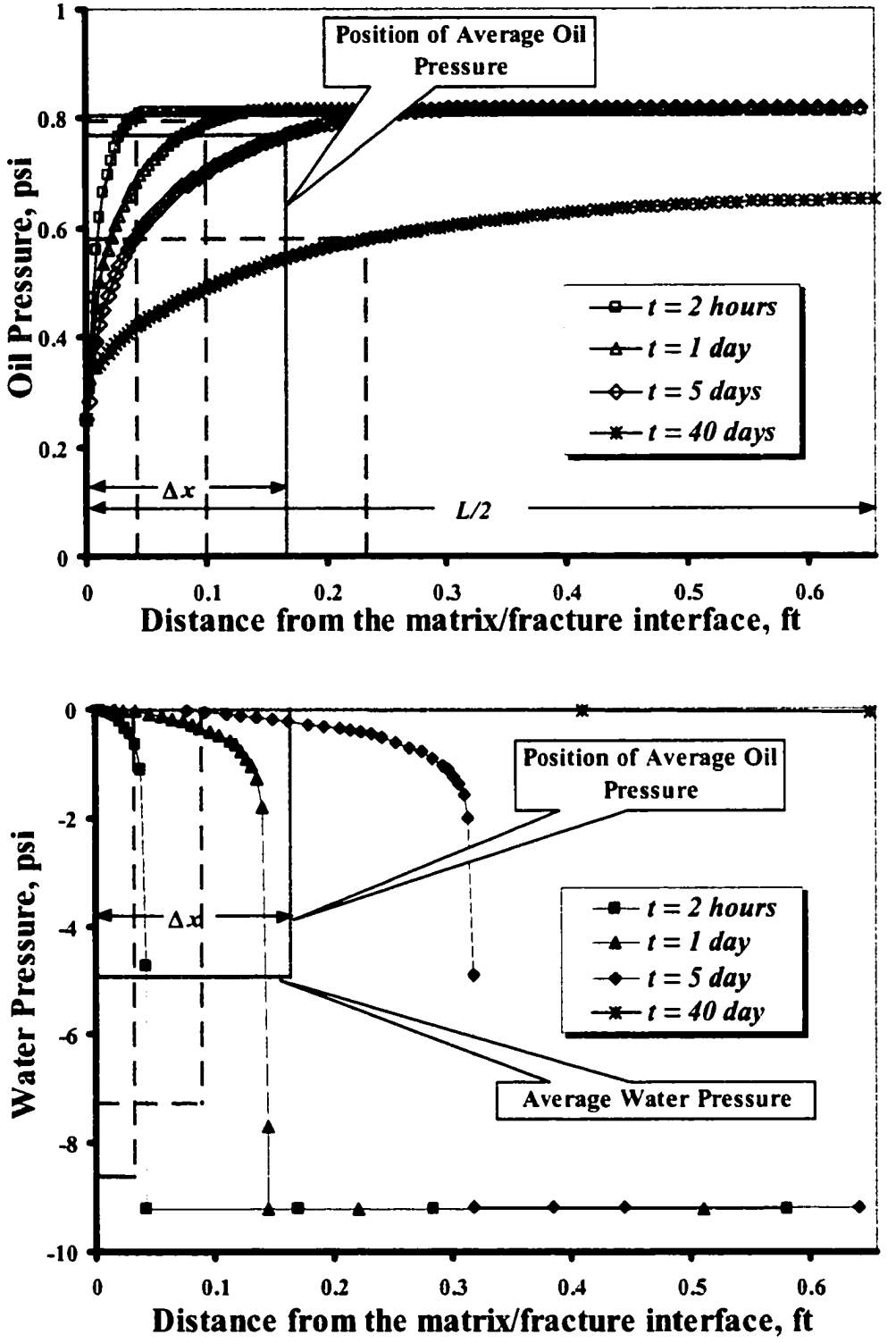

Fig. 7.4 – The position of the average oil pressure does not coincide with the position of the average water pressure, for instance at t = 5 days. The difference in locations of these two points is caused by the capillary pressure in the matrix block.

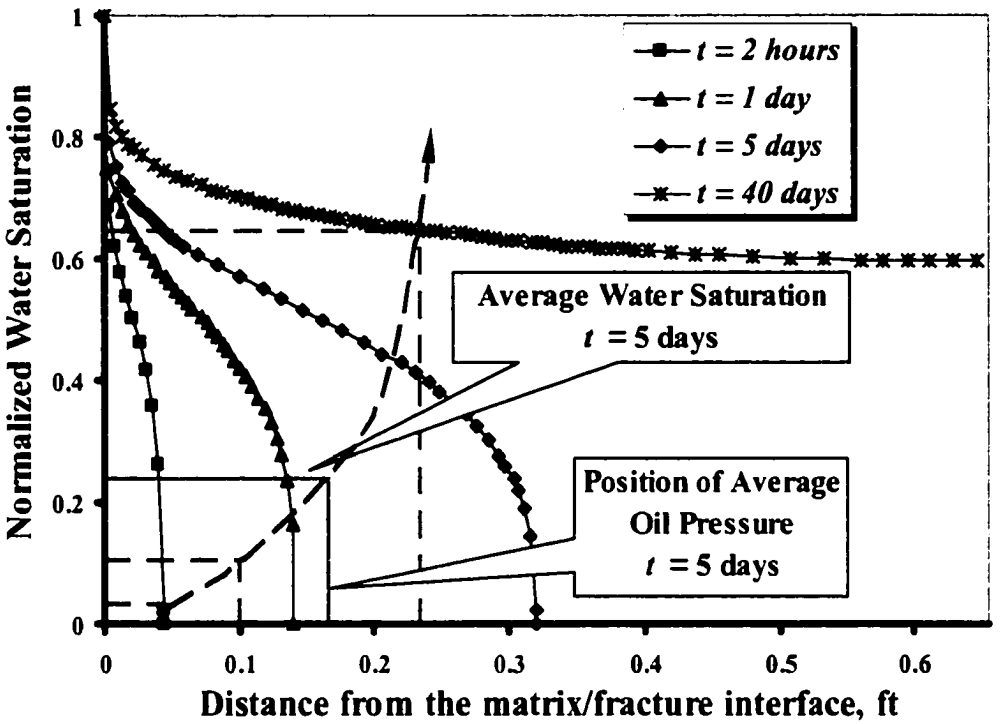

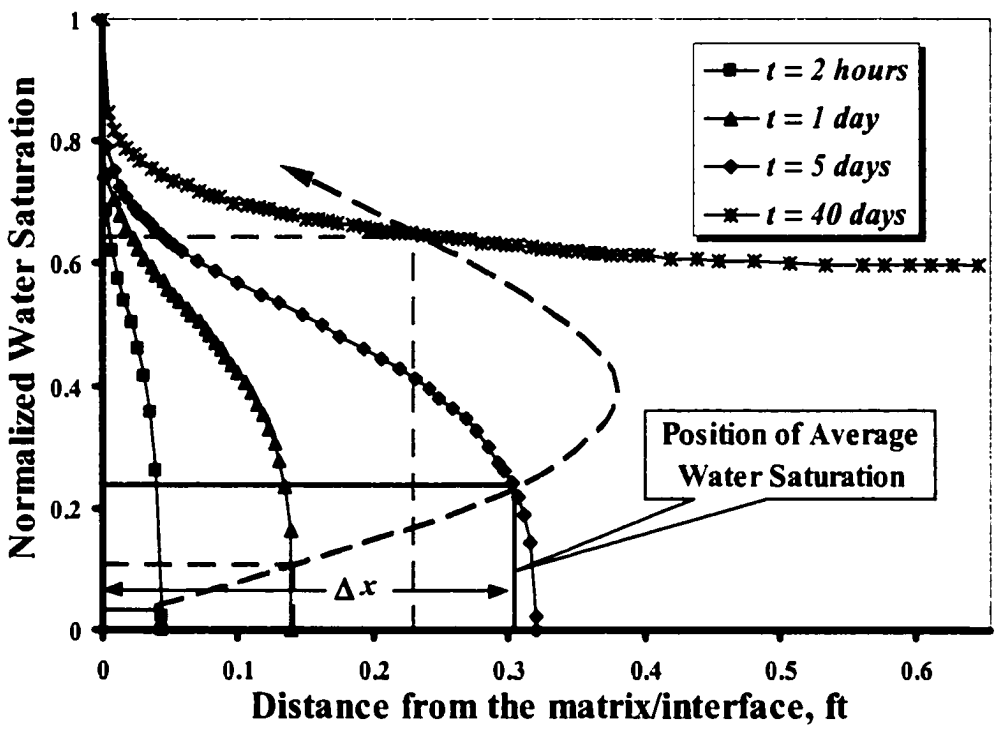

Fig. 7.5 – The position of the average oil pressure does not always coincide with the position of the average water saturation, for instance at t = 5 days. The distance of average saturation value on the water saturation curve, Δx, goes to a maximum and then reduces.

If the distance Δx is plotted along with the average value of water pressure at t = 5 days in a figure of water pressure as a function of position, x, the intersection point would not be on the water pressure curve. This observation implies that two different Δx are needed to describe the transient effects of pressure gradients in the matrix block. Because Δx for oil phase in Eq. 6.3 would be different if a similar expression is written for the water phase, a different time-dependent flow correction factor is required to compute the interporosity flow rate for the water phase using an expression similar to Eq. 6.4. This conclusion is also obtained by observing the intersection point of the average oil-phase pressure and the average water saturation in Fig. 7.5, for instance at t = 5 days.

An important difference in the transient behavior of the pressure gradients is better seen in Fig. 7.5. In the case of the oil phase, Δx increases from a value of zero to a steady state value between the matrix/fracture interface and the matrix-block mid point. This variation is captured by a F_c that decreases from very large values to a steady-state value computed for single-phase flow, F_c = 2.47 (see Figs. 5.1 and 6.3). On the other hand for the water phase, Δx initially increases to reach a maximum and then decreases.

Therefore, the F_c for water should decrease until it reaches a minimum and then should increase to obtain the typical value for single-phase flow, F_c = 2.47.

This discussion is confirmed by computing the time-dependent flow correction factor for the water phase using output data from numerical simulations presented in Chapter 6. This correlation is based on the interporosity rate given by:

$$q_w = F_c A k_m \frac{k_{rw}}{\mu_w} \frac{\left(\overline{p}_{wm} - p_{wf}\right)}{\frac{L}{2}} \qquad \text{.....7.16}$$

Thus, the flow correction factor for the water phase can be computed from fine-grid numerical simulations and Eq. 7.16 as follows:

$$F_c = \frac{q_w \mu_w L}{2Ak_m k_{rw}^{\bullet}\left(\overline{p}_{wm} - p_{wf}\right)} \quad \text{.....7.17}$$

Data to compute F_c from Eq. 7.17 is the same as used in Chapter 6. In this case, there is no problem with the relative permeability at the matrix/fracture interface, since the value is very close to the end point of the relative permeability curve for a water-wet system. A difficulty is found during the estimation of F_c from Eq. 7.17 because the difference between the average water pressure in the matrix and the fracture tends to zero at the latest stages of the imbibition process when capillary forces are weak as observed in **Fig. 7.6**. In this figure, dimensionless time given by Eq. 6.12 is used. A correlation that fits the data for the time-dependent flow correction factor shown in **Fig. 7.7** is given by the following expressions:

$$F_c = 1.0\times10^{-1}\left(1+\frac{1.20\times10^{-2}}{t_D}\right),\ t_D \le 0.3 \quad \text{.....7.18,}$$

$$F_c = 1.0\times10^{-1}\left(1+2.75\times10^{-1}t_D^2\right),\ 0.3 < t_D \le 4 \quad \text{.....7.19,}$$

and,

$$F_c = 7.37\times10^{-3}\left(-t_D^2+4.03\times10^{1}t_D-7.12\times10^{1}\right),\ 4 < t_D \le 20 \quad \text{.....7.20.}$$

For $t_D > 20$, a flow correction factor value of $F_c = 2.47$ should be used since, at that time, the only mobile phase would be water, and the flow correction factor for single-phase flow applies.

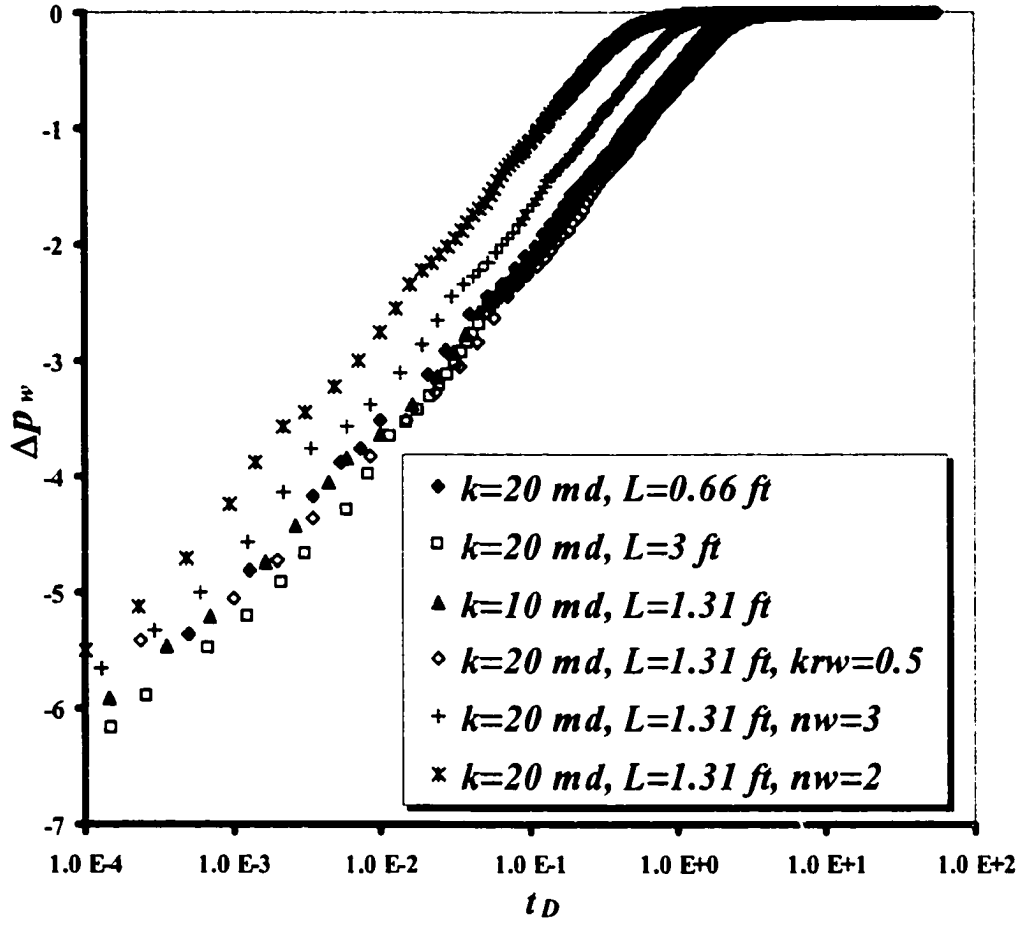

Fig. 7.6 –Difference between the average water-phase pressure in the matrix and the water pressure in the fracture reduces to almost zero at a dimensionless time corresponding to the transition time computed from Eq. 6.16 and shown in Fig. 6.3. At transition time, water fronts coming from two parallel fractures interfere with each other at the matrix-block center (see Fig. 6.4).

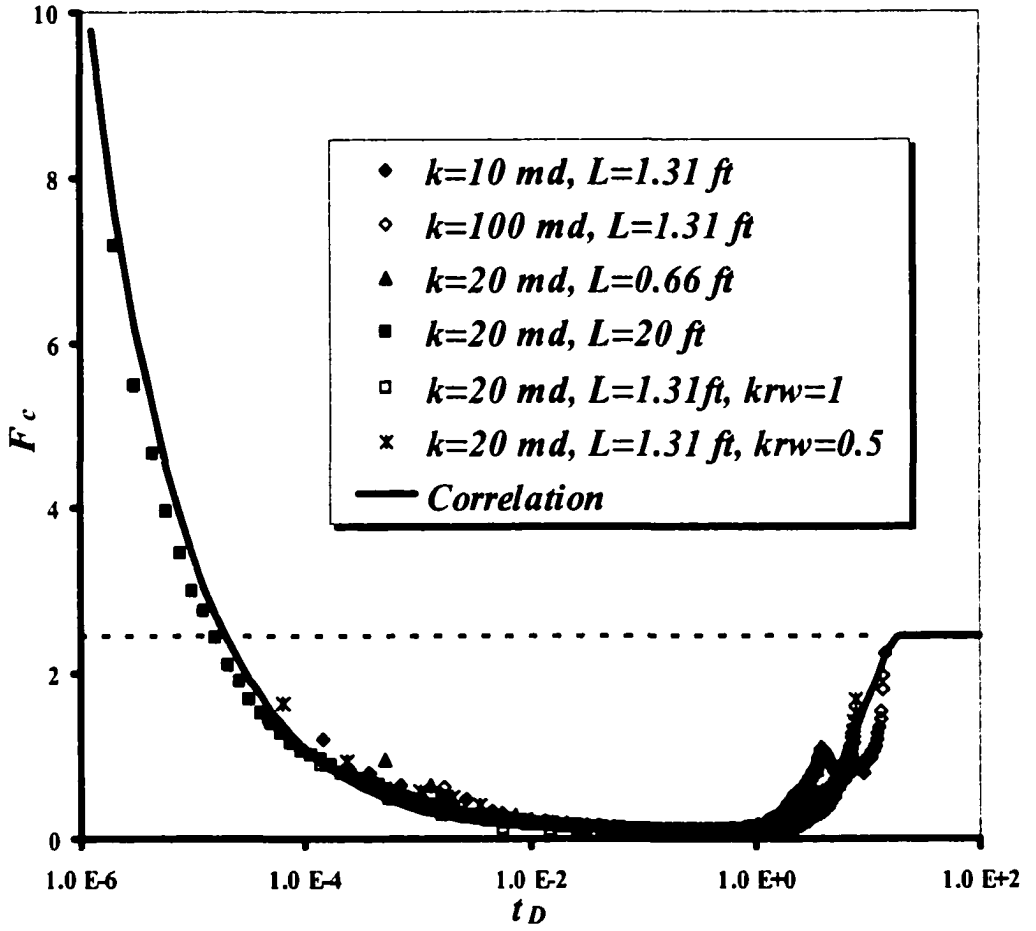

Fig. 7.7 – Time-dependent flow correction factor derived for the water phase. Before the dimensionless transition time, t_{Dt}, the F_c curve resembles the single-phase flow correlation. After t_{Dt}, division by very small values of pressure differences (see Fig. 7.6) causes some numerical errors. Data points in this part of the figure are used to generate a correlation that best fit the general trend toward the known value of F_c for single-phase flow.

7.3.2 Numerical Solution

Formulae previously presented in this chapter were implemented in a dual-porosity, dual-permeability model. A simulation run using input data described in Appendix C was performed and output was compared with results using a constant shape factor.

Numerical simulation results plotted in **Figs. 7.8** and **7.9** indicate that the proposed model predicts earlier water breakthrough with a more rapid oil production rate decline after breakthrough than models that use a constant shape factor. After 8 years of production, oil production would be more stable according to the proposed model than the one predicted with a constant shape factor.

These results can be explained based on two important characteristics of the present model: the ability to capture the time-dependent effects of saturation gradients and the consideration of fluid mobility restrictions at the matrix/fracture interface.

This study has shown that it is very important to take into account the water front shifting from the matrix/fracture interface to the matrix-block center. This physical phenomenon causes the presence of initially high flow correction factors and, consequently, high interporosity rates.

However, as water imbibes into the matrix, the flow correction factor for water indicates a slowing water motion because of the oil phase pressure gradient. Water pressure and oil pressure gradients are in opposite direction, causing an additional restriction to water flow. After the water front reaches the matrix-block center, small quantities of oil flow in the matrix, producing a reestablishment of the ability of water to move as if it were a single phase in the matrix block. Thus, the increase of water saturation at the interface limits the ability of oil to move into the fracture.

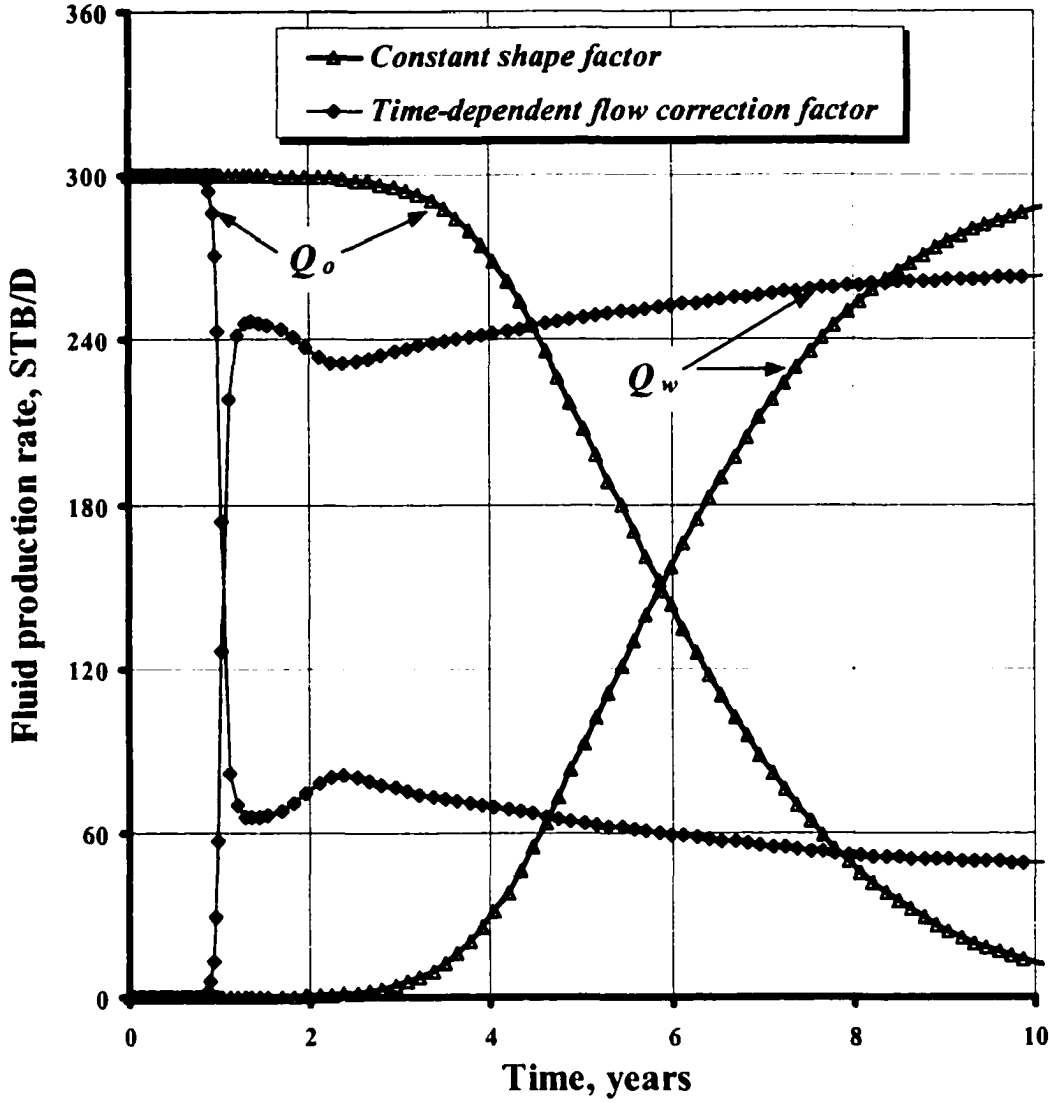

Fig. 7.8 – Proposed model predicting an early water breakthrough because it considers the restriction to oil outflow as a result of high water saturation at the interface, and the restriction to water imbibition as a result of oil-pressure gradients in the matrix. Water-pressure and oil-pressure gradients are vector quantities with the same orientation but opposite direction during countercurrent imbibition.

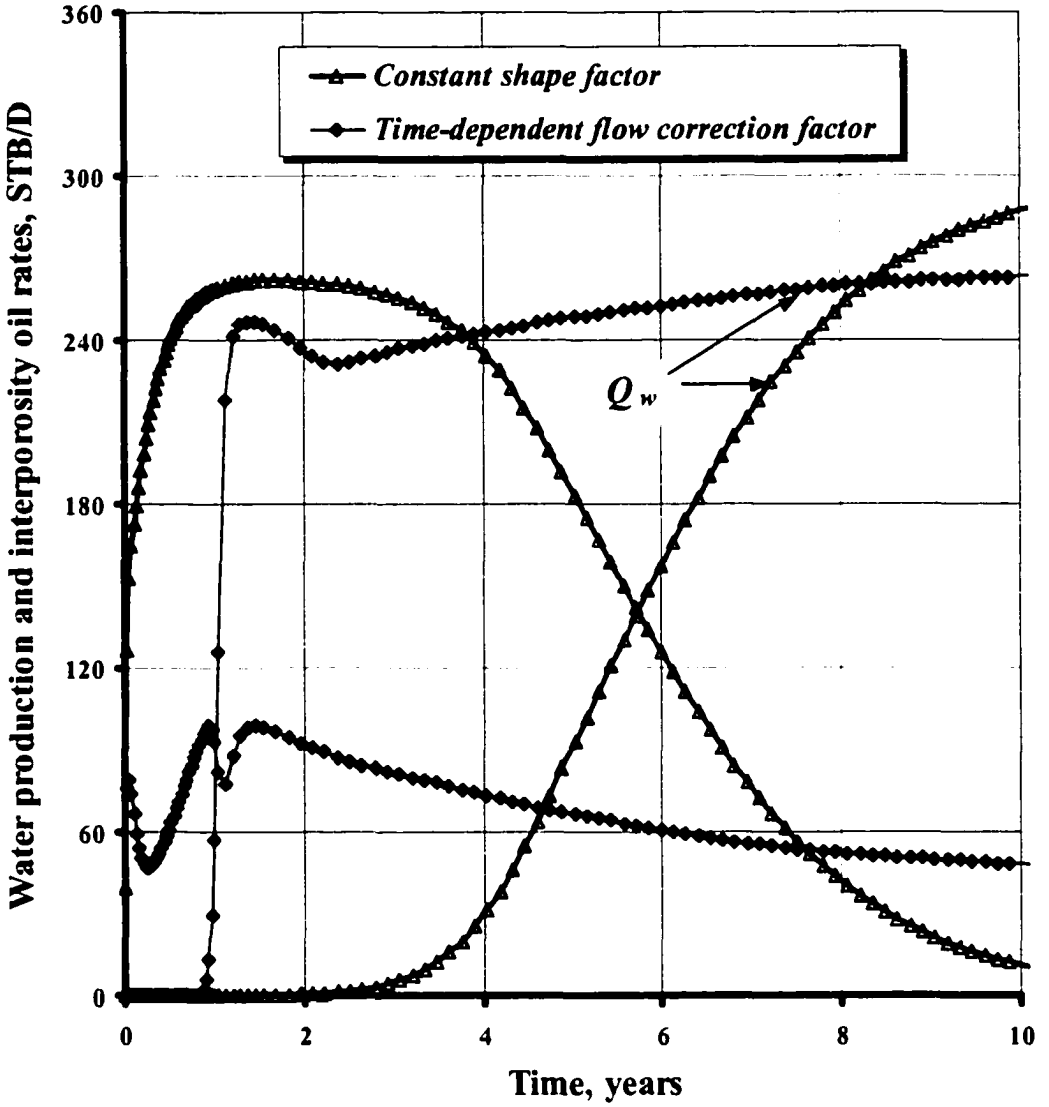

Fig. 7.9 – Because the time-dependent flow correction factors derived in the present study predict lower interporosity oil rates, more water flows along the fracture causing water breakthrough to occur earlier than the prediction assuming a constant shape factor approach. Once high water saturations are present in the fracture, the proposed model predicts higher interporosity rates; and, therefore, higher oil production rates (see Fig. 7.8).

This interference is better considered in the proposed model. Common approaches use oil relative permeability evaluated at the average water saturation in the matrix to compute the oil expelled from the matrix when water is imbibing. As seen in Fig. 6.10, interporosity flow rate is over-predicted by not taking into account the restriction to oil outflow at the interface. In this particular example of waterflooding, the water breakthrough time and oil recovery predicted by the present model are about the half of those predicted by current numerical simulators using constant shape factors, based on a 10 year simulation.

CHAPTER 8

CONCLUSIONS AND RECOMMENDATIONS

8.1 Conclusions

- An interporosity flow equation considering time-dependent effects due to the shifting of the average oil-pressure and water-saturation locations in the matrix block from the fracture face to the block center during matrix-fracture flow can be adequately incorporated in a standard finite-difference scheme.

- Darcy's law may be used to compute the interporosity flow rate for the oil phase if a correction factor that accounts for the shifting of the average pressure and saturation position within the matrix block is defined.

- Fine-grid numerical simulation allowed the development of dimensionless correlations for flow correction factors for single-phase, gas-condensate and immiscible two-phase systems.

- The interporosity rate is strongly dependent on the matrix pressure gradient. For single-phase systems, numerical experiments indicated that the flow correction factor curve remains nearly unchanged in spite of pressure gradient distortions. This fact

validates the use of the proposed flow correction factor to situations where low fracture permeability (dual-permeability situations) and intersecting fractures are present.

- Time-dependent flow correction factor effects were shown to be more important in oil recovery by water injection than the single-phase fluid production during reservoir depletion of a naturally fractured reservoir. In the immiscible two-phase system, there is a slow moving saturation gradient that propagates across the matrix in addition to the rapidly moving pressure gradient.

- The flow correction factor for single-phase flow converges to a steady-state value at a speed proportional to the reciprocal of total compressibility, while the flow correction factor for two-phase flow converges at a speed proportional to the slope obtained from the capillary pressure curve evaluated at the average water saturation present at the matrix/fracture interface. Therefore, the single-phase flow correction factor converges much more rapidly to its steady-state value than the two-phase flow correction factor.

- Time-dependent flow correction factor effects on single-phase interporosity flow are important in short flow tests such as transient pressure tests. However, transient effects in single-phase systems may be neglected for long-term production forecasts. For immiscible two-phase systems, time-dependent effects cannot be neglected.

- For two-phase interporosity flow, the water front shifting is primarily driven by capillary forces. Therefore, the previously proposed constant shape factors do not accurately represent the physical processes involved during water imbibition in a water-wet matrix block. The variable flow correction factors provide a better model for interporosity mass exchange because they are functions of the variables controlling the imbibition process as well as variables readily obtained from the simulator.

- For gas-condensate systems, the use of pseudofunctions is necessary to apply the correlation developed for single-phase systems in the estimation of the interporosity flow rate. The pseudopressure function includes the effect of relative permeability reduction due to the presence of the condensate while the pseudotime function accounts for the fluid compressibility effects. An approximation to compute the integral for the average pseudopressure was also discussed.

- The proposed interporosity flow rate equation incorporates both fracture and matrix geometric characteristics while retaining effective fluid mobility at the matrix/fracture interface as the main restriction to flow.

- The new interporosity flow rate equation is convenient to implement in current dual-porosity, dual-permeability reservoir simulators, and properly accounts for the physics of the imbibition processes. An approach to handle the interplay between the viscous and capillary force effects on the interporosity flow was proposed.

- Neglecting the time-dependency of the shape factor can introduce significant errors in numerical simulation of waterflooding in naturally fractured reservoirs. Compared with the constant shape factor approach, a numerical simulation example showed shorter water breakthrough times and more stable oil production rates after breakthrough.

8.2 Recommendations

- The Darcy's law assumption presents the interporosity flow rate to be directly proportional to the matrix/fracture interface area. An approach proposed in this study, assuming fractures as parallel plates, requires an average fracture aperture. Methodologies to obtain realistic interface areas or fracture apertures are required. Values obtained in cores, well logs, and outcrops may not be representative of the actual values for these fracture properties in the reservoir because of the space variability of fractures and the effect of the in-situ stresses. However, values measured from cores, well logs and outcrops should be used as a starting point.

- Motion of a water front down in a fracture could be represented by a single flow correction factor that accounts for three flow regimes. First, a flow period where the fracture is being depleted while some imbibition takes place. Second, a flow period where matrix is being depleted because of the countercurrent imbibition before the water front reaches the matrix-block center. Finally, matrix depletion by imbibition after water fronts are interfering each other at the matrix-block center. This approach

requires the average or representative fracture length besides the fracture spacing. Such an approach was not explored in this study and is recommended.

- Effects on the flow correction factor because of fractures intersecting at different angles should be considered. This study concluded that some pressure gradient distortions caused by high permeability ratios result in some insignificant effects on interporosity flow. However, by definition, the flow correction factor is a function of how a pressure gradient propagates in a matrix block with a specific shape (not size), and therefore, fractures intersecting at different angles within a simulation gridblock may cause significant deviations from the proposed flow correction factor correlation.

- Effects due to matrix and fracture deformation should be incorporated in the derivation of flow correction factors. It is well known that in some naturally fractured reservoirs the geomechanics aspects such as the in-situ stress and the poroelastic behavior of fractured rocks play an important role in hydrocarbon recovery. The geomechanics effects are observed in variations of the stress-dependent permeability and porosity, which are important parameters in computing flow correction factors.

NOMENCLATURE

a = Matrix/fracture interface flow constant

A = Total fracture area, ft^2

A_o = Half fracture area, ft^2

B_α = Formation volume factor of phase α, rb/STB

c_f = Fracture compressibility, psi^{-1}

c_m = Matrix compressibility, psi^{-1}

c_t = Total compressibility, psi^{-1}

C_1, C_2, C_3 = Constants in the flow correction factor correlation

D = Reservoir depth, ft

f_{kn} = Parameter in Eq. 6.13, dimensionless

F_c = Flow correction factor, dimensionless

g = Acceleration of gravity, ft/sec^2

k = Absolute permeability, md

k_{ro} = Relative permeability to oil, dimensionless

k_{ro}^* = End-point of the relative permeability to oil, dimensionless

k_{ro}^o = Relative permeability to oil at the matrix/fracture interface, dimensionless

k_{rw} = Relative permeability to water, dimensionless

k_{rw}^* = End-point of the relative permeability to water, dimensionless

n_o = Exponent of the relative permeability to oil, dimensionless

n_w = Exponent of the relative permeability to water, dimensionless

n = Number of normal sets of fractures

L = Fracture spacing, ft

L_f = Fracture length, ft

q = Interporosity flow rate, rb/day

q_t = Interporosity molar rate, lb-mole/day

$\tilde{q}_\alpha$ = Interporosity flow rate per unit volume of rock, day^{-1}

Q = Flow rate, STB/D

p = Pressure, psia

p_c = Capillary pressure, psia

S_{iw} = Connate water saturation, fraction

S_{or} = Residual oil saturation, fraction

S_w^* = Water saturation at the matrix/fracture interface, fraction

S_α = Saturation of phase α, fraction

t = Time, days

t_{Dt} = Dimensionless transition time

V = Bulk volume, ft^3

w_f = Fracture width, ft

β = Matrix/fracture interface flow constant

γ = Matrix/fracture interface flow constant

ϕ = Porosity, fraction

μ = Viscosity, cp

ρ = Density, lb/ft^3

Φ = Flow potential, psia

σ = Shape factor, ft^{-2}

ω_K = Permeability ratio, dimensionless

Subscripts

b = Bubble point

D = Dimensionless

f = Fracture

i = Initial value

m = Matrix

o = Oil or condensate phase

p = Pseudofunction

w = Water phase

x = x-direction

y = y-direction

z = z-direction

α = Water or oil phase

REFERENCES

1. Jaeger, J.S. and Cook, N.G.W.: *Fundamentals of Rock Mechanics*, third edition, Chapman and Hall Ltd., New York City (1979).
2. Aguilera, R.: *Naturally Fractured Reservoirs*, second edition, PennWell Pub. Co., Tulsa (1995).
3. Reiss, L.H.: *The Reservoir Engineering Aspects of Fractured Reservoirs*, Golf. Pub. Co., Houston (1980).
4. van Golf-Racht, T.D.: *Fundamentals of Fractured Reservoir Engineering*, Elsevier Scientific Pub. Co., Amsterdam (1982).
5. Nelson, R.A.: *Geologic Analysis of Naturally Fractured Reservoirs*, Golf. Pub. Co., Houston (1985).
6. *Rock Fractures and Fluid Flow: Contemporary Understanding and Applications*, Committee on Fracture Characterization and Fluid Flow, National Academy Press, Washington, D.C. (1996).
7. Livak, B.L.: "Simulation and Characterization of Naturally Fractured Reservoirs," Prod., Reservoir Characterization Technical Conference, Dallas, Academic Press, New York City (1985).
8. Gilman, J.R. and Kazemi, H.: "Improved Calculations for Viscous and Gravity Displacement in Matrix Blocks in Dual-Porosity Simulators," *JPT* (Jan. 1988) 60-70.

9. Firoozabadi, A. and Ishimoto, K: "Theory of Reinfiltration in Fractured Porous Media: Part I – One-Dimensional Model," paper SPE 21796 presented at the Western Regional Meeting, Long Beach, California, March 20-22, 1991.

10. Barkve, T. and Firoozabadi, A.: "Analysis of Reinfiltration in Fractured Porous Media," paper SPE 24900 presented at the Annual Technical Conference and Exhibition, Washington, D.C., Oct. 4-7, 1992.

11. Labastie, A.: "Capillary Continuity between Blocks of a Fractured Reservoir," paper SPE 20515 presented at the SPE Annual Technical Conference and Exhibition, New Orleans, Sept. 23-26, 1990.

12. Tan, J.C.T. and Firoozabadi, A.: "Dual-Porosity Simulation Incorporating Reinfiltration and Capillary Continuity Concepts: Part I – Single Gridcell," paper SPE 29113 presented at the SPE Reservoir Simulation Symposium, San Antonio, Feb. 12-15, 1995.

13. Bourbiaux, B. and Kalaydjian, F.J.: "Experimental Study of Cocurrent and Countercurrent Flows in Natural Porous Media," *SPERE* (Aug. 1990) 361-368.

14. Pooladi-Darvish, M. and Firoozabadi, A.: "Cocurrent and Countercurrent Imbibition in a Water-Wet Matrix Block," *SPEJ* (March 2000) 3-11.

15. Reis, J. and Cil, M.: "Analytical Models for Capillary Imbibition: One-Dimensional Matrix Blocks," *In Situ* (1999) **23** (3) 243-270.

16. Agarwal, B., Hermansen, H., Sylte, J.E., and Thomas, L.K.: "Reservoir Characterization of Ekofisk Field: A Giant, Fractured Chalk Reservoir in the Norwegian North Sea – History Match," *SPEREE* (Dec. 2000), 534-543.

17. Warren, J.E. and Root, P.J.: "The Behavior of Naturally Fractured Reservoirs," *SPEJ* (Sep. 1963) 245-255.

18. Kazemi, H.: "Pressure Transient Analysis of Naturally Fractured Reservoirs with Uniform Fracture Distribution," *SPEJ* (Dec. 1969) 451-462; *Trans.*, AIME, **246**.

19. Abdassah, D. and Ershaghi, I.: "Triple-Porosity Systems for Representing Naturally Fractured Reservoirs," *SPEFE* (April 1986) 113-127.

20. Barenblatt, G.I., Zheltov, I.P., and Kochina, I.N.: "Basic Concepts in the Theory of Seepage of Homogenous Liquids in Fissured Rocks (Strata)," *J. Appl. Math. Mech.* (1960) 24, 1286-1303.

21. Hill, A.C. and Thomas, G.W.: "A New Approach for Simulating Complex Fractured Reservoirs," paper SPE 13537 presented at the SPE Reservoir Simulation Symposium, Dallas, Feb. 10-13, 1985.

22. Bourbiaux, B., Granet, S., Landereau, P., Noetinger, B., Sarda, S., and Sabathier, J.C.: "Scaling Up Matrix-Fracture Transfer in Dual-Porosity Models: Theory and Application," paper SPE 56557 presented at the SPE Annual Technical Conference and Exhibition, Houston, Oct. 3-6, 1999.

23. Evans, R.D.: "A Proposed Model for Multiphase Flow Through Naturally Fractured Reservoirs," *SPEJ* (Oct. 1982) 669-680.

24. Kazemi, H. and Gilman, J.R.: *Multiphase Flow in Fractured Petroleum Reservoirs*, in Bear, J., Tsang, C-F, and de Marsily, G. (Eds.): *Flow and Contaminant Transport in Fractured Rock*, Academic Press, Inc., San Diego, California (1993).

25. de Swaan, A.: "Analytic Solutions for Determining Naturally Fractured Reservoir Properties by Well Testing," *SPEJ* (June 1976) 117-122; *Trans.*, AIME, **261**.

26. Najurieta, H.L.: "A Theory for Pressure Transient Analysis in Naturally Fractured Reservoirs," *JPT* (July 1980) 1241-1250.

27. Penuela, G., Civan, F., Hughes, R.G., and Wiggins, M.L.: "Time-Dependent Shape Factors for Interporosity Flow in Naturally Fractured Gas-Condensate Reservoirs," paper SPE 75524 presented at the SPE Gas Technology Symposium, Calgary, April 30 – May 2, 2002.

28. Kazemi, H., Merrill, L.S., Porterfield, K.L., and Zeman, P.R.: "Numerical Simulation of Water-Oil Flow in Naturally Fractured Reservoirs," *SPEJ* (Dec. 1976) 317-326.

29. Thomas, L.K., Dixon, T.N., and Pierson, R.G.: "Fractured Reservoir Simulation," *SPEJ* (Feb.1983) 42-54.

30. Coats, K.H.: "Implicit Compositional Simulation of Single-Porosity and Dual-Porosity Reservoirs," paper SPE 18427 presented at the SPE Reservoir Simulation Symposium, Houston, Feb. 6-8, 1989.

31. Lim, K.T. and Aziz, K.: "Matrix-Fracture Transfer Shape Factors for Dual-Porosity Simulators," *J. Pet. Sci. and Eng.* (1995) 13, 169-178.

32. Quintard, M. and Whitaker, S.: "Transport in Chemically and Mechanically Heterogeneous Porous Media," *Adv. in Water Res.*, (1996) **19** (1), 29-60.

33. Noetinger, B. and Estebenet, T.: "Application of Random Walk Methods on Unstructured Grid to Up-Scale Fractured Reservoirs," paper presented at the 1998 European Conference on Mathematics of Oil Recovery, Peebles, Scotland, Sep 8-11.

34. Noetinger, B., Estebenet, T., and Landereau, P.: "Up-scaling of Double Porosity Fractured Media Using Continuous-Time Random Walks Methods," *Transport in Porous Media*, (2000) **39** (3), 315-337.

35. Duguid, J.O. and Lee, P.C.Y.: "Flow in Fractured Porous Media," *Water Resour. Res.* (1977) **13** (3), 558-566.

36. Birks, J.: "A Theoretical Investigation into the Recovery of Oil from Fissured Limestone Formations by Water-Drive and Gas Cap Drive," *Proc.*, Fourth World Pet. Cong., Rome (1955) 425-440.

37. Aronofsky, J.S., Masse, L., and Natanson, S.G.: "A Model for the Mechanism of Oil Recovery from the Porous Matrix Due to Water Invasion in Fractured Reservoirs," *Trans.*, AIME (1958) **213**, 17-19.

38. Mattax, C.C. and Kyte, J.R.: "Imbibition Oil Recovery from Fractured, Water-Drive Reservoirs," *SPEJ.* (June 1962) 177-184; *Trans.*, AIME, **225**.

39. Gilman, J.R. and Kazemi, H.: "Improvements in Simulation of Naturally Fractured Reservoirs," *SPEJ* (Aug. 1983) 695-707.

40. Sonier, F., Bouillard, F., and Blaskivoch, F.T.: "Numerical Simulation of Naturally Fractured Reservoirs." *SPERE* (Nov. 1988) 1114-1122.

41. Coats, K.H., Dempsey, J.R., and Henderson, J.H.: "The Use of Vertical Equilibrium in Two-Dimensional Simulation of Three-Dimensional Reservoir Performance," *SPEJ* (March 1971) 63-71.

42. Rossen, R.H. and Shen, E.I.: "Simulation of Gas/Oil Drainage and Water/Oil Imbibition in Naturally Fractured Reservoirs," *SPERE* (Nov. 1989) 464-470; *Trans.*, AIME, **287**.

43. ECLIPSE 100 Reference Manual, Schlumberger (2000).

44. Pruess, K. and Narasimhan, T.N.: "A Practical Method for Modeling Fluid and Heat Flow in Fracture Porous Media," *SPEJ* (Feb. 1985) 14-26.

45. Gilman, J.R.: "An Efficient Finite-Difference Method for Simulating Phase Segregation in Matrix Blocks in Double-Porosity Reservoirs," *SPERE* (July 1986) 63-71

46. Beckner, B.L., Chan, H.M., McDonald, A.E., Wooten, S.O., and Jones, T.A.: "Simulating Naturally Fractured Reservoirs Using a Subdomain Method," paper SPE 21241 presented at the SPE Symposium on Reservoir Simulation, Anaheim, California, Feb. 17-20, 1991.

47. Penuela, G., Hughes, R.G., Civan, F., and Wiggins, M.L.: "Time-Dependent Shape Factors for Secondary Recovery in Naturally Fractured Reservoirs," paper SPE 75234 presented at the SPE/DOE Improved Oil Recovery Symposium, Tulsa, April. 13-17, 2002.

48. de Swaan, A.: "A Theory of Waterflooding in Fractured Reservoirs," *SPEJ* (April 1978) 117-122; *Trans.*, AIME, **265**.

49. Kazemi, H., Gilman, J.R., and Elsharkawy, A.M.: "Analytical and Numerical Solution of Oil Recovery From Fractured Reservoirs With Empirical Transfer Functions," *SPERE* (May 1992) 219-227.

50. Civan, F.: "Waterflooding of Naturally Fractured Reservoirs: An Efficient Simulation Approach," paper SPE 25449 presented at the Production Operations Symposium, Oklahoma City, March 21-23, 1993.

51. Civan, F.: "Quadrature Solution for Waterflooding of Naturally Fractured Reservoirs," *SPEREE* (April 1998) 141-147.

52. Gupta, A. and Civan, F.: "An Improved Model for Laboratory Measurement of Matrix to Fracture Transfer Function Parameters in Immiscible Displacement," paper

SPE 28929 presented at the SPE Annual Technical Conference and Exhibition, New Orleans, Sep. 25-28, 1994.

53. Civan, F. and Rasmussen, M.L.: "Asymptotic Analytical Solutions for Imbibition Waterfloods in Fractured Reservoirs," *SPEJ* (June 2001) 171-181.

54. Reis, J. and Cil, M.: "Analytical Models for Capillary Imbibition: Multidimensional Matrix Blocks," *In Situ* (2000) **24** (1) 79-106.

55. Dean, R.H. and Lo, L.L.: "Simulations of Naturally Fractured Reservoirs," *SPERE* (May 1988) 638-648.

56. Greenkorn, R.A., Johnson, C.R., and Shallenberger, L.K.: "Directional Permeability of Heterogeneous Anisotropic Porous Media," *SPEJ* (June 1964) 124-132.

57. Snow, D.T.: "Anisotropic Permeability of Fractured Media," *Water Resour. Res.* (1969) **5** (6), 1273-1289.

58. Pooladi-Darvish, M. and Firoozabadi, A.: "Experiments and Modeling of Water Injection in Water-Wet Fractured Porous Media," *JCPT* (March 2000) 31-42.

59. Harstad, H., Teufel, L.W., and Lorenz, J.C.: *Characterization and Simulation of Fluid Flow in Natural Fracture Networks*, in Hoak, T.E., Klawitter, A.L., and Blomquist, P.K. (Eds.): *Fractured Reservoirs: Characterization and Modeling*, Rocky Mountain Association of Geologists, Denver, Colorado (1997).

60. Perez, M.A., Gibson, R.L., and Toksöz, N.: "Detection of Fracture Orientation from Azimuthal Variation of P-wave AVO Responses," *Geophysics* (1999) **64** (4), 1253-1265.

61. Perez, M.A., Grechka, V., and Michelena R.J.: "Fracture Detection in a Carbonate Reservoir using a Variety of Seismic Methods," *Geophysics* (1999) **64** (4), 1266-1276.

62. Ata, E. and Michelena, R. J.: "Mapping Distribution of Fractures in a Reservoir with P-S Converted Waves," *The Leading Edge* (1995) **12**, 664-676.

63. Avila, R., Gupta, A., and Penuela, G.: "An Integrated Approach to the Determination of Permeability Tensors for Naturally Fractured Reservoirs," paper 2000-47 presented at the Canadian International Petroleum Conference of the Petroleum Society in Calgary, June 4-8, 2000.

64. Panfilov, M.: *Macroescale Models of Flow Through Highly Heterogeneous Media*, Kluwer Academic Publishers, Dordrecht (2000) 11-13.

65. Chang, M-M., Sarathi, P., Heemstra, R.J., Cheng, A.M., and Pautz, J.F.: "Users Guide and Documentation Manual for BOAST-VHS for the PC," final report, Contract No. DE-FC22-83FE60149, U.S. DOE, Bartlesville, Oklahoma (Jan. 1992).

66. Jones, J.R. and Raghavan, R.: "Interpretation of Flowing Well Response in Gas-Condensate Wells," *SPEFE* (Sept. 1988) 578-594.

67. Lee, W.J. and Holditch, S.A.: "Application of Pseudotime to Buildup Test Analysis of Low-Permeability Gas Wells With Long-Duration Wellbore Storage Distortion," *JPT* (Dec. 1982) 2877-2887.

68. Penuela, G. and Civan, F.: "Gas-Condensate Well Test Analysis with and without Relative Permeability Curves," paper SPE 63160 presented at the Annual Technical Conference and Exhibition, Dallas, Oct. 1-4, 2000.

69. Penuela, G. and Civan, F.: "Prediction of Gas-Condensate Well Productivity," *J. Pet. Sci. and Eng.* (2000) 28, 95-110.

70. Penuela, G.: "Prediction of the Gas-Condensate Well Productivity and Field Implementation Using a Compositional Model," MS thesis, U. of Oklahoma, OK (1999).

71. McWhorter, D.B. and Sunada, D.K.: "Exact Integral Solutions for Two-Phase Flow," *Water Resour. Res.* (March 1990) 26, 399-413.

72. Rapoport, L.A.: "Scaling Laws for Use in Design and Operation of Water/Oil Flow Models," *Trans.*, AIME (1955) 204, 143.

73. Wiggins, M.L, Brown, R.L., Civan, F., and Hughes, R.G:" Development of Reservoir Characterization Techniques and Production Models for Exploiting Naturally Fractured Reservoirs," U.S. DOE final report, grant No. DE-AC26-99BC15212 (in progress).

74. Firoozabadi, A. and Thomas, L.K.: "Sixth SPE Comparative Solution Project: Dual-Porosity Simulators," *JPT* (June 1990) 710-717.

75. Walas, S.M.: *Modeling with Differential Equations in Chemical Engineering*, Butterworth Heinemann Pub., Boston (1991).

APPENDIX A

ANALYTICAL SOLUTION OF THE 1D SINGLE-PHASE FLOW PROBLEM

In this appendix, the time-dependent flow correction factor to estimate the single-phase interporosity flow is analytically derived.

The pressure diffusivity equation for a 1D linear system representing single-phase fluid flow from the matrix to the fracture surface is given by:

$$\frac{\partial p_m}{\partial t} = \frac{k_m}{\phi_m \mu c_t} \frac{\partial^2 p_m}{\partial x^2} \quad \text{.....A.1}$$

and is subject to the following initial and boundary conditions[31] (see Fig. 3.2b):

$$p_m = p_i, \; -L/2 \le x \le L/2, \quad t = 0 \quad \text{.....A.2,}$$

$$p_m = p_f, \quad x = -L/2, \quad t > 0 \quad \text{.....A.3,}$$

$$p_m = p_f, \quad x = L/2, \quad t > 0 \quad \text{.....A.4.}$$

The analytic solution to Eqs. A.1 through A.4 is given by:[31]

$$\frac{\bar{p}_m - p_f}{p_i - p_f} = \sum_{j=0}^{\infty} \frac{8}{(2j+1)^2 \pi^2} \exp\left[-\frac{(2j+1)^2 \pi^2 k_m t}{\phi_m \mu c_t L^2} \right] \quad \text{.....A.5.}$$

In the dual-porosity model, it is assumed that the interporosity flow rate per unit volume of rock is related to the rate of accumulation in the matrix according to the following relation:[17]

$$\tilde{q} = -\phi_m c_t \frac{\partial \bar{p}_m}{\partial t} \quad \text{.....A.6.}$$

Taking the partial derivative of Eq. A.5 with respect to time and then substituting the resulting expression into Eq. A.6, the total interporosity flow rate can be computed as:

$$q = \frac{8V}{L^2}\frac{k_m}{\mu}(p_i - p_f)\sum_{j=0}^{\infty}\exp\left[-\frac{(2j+1)^2\pi^2 k_m t}{\phi_m \mu c_t L^2}\right] \quad \text{.....A.7}$$

where V is the bulk volume of the matrix from which fluids are produced into the fracture.

The flow correction factor is computed by solving Eq. 4.5 for F_c, given by:

$$F_c = \frac{q\mu L}{2Ak_m(\bar{p}_m - p_f)} \quad \text{.....A.8.}$$

Consider two parallel fractures that limit a matrix block with a fracture spacing L. Each fracture is in contact with the matrix along a surface A_o so that the total matrix volume is LA_o and $A \approx 2A_o$. Therefore, substitution of the pressure difference, $\bar{p}_m - p_f$, computed from Eq. A.5 and the interporosity flow rate, q, from Eq. A.7 into A.8 yields:

$$F_c = \frac{\pi^2}{4}\frac{\sum_{j=0}^{\infty}\exp\left[-(2j+1)\pi^2 t_D\right]}{\sum_{j=0}^{\infty}(2j+1)^{-2}\exp\left[-(2j+1)\pi^2 t_D\right]} \quad \text{.....A.9}$$

where the dimensionless time is defined by:

$$t_D = \frac{k_m}{\phi_m \mu c_t L^2} t \quad \text{A.10}$$

At large dimensionless time, Eq. A.9 converges to $F_c = \pi^2/4$.

The asymptotic behavior of F_c can be also theoretically calculated by using the constant shape factor proposed by Lim and Aziz[31] for one set of parallel fractures. They eliminated the time parameter in Eq. A.7 by introducing a constant shape factor into Eq. 2.2, resulting in a total interporosity flow rate equation given by:

$$q = \frac{\pi^2}{L^2} V \frac{k_m}{\mu} \left(\overline{p}_m - p_f \right) \quad \text{A.11.}$$

The total interporosity flow rate can be calculated by introducing $V = LA_o$ into Eq. A.11:

$$q = \frac{\pi^2}{L^2} LA_o \frac{k_m}{\mu} \left(\overline{p}_m - p_f \right) \quad \text{A.12.}$$

This equation can be rearranged by approximating the total fracture surface area as $A \approx 2A_o$ in order to get the following expression:

$$q = \frac{\pi^2}{4} A \frac{k_m}{\mu} \frac{\left(\overline{p}_m - p_f \right)}{\frac{L}{2}} \quad \text{A.13.}$$

Thus, comparing Eq. 4.5 with Eq. A.13, the steady-state value of F_c is given by:

$$F_c = \frac{\pi^2}{4} \approx 2.47 \quad \text{A.14.}$$

APPENDIX B

ANALYTICAL SOLUTION OF THE 1D GAS-CONDENSATE FLOW PROBLEM

In this Appendix, the flow correction factor for computing the interporosity molar flow rate in a gas-condensate system is analytically derived.

The model assumes a matrix block that is homogenous, isotropic and of uniform-thickness, bounded by two parallel fractures that are kept at constant pressure, p_f, below the dew point pressure of the gas, p_{dew}. The model neglects gravity, capillary, inertial and rock compressibility effects. Consequently, the diffusivity equation for this 1D linear system describing the gas-condensate flow from the matrix to the fracture surface is expressed as follows:

$$\frac{\partial\left(\rho_o S_o + \rho_g S_g\right)}{\partial t} = \frac{k_m}{\phi_m}\frac{\partial}{\partial x}\left[\left(\rho_o \frac{k_{ro}}{\mu_o} + \rho_g \frac{k_{rg}}{\mu_g}\right)\frac{\partial p_m}{\partial x}\right] \quad \text{.....B.1.}$$

The initial and boundary conditions are given by Eqs. A.2 through A.4. In order to linearize Eq. B.1, define a the pseudopressure function as:[66]

$$p_p = \int_{p_{ref}}^{p}\left(\rho_o \frac{k_{ro}}{\mu_o} + \rho_g \frac{k_{rg}}{\mu_g}\right)dp \quad \text{.....B.2.}$$

Penuela and Civan[68,69] proposed the following pseudotime function to complete the linearization of Eq. B.1:

$$t_p = \int_{t_{ref}}^{t} \left(\frac{\partial(\rho_o S_o + \rho_g S_g)}{\partial p_p} \right)^{-1} dt \quad \text{.....B.3.}$$

Substitution of Eq. B.2 and B.3 into B.1 yields:

$$\frac{\partial p_p}{\partial t_p} = \frac{k_m}{\phi_m} \frac{\partial^2 p_p}{\partial x^2} \quad \text{.....B.4.}$$

Using the pseudofunction definitions given by Eqs. B.2 and B.3, the initial and boundary conditions expressed in Eqs. A.2 through A.4 become (see Fig. 3.2b):

$$p_p = p_{pi}, \quad -L/2 \le x \le L/2, \quad t_p = 0 \quad \text{.....B.5,}$$

$$p_p = p_{pf}, \quad x = -L/2, \quad t_p > 0 \quad \text{.....B.6,}$$

$$p_p = p_{pf}, \quad x = L/2, \quad t_p > 0 \quad \text{.....B.7.}$$

Hence, the analytic solution to Eqs. B.4 through B.7 is identical to the solution given for the single-phase fluid problem in Appendix A but in terms of the prescribed pseudofunctions:

$$\frac{\bar{p}_p - p_{pf}}{p_{pi} - p_{pf}} = \sum_{j=0}^{\infty} \frac{8}{(2j+1)^2 \pi^2} \exp\left[-\frac{(2j+1)^2 \pi^2 k_m t_p}{\phi_m L^2} \right] \quad \text{.....B.8.}$$

It is also assumed that the interporosity molar flow rate per unit volume of rock is related to the rate of mass accumulation expressed in moles of hydrocarbons in the matrix according to the following relation:

$$\tilde{q}_t = -\phi_m \frac{\partial(\rho_o S_o + \rho_g S_g)}{\partial t} \quad \text{B.9}$$

where density and saturation values are volume-weighted average quantities over the total rock volume, V. Then, substitution of the pseudotime function (Eq. B.3) into Eq. B.9 yields:

$$\tilde{q}_t = -\phi_m \frac{\partial \bar{p}_p}{\partial t_p} \quad \text{B.10.}$$

Thus, taking the partial derivative of Eq. B.8 with respect to pseudotime and then substituting the resulting expression into Eq. B.10, the total interporosity molar rate can be expressed as:

$$q_t = \frac{8Vk_m}{L^2}(p_{pi} - p_{pf}) \sum_{j=0}^{\infty} \exp\left[-\frac{(2j+1)^2 \pi^2 k_m t_p}{\phi_m L^2} \right] \quad \text{B.11.}$$

Consequently, the flow correction factor is computed by solving Eq. 5.4 for F_c, given by:

$$F_c = \frac{q_t L}{2Ak_m(\bar{p}_p - p_{pf})} \quad \text{B.12.}$$

If the pseudopressure difference (Eq. B.8) and the interporosity flow rate (Eq. B.11) are substituted into Eq. B.12, Eq. A.9 is obtained but with the following definition for dimensionless time:

$$t_D = \frac{k_m}{\phi_m L^2} t_p \quad \text{B.13.}$$

The use of the pseudotime function introduces small errors into Eq. B.4, which may be neglected. The reason for the errors is that in some cases the pseudopressure value in the left hand side of Eq. B.4 obtained from Eqs. B.9 and B.10 is not the same as the

pseudopressure value in the right hand side of Eq. B.4, which may be the case at the beginning of the simulation run. Note that the left hand side of Eq. B.4 requires the pseudopressure averaged over the matrix block while it needs pseudopressure values as function of space on the right hand side. For a detailed analysis on linearization by means of a pseudotime function, the reader is referred to Lee and Holditch.[67]

APPENDIX C

NUMERICAL SIMULATION OF A NATURALLY FRACTURED RESERVOIR: INPUT AND OUTPUT DATA ANALYSIS

This appendix gives a description of input data required for a typical simulation of a naturally fractured reservoir using constant shape factors. Simulation output data are then presented in a graphical form to investigate the forces acting in different flow stages as the water front flows along the fracture system. Qualitative results from this exercise provide the basis for the implementation of a generalized model for fluid exchange described in Chapter 7.

C.1 Input Data Description

Input data presented in the following section are taken from the sixth SPE comparative project for dual-porosity simulators.[74] Fluid PVT data and some of the fluid-rock properties for that project were originally presented by Thomas *at al.*[29]

The naturally fractured reservoir is simulated as a single-layer formation using a 40×1×1 parallel Cartesian grid whose dimensions are shown in **Table C.1**. The reservoir is composed of a matrix system with ϕ_m = 29% and k_m = 1 md. It is assumed that the fracture network consists of a single set of parallel fractures with ϕ_f= 1%, k_f= 90 md and a fracture spacing of L = 5 ft. Therefore, the matrix-block shape factor using Lim and

Aziz's approximation[31] for one set of parallel fractures from Table 2.1 is σ= 0.396 ft^2. This reservoir configuration represent an example of a dual-porosity system with a permeability ratio ω_K= 0.011.

TABLE C.1 – GRIDBLOCK AND RESERVOIR ROCK BASIC DATA

Number of grid-blocks in the x-direction, n_x	40
Number of grid-blocks in the y-direction, n_y	1
Number of grid-blocks in the z-direction, n_z	1
Grid-block size in the x-direction, Δx, ft	50
Grid-block size in the x-direction, Δy, ft	1000
Grid-block size in the x-direction, Δz, ft	50
Matrix porosity, ϕ_m, *fraction*	0.29
Matrix permeability, k_m, md	1.0
Matrix compressibility, c_m, psi^{-1}	3.5×10^{-6}
Fracture porosity, ϕ_f, *fraction*	0.01
Fracture permeability, k_f, md	90
Fracture compressibility, c_f, psi^{-1}	3.5×10^{-6}
Connate water saturation in the matrix, S_{wc}, %	20
Initial pressure, p_i, psig	6000
Fracture spacing, L, ft	5

Relative permeability and water-oil capillary pressure data shown in **Table C.2** were taken from Thomas *et al.*[29] and Firoozabadi and Thomas,[74] respectively. This set of data represents a matrix system with intermediate wettability. Zero capillary pressure and relative permeability as linear functions of saturation were used for the fracture system. Relative permeabilities for the interporosity flow is computed using the Thomas *et al.*[29] approach, which computes the relative permeability at the interface for fluids flowing from the fracture to the matrix as follows:[29]

$$k_{rw} = k_{rw}(p_{cwo} = 0)S_{wf} \quad \text{C.1,}$$

and,

$$k_{ro} = k_{ro}(S_{wm})S_{of} \quad \text{C.2.}$$

For fluids flowing from the matrix to the fracture, water saturation in the matrix is used to estimate relative permeabilities at the interface. In Eqs. C.1 and C.2, relative permeabilities are obtained from the input values for fluid-rock properties in the matrix given in Table C.2.

TABLE C.2 – FLUID-ROCK PROPERTIES IN THE MATRIX SYSTEM

S_α	k_{rw}	k_{ro}	P_{cow} *psi*
0	0	0	1
0.1	0	0	1
0.2	0	0	1
0.25	0	0.005	0.5
0.3	0.042	0.01	0.3
0.35	0.1	0.02	0.15
0.4	0.154	0.03	0
0.45	0.22	0.045	-0.2
0.5	0.304	0.06	-1.2
0.6	0.492	0.11	-4
0.7	0.723	0.18	-10
0.75	0.86	0.23	-40
0.8	1	0.23	-40
1	1	0.23	-40

In Table C.2, S_α represents phase saturation. For instance, fluid-rock properties at S_w=0.3 are k_{rw} = 0.042, k_{ro} = 0.18, and p_{cow} = 0.3 psi.

PVT data of oil is divided into two sets. One set corresponds to undersaturated properties relative to a bubble-point pressure p_b = 5545 psig (**Table C.3**). Saturated

values are shown in **Table C.4**. In this simulation, pressures remain above the bubble-point pressure; and, therefore mainly undersaturated values are used.

TABLE C.3 – UNDERSATURATED OIL PROPERTIES

Oil density, ρ_o, lb/ft^3	51.14
Oil viscosity at p_b, μ_o, cp	0.21
Slope of μ_o above p_b, $d\mu_o/dp$, cp/psi	1.72×10^{-5}
Oil formation volume factor at p_b, B_o, RB/STB	1.8540
Slope of B_o above p_b, dB_o/dp, RB/STB/psi	-4.0×10^{-5}

TABLE C.4 – SATURATED OIL PROPERTIES

p *psig*	μ_o *cp*	B_o *RB/STB*	R_{so} *SCF/STB*
1674	0.529	1.3001	367
2031	0.487	1.3359	447
2530	0.436	1.3891	564
2991	0.397	1.4425	679
3553	0.351	1.5141	832
4110	0.31	1.5938	1000
4544	0.278	1.663	1143
4935	0.248	1.7315	1285
5255	0.229	1.7953	1413
5545	0.21	1.854	1530
7000	0.109	2.1978	2259

PVT data of water are basically $\mu_w = 0.35$ cp, $B_w = 1.07$ RB/STB, $c_w = 3.5\times10^{-6}$ psi^{-1} and $\rho_w = 65$ lbm/ft^3.

A simulation run was performed by using a producer located at grid-block indexed (1,1,1) and an injector at (40,1,1). Fluid withdrawal was constrained by total liquid production of 300 STB/D while water injection was initially controlled by a constant rate

of 300 STB/D but constrained by a maximum bottomhole pressure of 6100 psig. Results from a simulation run time of 10 years are reported in the following.

C.2 Output Data Analysis

Fluid production rates are shown in **Fig. C.1** along with the effective interporosity oil rate during 10 years of water injection.

Oil production rate, Q_o, remained constant until water breakthrough, which occurred approximately after 2.5 years of water injection. During this period of constant oil production, the effective interporosity oil rate, $q_{o\ eff}$, increased until reaching an equilibrium flow rate that was also affected by the water breakthrough. The rate difference between the Q_o and $q_{o\ eff}$ represents the rate of oil production from the fracture system.

The interporosity rate in Fig. C.1 represents the effective oil production from the matrix as a result of the interplay between the viscous and capillary forces. **Figure C.2** shows the actual interporosity flow rate along the fracture that connects the producer located at $x = 0$ and the injector. It is observed that oil is initially injected into the matrix (forced drainage) as a consequence of high pressure in the fractures. With water imbibition, the oil-phase pressure gradient is reversed and oil begins to flow into the fracture. As a consequence of fluid exchange, water in the fracture does not move as a piston-like front as shown in **Fig. C.3**. For comparison, **Fig. C.4** shows water saturation profiles in the fracture system at three different times along with the interporosity oil rate. It is observed that ahead of the saturation front, oil interporosity rate is very small except

close the producer, where a large pressure drawdown at the well causes a large pressure difference between the matrix and the fractures, and therefore high interporosity flow.

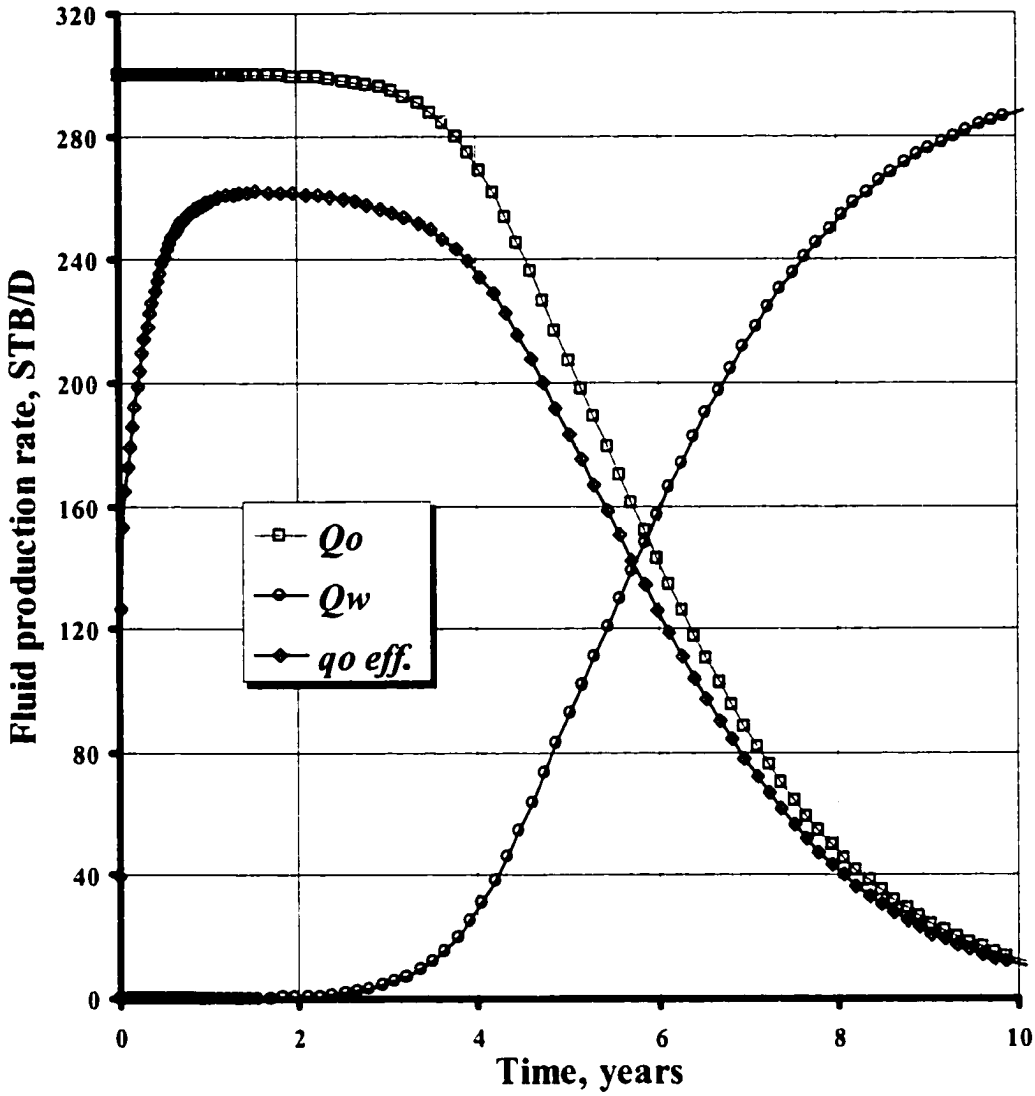

Fig. C.1 – Fluid production in a naturally fractured reservoir under waterflooding. Oil recovery from the matrix is affected by the water breakthrough at the producer. After breakthrough, oil production rate drops to values similar to the interporosity oil rate.

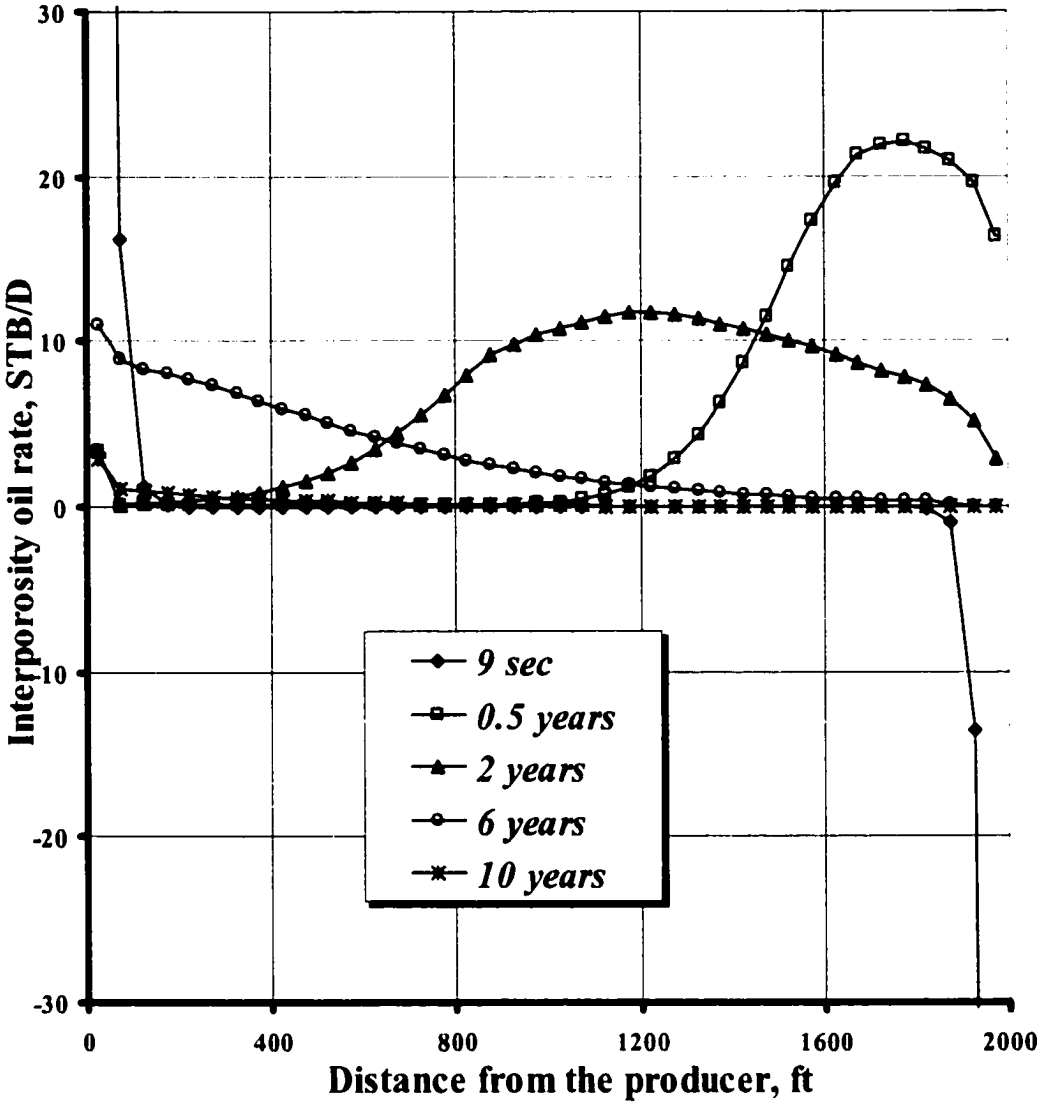

Fig. C.2 – Interporosity oil rate as a function of position and time. Distance is measured along the fracture that connects the producer (x = 0) and the injector (x = 2000 ft). Initially, oil is injected into the matrix in the region close to the injector as a result of high pressures in the fracture. As water flows through the fracture, capillary forces are responsible for most of the fluid exchange.

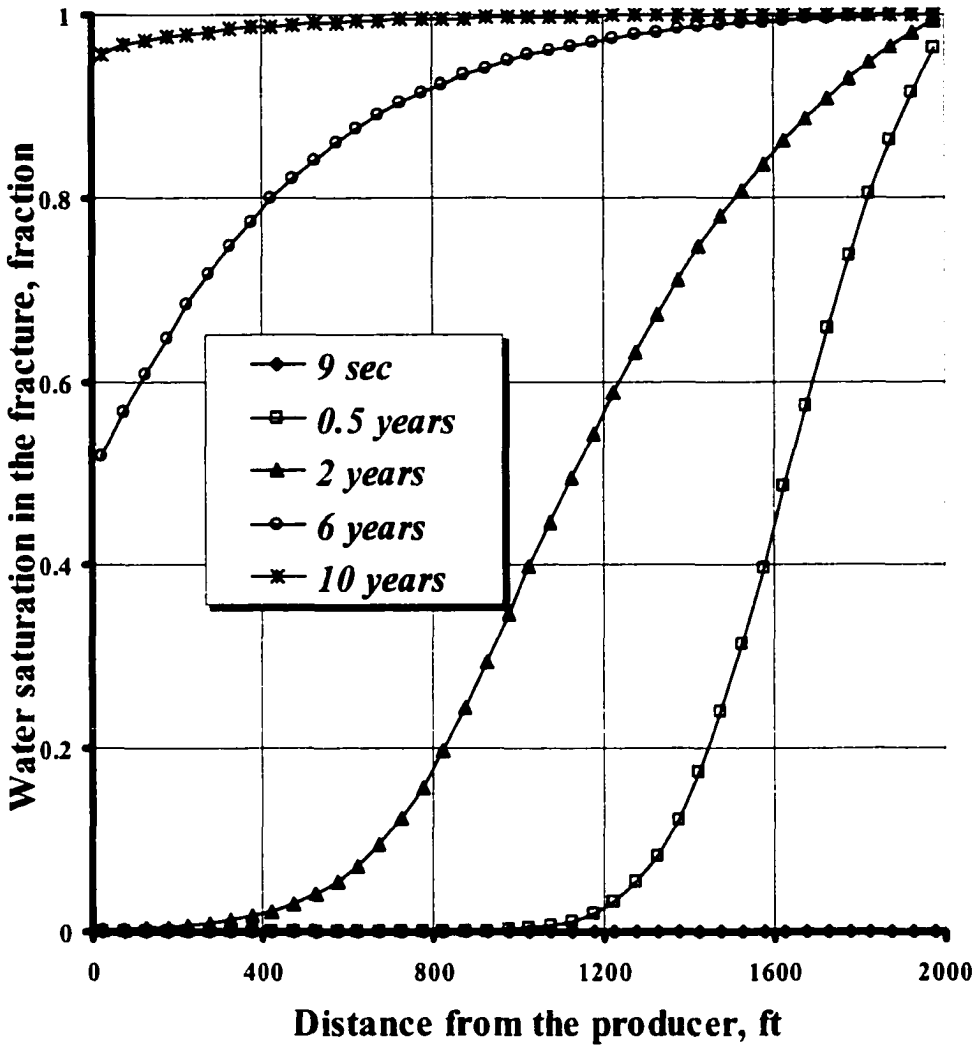

Fig. C.3 – Water saturation profiles observed along the fracture that connects the producer with the water injector located at x = 2000 ft. As water contacts new matrix surfaces, capillary forces act and countercurrent imbibition occurs. Ahead of the water front, viscous forces contribute to the interporosity flow rate through the pressure differences between the matrix and the fracture.

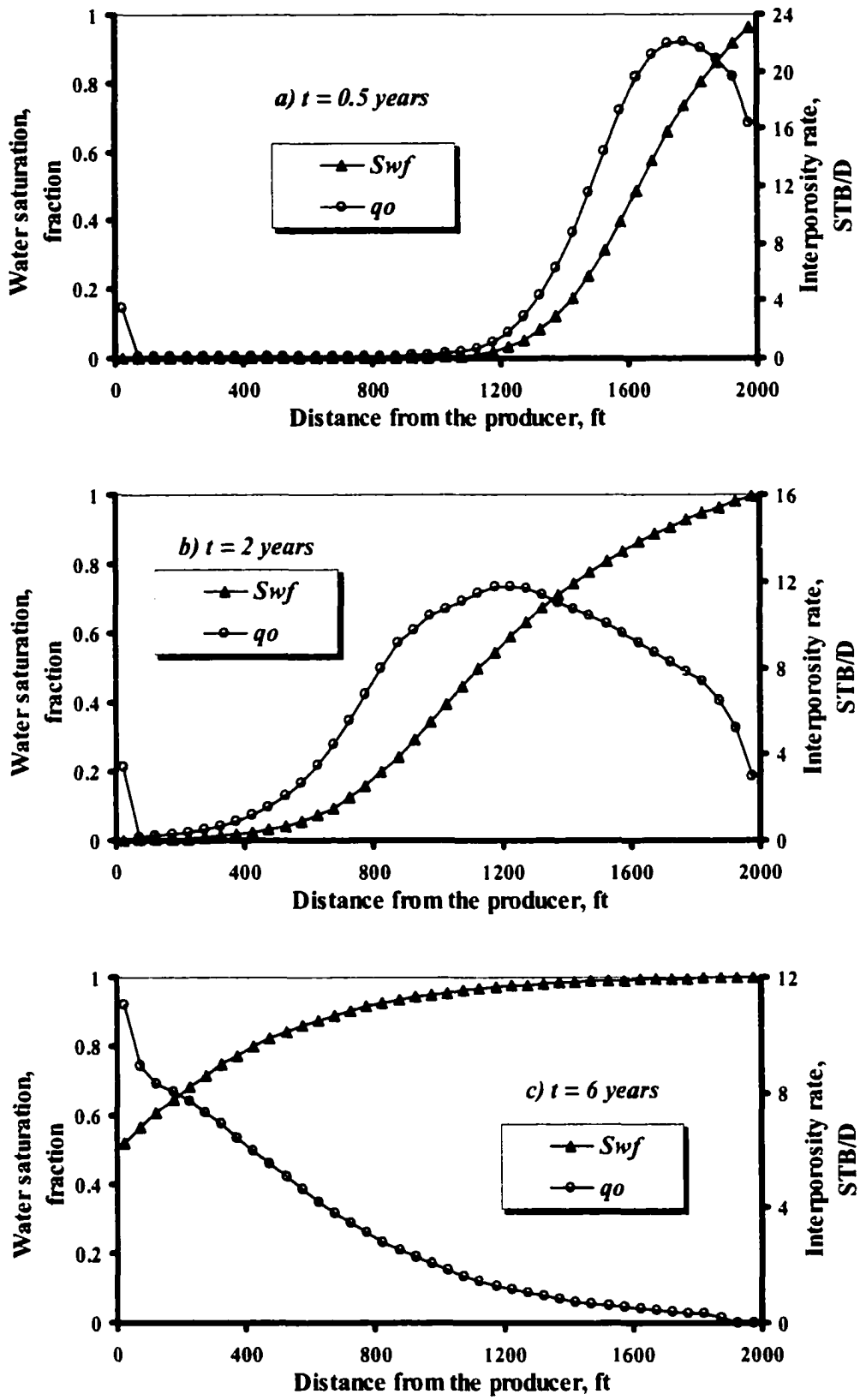

Fig. C.4 – Fracture water saturation profiles and interporosity oil rate at different times.

Single-phase flow is not only observed before water breakthrough at the producer; water injection in the matrix is also observed after long time of injection in the near wellbore region of the water injector (**Fig. C.5**). After 10 years of injection, oil outflow from the matrix is negligible (see Fig. C.2) while there is virtually single-phase water injection into the matrix (Fig. C.5c).

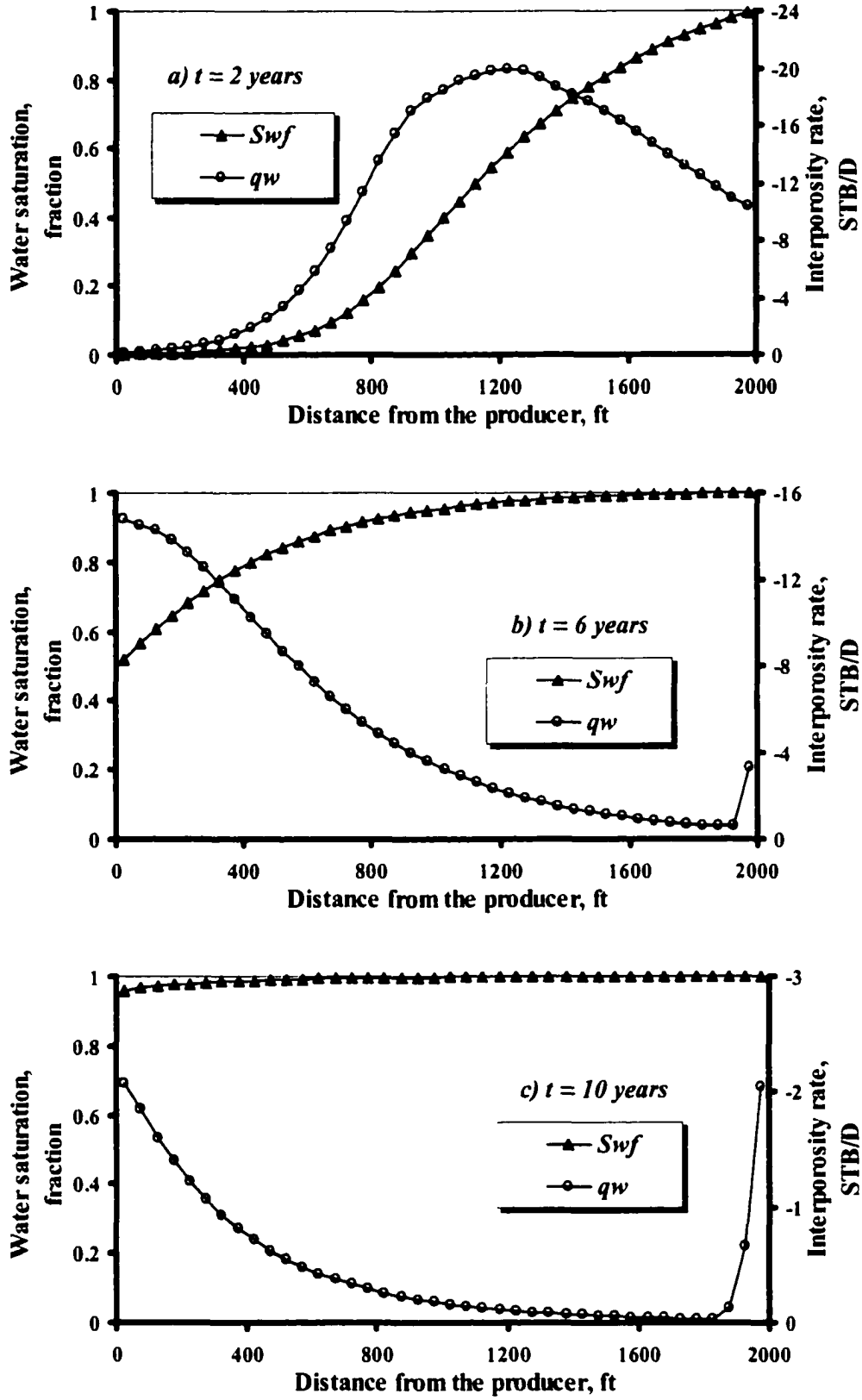

Fig. C.5 – Fracture water saturation profiles and interporosity water rate at different times.